

TOWARD HIGH-RESOLUTION FLOOD FORECASTING FOR LARGE
URBAN AREAS - NEW SOLUTIONS FOR 1D ROUTING

by

BEHZAD NAZARI

Presented to the Faculty of the Graduate School of
The University of Texas at Arlington in Partial Fulfillment
of the Requirements
for the Degree of

DOCTOR OF PHILOSOPHY

THE UNIVERSITY OF TEXAS AT ARLINGTON

May 2017

Copyright © by Behzad Nazari 2017

All Rights Reserved



Acknowledgements

I am extremely grateful to my advisor Dr. Dong-Jun Seo for his tremendous support during my PhD study. I would also like to thank my dissertation committee Drs. Nick Fang, Habib Ahmari, Jean Gao, and Ranjan Muttiah for their comments. In addition, I am grateful to Dr. Sunghee Kim, Ms. Hamideh Habibi, Drs. Arezoo Rafieeiniasab and Amir Norouz, and all other members of our research group at the Urban Water Institute for their support.

Also, I would like to express my gratitude to many others who helped me during my PhD study including: Ms. Laura Pham and Mr. Timothy B. Royer at the City of Fort Worth; Ms. Mandy Clark and Ms. Amy Cannon at the City of Arlington; Mr. Zhengtao Cui, Mr. Brian Cosgrove, Mr. Victor Koren, Mr. Mike Smith, Mr. Seann Reed, and Mr. Dave Streubel at the National Weather Service.

This research was supported by the NSF under Grants IIPS-1237767 and CyberSEES-1442735. I would also like to thank Computational Hydraulics International (CHI) for providing me with a student license for PCSWMM.

Finally, I must express my gratitude to my parents, family, and friends for all their support and encouragement.

April 21, 2017

Abstract

TOWARD HIGH-RESOLUTION FLOOD FORECASTING FOR LARGE URBAN AREAS - NEW SOLUTIONS FOR 1D ROUTING

Behzad Nazari, PhD

The University of Texas at Arlington, 2017

Supervising Professor: Dong-Jun Seo

The ability to forecast flow, depth, and velocity in flooding events is one of the most important needs in highly populated urban areas. Urbanization and climate change highlight the necessity to understand and accurately predict water-related hazards in urban areas due to extreme precipitation. Towards that end, this study initially assesses the impact of changes in precipitation magnitude and imperviousness on urban inundation in a flooding prone urban catchment in the Dallas-Fort Worth Metroplex. Consequently, this study focuses on identifying potential alternatives to the conventional inundation models to improve operational viability of real-time flood forecasting in urban areas by downscaling coarse-resolution model output. Taking advantage of high-resolutions physiographic information, the problem is then transformed into developing efficient methods for routing flow in a network of 1D channels to represent sub-

grid variability of hydraulic parameters within coarse 2D cells. Accordingly, two existing methods for such a routing problem are discussed, i.e., the diffusion wave routing and nonlinear routing with power-law storage functions. Each of the aforementioned methods is then solved innovatively to improve their efficiency for real-time routing of flow through many small streams quickly over a large area. In this work, two new methods for solving the 1-dimensional linear diffusion wave equation for finite domain is presented. Referred to as the Continuous Time Discrete Space (CTDS) methods, they yield explicit symbolic expressions for time-continuous solutions at discrete points in space. As such, the methods provide a powerful tool for very easily obtaining accurate diffusive wave solutions in lieu of numerical integration when predictions are desired only at specific locations along the channel. The proposed methods are easy to implement and may be used in a variety of routing applications where accurate explicit symbolic solutions are desired for linear advection-diffusion at specific locations. Also, a new direct solution for nonlinear reservoir routing with a general power-law storage function is presented. The resulting implicit solution is expressed in terms of the incomplete Beta function and is valid for inflow hydrographs that may be approximated by a series of pulses of finite duration. A separate solution for zero inflow representing recession is also presented. The new analytical solution extends the previous results reported in the literature which provide direct solutions only for certain exponents in the power-law storage function. In

addition to the wide spectrum of applications that require modeling of nonlinear reservoirs or open channels, the direct solution may also be used for physically-based semi-distributed routing of hillslope flow following simplification of the flow paths as a dendritic network of nonlinear reservoirs. The proposed solutions offer new pathways for simple and efficient modeling of flood waves in real-world applications with minimal computational effort that makes them suitable candidates for flood forecasting in large urban areas.

Table of Contents

Acknowledgements.....	iii
Abstract.....	iv
Chapter 1 General Introduction	1
Chapter 2 Assessing The Impact of Variations in Hydrologic, Hydraulic And Hydrometeorological Controls on Inundation in Urban Areas	15
Chapter 3 Quasi-Analytical Solution for 1-Dimensional Diffusion Wave Equation with Lateral Inflow Using Continuous-Time Discrete- Space Methods	49
Chapter 4 Analytical Solution for Nonlinear Reservoir Routing with Power-Law Storage Function	115
Chapter 5 General Conclusions	145

Chapter 1

General Introduction

The complex system of water cycle in an urban environment, or the urban hydrological system (see Fig 1), is not fully understood (Salvadore et al., 2015). Among water-related hazards in large population centers, flooding and inundation pose arguably the largest threat. As a part of this research, detailed geo-spatial and statistical analyses are performed to improve understanding of urban flooding by assessing the sensitivity of inundation to urbanization and climate change.

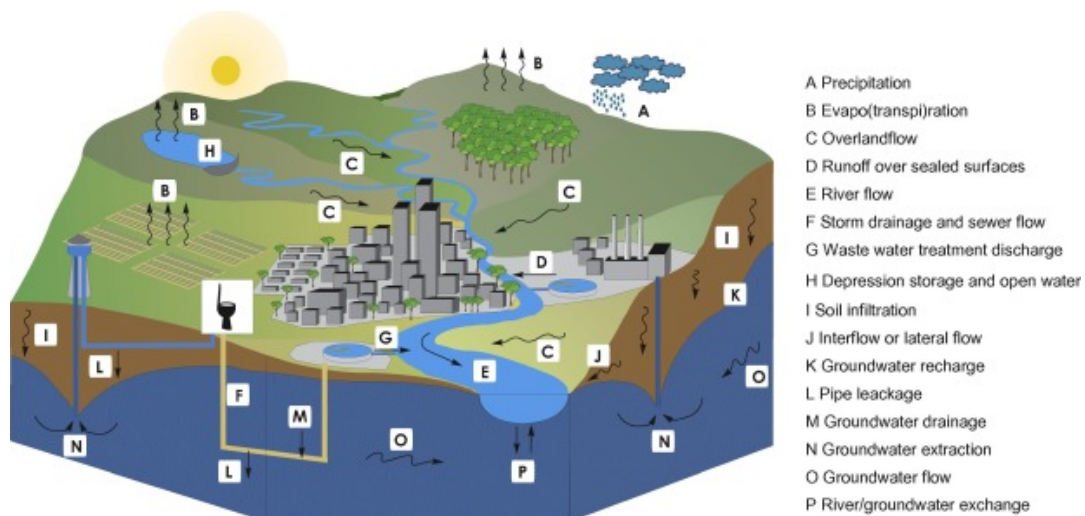


Figure 1 Water cycle in an urban area (Salvadore et al., 2015).

Detailed inundation mapping is an effective tool for mitigating flood hazards in highly urbanized areas. Recent advances in computing, data science and technology, and remote sensing have led to emergence of new breeds of models for urban flood modeling (Chang et al., 2015, Gires et al., 2014). High-resolution urban inundation mapping, however, is still a relatively new area of

research and remains a large challenge particularly for large urban areas due to extremely large computational and modeling costs. Hydraulic models for flood forecasting and inundation mapping solve the mathematical equations of flow, or the Saint Venant equations, to obtain depth and velocity (Dutta et al. 2003). Depending on the purpose of modeling, data availability, and computational resources, the governing equations of flood flow are usually discretized and solved in either one or two dimensions. One-dimensional (1D) models are easy to set up and calibrate (Seyoum *et al.*, 2011), computationally inexpensive and relatively easy to parameterize (Horrit and Bates, 2001). However, 1-D models fail to capture the distributed nature of flood hydraulics in certain cases of urban flooding (Bernard *et al.*, 2007). Two dimensional (2D) models, on the other hand, can produce areal inundation maps. High-resolution 2D hydraulic modeling, however, is difficult to perform and computationally too expensive (Leandro, 2008; Seyoum *et al.*, 2011) for large urban areas, particularly for real-time forecasting. The above limitations spurred efforts to develop methods that make use of the simplicity of hydrologic and hydraulic 1D models but at the same time address their inadequacies when and where necessary. Among the methods emerged are the 1D-2D models (Bernard *et al.*, 2007; Leandro, 2008; Seyoum *et al.*, 2011; Simões *et al.*, 2011, Gires *et al.*, 2013) which simulate the flows in channels and pipes in 1D and the overland surcharge flow in 2D (see Fig 2). The goal of this research is to: 1) assess the feasibility of hydraulic and hydrologic

modeling for real-time flood forecasting for large urban areas using the 1D-2D approach, 2) formulate potential alternative approaches, and 3) develop core modeling elements in support of such approaches.

For 1), the possibility of operational real-time flood forecasting for select locations, or hot spots, in the City of Fort Worth was considered using the Computational Hydraulics International’s 1D-2D PCSWMM model. It was found that high-resolution 1D-2D hydraulic models are computationally too expensive for real-time inundation mapping in large urban areas. For instance, high-resolution 1D-2D simulation of inundation in Edgecliff Branch Catchment of Sycamore Creek (~12.17 km²) takes approximately 10 to 15 minutes while a target simulation time of 5 to 10 minutes is desired to produce actionable forecasts. This conclusion is in agreement with previous studies, even the most

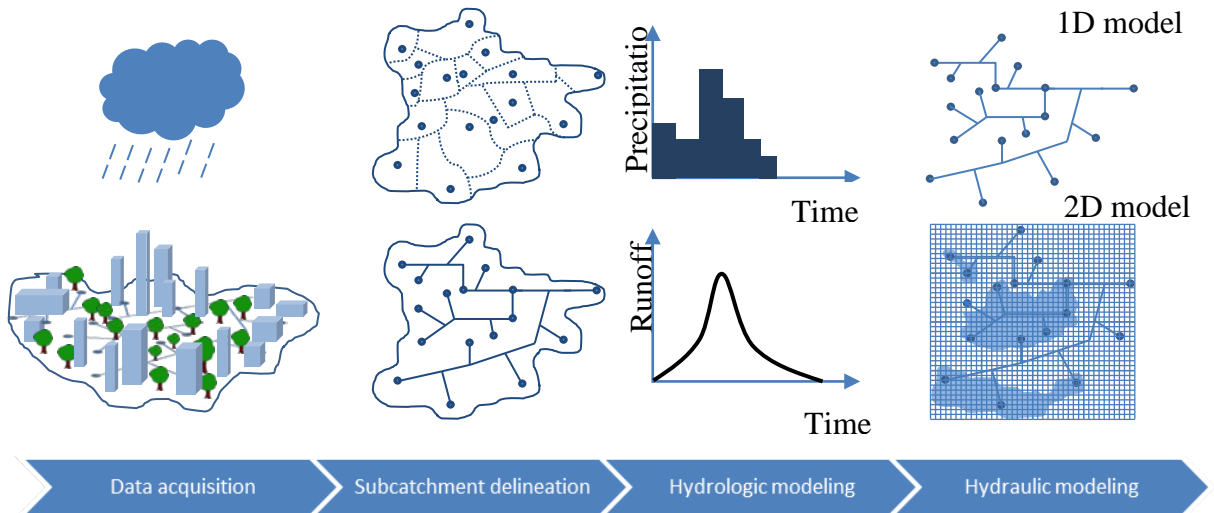


Figure 2 General framework of 1D-2D models

recent ones that consider the latest developments. For example, Russo et al. (2015) reports that using a specific GPU card (as opposed to the commercial software package used in the current study) significantly reduces the computational time of a 1D-2D model from about 2 hours to 3-4 minutes for a 3-hr simulation period. The above modeling used a sophisticated adaptive mesh of 400,000 cells for a 44 km² domain in Barcelona, Spain. Inundation mapping for larger urban areas such as the City of Dallas, which has 20 times the area, will take much longer. Just as importantly, detailed modeling of such a large area will require very large human resources. As such, real-time inundation mapping using high-resolution 1D-2D models is currently practical only for smaller urban catchments. The detailed high resolution 1D-2D modeling of the study area in the City of Fort Worth nevertheless allowed detailed geo-spatial and statistical analyses of inundation due to urbanization and climate change to improve understanding of urban flooding. Chapter 2 discusses the results of this element obtained via multi-dimensional sensitivity analysis (Nazari et al. 2016).

Although high-resolution modeling is very effective in conveying flood hazards, the model should be kept as simple as possible while still being physically realistic (Hunter et al., 2007). In addition, many studies (see Hunter et al., 2007 and references therein) suggest that the uncertainties in topography and boundary conditions influence the simulated results of hydraulic models more than those introduced by appropriately simplified process modeling. Moreover,

hydraulic models with reduced complexity combined with detailed descriptions of topography are easier to calibrate (Hunter et. al., 2007), a rather important point in that lack of data for calibration and validation poses one of the biggest challenges for modeling. Also, high resolution 1D-2D models make difficult uncertainty assessment using standard Monte Carlo methods as it is impractical to make a very large number of runs. Therefore, it is highly desirable to produce detailed descriptions of hydraulic variable without impractical high-resolution hydraulic modeling. Distributed hydrologic models such as the National Weather Service (NWS) Hydrology Laboratory Research Distributed Hydrologic Model (HLRDHM, Koren et al. 2004) have been shown to be a viable tool for real-time flood forecasting in large urban area if relatively coarse resolutions are chosen (Habibi et al., 2015). If one could effectively and efficiently downscale coarse-resolution model output by utilizing physiographic information such as elevation, building footprint, etc., to produce high-resolution hydraulic information such as flow, depth and velocity, one may overcome the limitations of 1D-2D modeling. The above problem amounts to mapping subgrid-scale variations of hydraulic variables given output from a lower-resolution hydraulic model. Such downscaling approaches have been used extensively in hydrometeorology for atmospheric variables but have not been explored as much for hydrologic or hydraulic variables. This work formulates such an approach and develop the key necessary elements.

One way to reduce the complexity of high-resolution 2D models is to represent the detailed hydraulics within a coarse-resolution 2D cell with a relatively dense network of 1D channels which may be identified based on physiographic features. Then, a physically-based and computationally-inexpensive 1D model with upstream and lateral flow may be used to route flow through many small streams quickly over a large area. Although the spatial resolution of such models is less than 2D models, it is hypothesized that the gain in computational feasibility marginalizes the reduction in spatial resolution. Successful application of efficient flood routing in large networks has already been verified by many researchers (Gupta and Waymire, 1998; Reggiani et al., 2001; Menabde and Sivapalan, 2001; Gupta, 2004; Mantilla and Gupta, 2005; Mantilla et al., 2006; Mandapaka et al., 2009; Small et al., 2013; Ayalew et al., 2014; Choi et al., 2015 among many others). Flow direction maps derived from high-resolution topographic data may be used to construct the downscaling 1D networks within each coarse-resolution cell. Modeling flow paths is important in determining the hydrologic response of urban catchments (Gironas et al., 2009, see also the references therein) for which numerous algorithms have been developed. In the widely used D8 method, an eight-cell neighborhood is assumed around each grid cell. As seen in Figure 3a-c, one may analyze the Digital Elevation Model (DEM) and identify the steepest descending slope at each grid cell as the most likely direction of flow at each cell as shown in Figure 3d (NWS,

2015; Maidment, 2002). The flow accumulation, which is defined as the total number of upstream pixels that flow into each cell, may be constructed by tracking the flow direction matrix (Figure 3e). Finally, flow accumulations may be used to construct the hillslope flow network as shown in Figure 3f. The cross-sectional geometries of the channels in the network may be extracted from the DEM. If DEM is not available, it may be possible to invoke self-similarity to estimate the hydraulic geometries of channels (Menabde and Sivapalan, 2001).

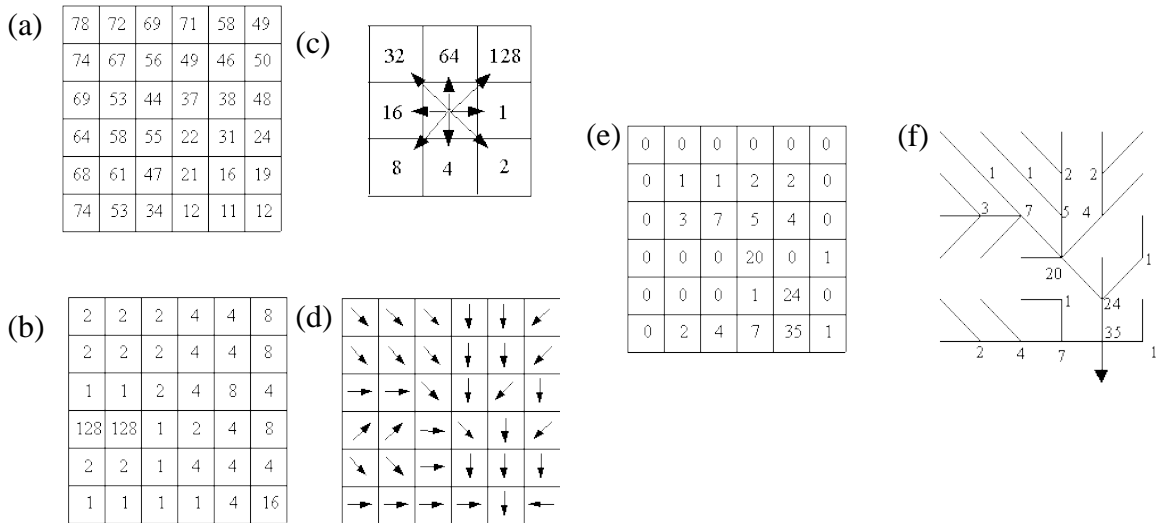


Figure 3 the process of producing a network of 1D channels to represent flow paths

The resulting downscaling problem amounts to solving equations of conservation of mass and momentum on the reduce 1D network of channels using the inflow boundary conditions derived from the coarse-resolution model output (see Fig 4).

This research develops two models to solve 1D linear diffusion wave equation with lateral inflow (Chapter 3) and nonlinear routing (Chapter 4) through

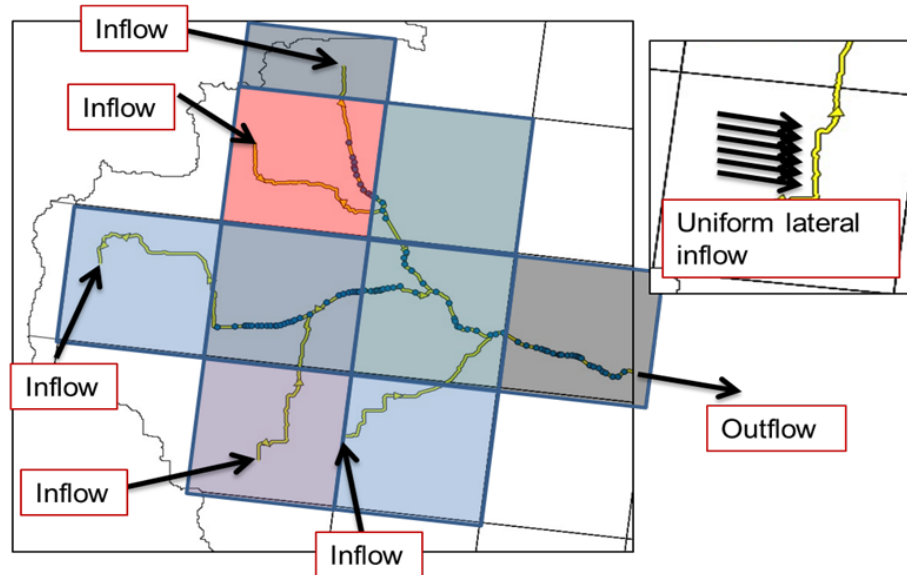


Figure 4 the general framework of downscaling coarse-resolution model output to the boundary conditions of a higher-resolution reduced hydraulic model

a network of channels. The newly proposed methods use innovative efficient solutions and hence offer a generalized approach that may be applied to large urban areas. Chapter 3 discusses the development of two new quasi-analytical symbolic solutions for 1D linear diffusion wave equation with lateral inflow for Neumann (known values of flux) or Dirichlet (known values of flow) downstream boundary conditions. The new methods produce explicit symbolic expressions for non-dimensionalized solutions for arbitrary inflow hydrographs. In addition, a generic unit response function to a constant inflow has also been developed (Chapter 2). It may be used to route flood hydrographs in wide-ranging real-world applications with minimal computational effort with the principles of

superposition and proportionality. Due to the linear nature of diffusive wave with constant coefficients, application of the principles of superposition and proportionality results in exact solutions at discretized nodes. Although this approach cannot be directly applied to nonlinear diffusive wave equation with flow-dependent coefficients, a common practice is to adopt a “layered” 1D diffusive wave routing which updates the value of coefficients based on the upstream flow magnitude. However, implementing such an approach requires additional research and evaluation which is outside the scope of current study. All newly developed explicit solutions to linear diffusive wave equation are closed-form and continuous functions of time, and hence do not suffer from numerical instabilities. Chapter 4 discusses the development of an analytical solution for nonlinear reservoir routing with a general power-law storage function. The new implicit solution is useful in practical modeling, design, forecasting and control when applied to single reservoirs, cascade of reservoirs, and/or networks of channels. In addition, an improved parametrization of nonlinear channel routing with general flow resistance and cross-sectional area as power-law storage function is presented (Chapter 4) which may serve as an improved solution technique for the downscaled 1D network of channels in large urban areas. Finally, Chapter 5 discusses general conclusions and broad implications of the present work and offers recommendations for future research. Figure 5

summarizes the general framework of the current research.

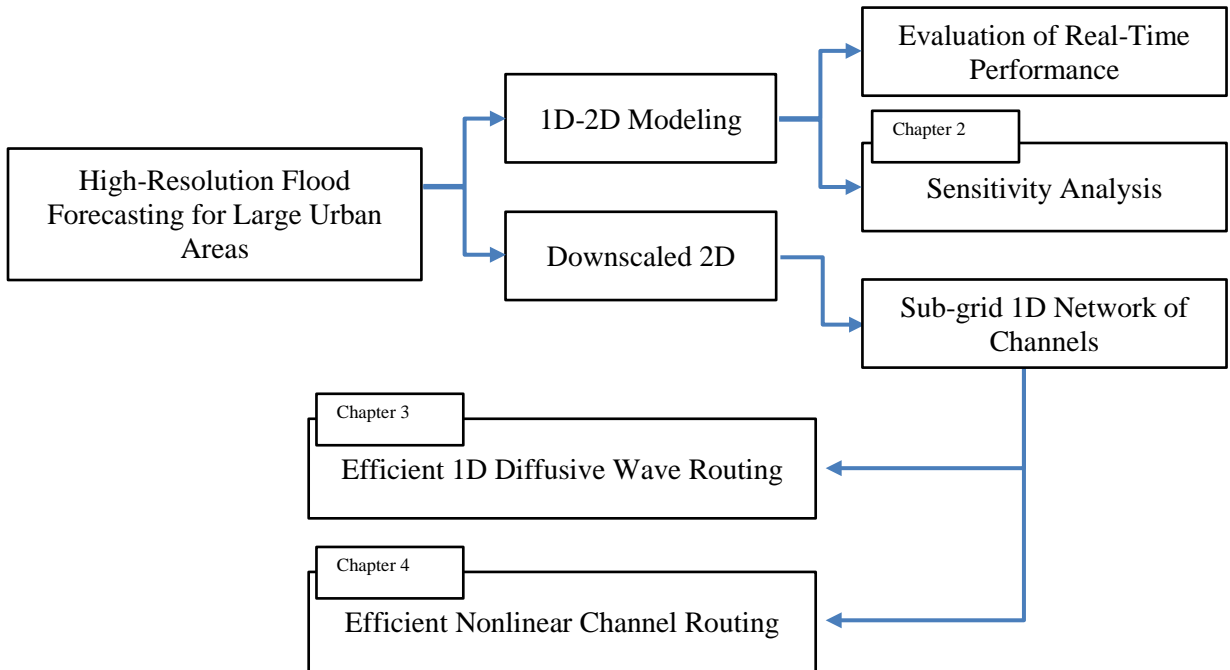


Figure 5 Topical organization and flow of the dissertation.

The main findings of this research are can be summarized as follows:

- Changes in precipitation and impervious cover have a large impact on local and catchment scale urban inundation.
- With climate change and continuing urbanization for accurate mapping of inundation in urban areas, high resolution rainfall forcing and physiographic information are essential.
- Quasi-analytical methods offer simple and computationally efficient solutions to the 1D linear diffusive wave equation. The obtained solutions are in very

good agreement with numerical integration methods and obviate the need for problem-specific model setup.

- Contrary to conclusions drawn from previous studies, it was found that the general nonlinear routing problem with power-law storage functions of any arbitrary exponent has an analytical solution. Many different components of the urban hydrological system could potentially be approximated by power-type storage functions and be solved by the presented solution.

References

- Ayalew, T. B., Krajewski, W. F., Mantilla, R., & Small, S. J. (2014). Exploring the effects of hillslope-channel link dynamics and excess rainfall properties on the scaling structure of peak-discharge. *Advances in Water Resources*, 64, 9-20.
- Akan, A. O., & Yen, B. C. (1981). Diffusion-wave flood routing in channel networks. *Journal of the Hydraulics Division*, 107(6), 719-732.
- Chang, T. J., Wang, C. H., & Chen, A. S. (2015). A novel approach to model dynamic flow interactions between storm sewer system and overland surface for different land covers in urban areas. *Journal of Hydrology*, 524, 662-679.
- Choi, C. C., Constantinescu, G., & Mantilla, R. (2015). Implementation of a hydraulic routing model for dendritic networks with offline coupling to a distributed hydrological model. *Journal of Hydrologic Engineering*, 20(11), 04015023.

- Dutta, D., Herath, S., & Musiaka, K. (2003). A mathematical model for flood loss estimation. *Journal of hydrology*, 277(1), 24-49.
- Hunter, N. M., Bates, P. D., Horritt, M. S., & Wilson, M. D. (2007). Simple spatially-distributed models for predicting flood inundation: a review. *Geomorphology*, 90(3), 208-225.
- Gires, A., Giangola-Murzyn, A., Abbas, J. B., Tchiguirinskaia, I., Schertzer, D., & Lovejoy, S. (2015). Impacts of small scale rainfall variability in urban areas: a case study with 1D and 1D/2D hydrological models in a multifractal framework. *Urban Water Journal*, 12(8), 607-617.
- Gupta, V. K., & Waymire, E. (1998). Some mathematical aspects of rainfall, landforms, and floods. *Advanced series in statistical sciences and applied probability*, 7, 129-172.
- Gupta, V. K. (2004). Emergence of statistical scaling in floods on channel networks from complex runoff dynamics. *Chaos, Solitons & Fractals*, 19(2), 357-365.
- Habibi, H., Nasab, A. R., Norouzi, A., Nazari, B., Seo, D. J., Muttiah, R., & Davis, C. (2016). High Resolution Flash Flood Forecasting for the Dallas-Fort Worth Metroplex. *Journal of Water Management Modeling*.
- Ochoa-Rodriguez, S., Wang, L., Willems, P., Van Assel, J., Gires, A., Ichiba, A., Bruni, G. & ten Veldhuis, M. (2013). Urban Pluvial Flood Modeling: Current

Theory and Practice. Paris:

RainGain.http://www.raingain.eu/sites/default/files/wp3_review_document.pdf.

Maidment, D. R. (2002). *Arc Hydro: GIS for water resources* (Vol. 1). ESRI, Inc.

Mantilla, R., & Gupta, V. K. (2005). A GIS numerical framework to study the process basis of scaling statistics in river networks. *IEEE Geoscience and Remote sensing letters*, 2(4), 404-408.

Mantilla, R., Gupta, V. K., & Mesa, O. J. (2006). Role of coupled flow dynamics and real network structures on Hortonian scaling of peak flows. *Journal of Hydrology*, 322(1), 155-167.

Mandapaka, P. V., Krajewski, W. F., Mantilla, R., & Gupta, V. K. (2009). Dissecting the effect of rainfall variability on the statistical structure of peak flows. *Advances in Water Resources*, 32(10), 1508-1525.

Menabde, M., & Sivapalan, M. (2001). Linking space–time variability of river runoff and rainfall fields: a dynamic approach. *Advances in Water Resources*, 24(9), 1001-1014.

Reggiani, P., Sivapalan, M., Hassanizadeh, S. M., & Gray, W. G. (2001, January). Coupled equations for mass and momentum balance in a stream network: theoretical derivation and computational experiments. In *Proceedings of the Royal Society of London A: Mathematical, Physical and Engineering Sciences* (Vol. 457, No. 2005, pp. 157-189). The Royal Society.

Salvadore, E., Bronders, J., & Batelaan, O. (2015). Hydrological modelling of urbanized catchments: A review and future directions. *Journal of hydrology*, 529, 62-81.

Small, S. J., Jay, L. O., Mantilla, R., Curtu, R., Cunha, L. K., Fonley, M., & Krajewski, W. F. (2013). An asynchronous solver for systems of ODEs linked by a directed tree structure. *Advances in Water Resources*, 53, 23-32.

Chapter 2

ASSESSING THE IMPACT OF VARIATIONS IN HYDROLOGIC, HYDRAULIC AND HYDROMETEOROLOGICAL CONTROLS ON INUNDATION IN URBAN AREAS¹

Behzad Nazari, Dong-Jun Seo, and Ranjan Muttiah

Published in Journal of Water Management Modeling DOI:

10.14796/JWMM.C408

¹ Used with permission from the CHI, the publisher of the Journal of Water Management Modeling, 2017

Abstract

There is a great need for timely prediction of the extent and depth of flooding and related hazards in highly populated urban areas such as the Dallas-Fort Worth Metroplex (DFW). The hydrologic, hydraulic and hydrometeorological processes involved and the large number of factors that control them are complex, inter-related and generally scale-dependent, which makes real-time prediction of flood inundation in urban areas particularly challenging. In addition, a large number of manmade structures such as channels, pipes, culverts, buildings, parking lots, manholes, etc., add complexity. With continuing urbanization and climate change, it is critical that the dynamics of urban flooding be better understood to improve prediction and to mitigate water-related hazards under changing conditions. In this work, we assess how different factors may impact urban flood inundation using the 1D-2D PCSWMM model through a series of controlled simulation experiments. The main study area is the 3.3 km² Forest Park-Berry Catchment in the City of Fort Worth in North Central Texas which has a high density of underground storm drainage. Specifically, we assess the impact of variations in precipitation and impervious cover on simulated inundation maps.

Keywords: Urban Flood Inundation Mapping, PCSWMM, Integrated 1D-2D Modelling.

Introduction

Urbanization and climate change increase risks for flooding in many urban areas. According to the Global Health Observatory data of the World Health Organization (WHO 2015), 54% of the global population live in urban areas as of 2014, an increase of 20% from 1960. O'Brien and Burn (2014) and references therein showed evidences of increasing amplitude and decreasing time-to-peak in flooding events as a result of increasing impervious areas. The annual flood loss data for the US (National Weather Service (NWS) 2015; see Figure 1) indicate that, although flood warning has been improving owing to the increase in both detection and understanding of the causes of heavy-to-extreme precipitation, floods still cause large losses with an annual average in the last 30 years of 89 fatalities and \$8.2 billion in damages (Kunkel et al. 2013 a, 2013b). Sharif et al. (2014) point out that the annual average number of fatalities in Texas is 16.8 with no apparent downward trend although a decline may be seen when normalized by population.

Urban flash flooding, or urban pluvial flooding, is defined as a condition where, as a result of heavy or prolonged rainfall, water escapes from or cannot enter the sewer system or minor urban watercourses, thus remaining on the surface and eventually entering buildings (Gires and ten Veldhuis 2013). The severity of this type of often short-term but high-peak flooding events depends on many different hydrologic, hydraulic and hydrometeorological factors. The

purpose of this work is to assess the different factors that control flood inundation in urban areas using an integrated 1D-2D PCSWMM model through a series of simulation experiments.

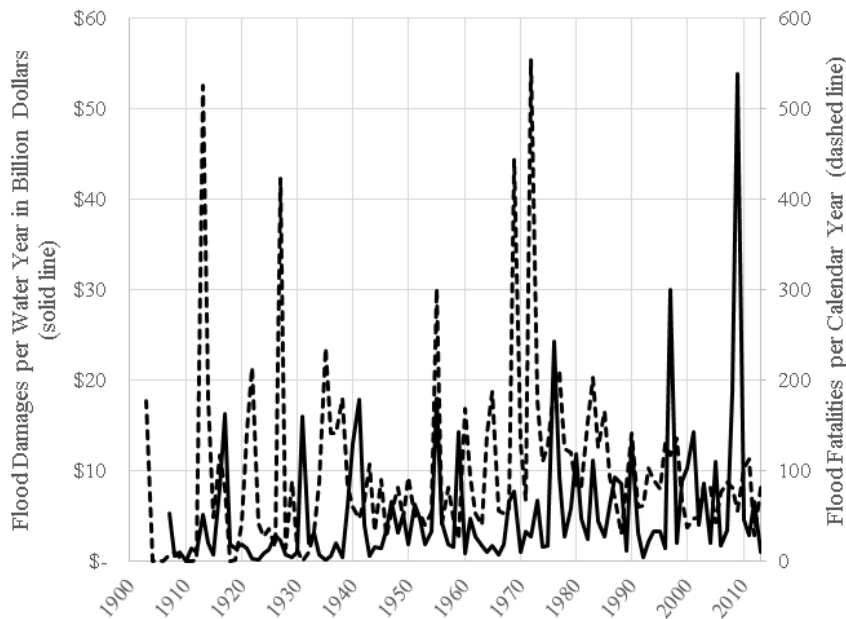


Figure 1 Annual (water year) flood damages and fatalities in United States (NWS 2015).

Study Area

The study area is in the City of Fort Worth in the Dallas-Fort Worth Metroplex (DFW) in North Central Texas. According to Zahran et al. (2008), Central Texas is the most flash flood-prone area in North America and DFW is located within the so-called “Flash Flood Alley”. Fort Worth is the 16th most populous city in the US with a population of 777,992 as of 2012 in an area of 904.4 km² that includes parts of Tarrant, Denton, and Wise Counties. It has had

the highest population growth among large US cities in the period of 2000 to 2013 with a 42.34% increase (Kezar 2014). On the other hand, Walsh et al. (2014) show that the amount of heaviest 1% daily precipitation has increased by 16% in Texas from 1958 to 2012 (Figure 2). Therefore, our study area makes an excellent subject for urban flooding studies under changing conditions.

The study basin is the Forest Park-Berry Catchment (3.28 km², see Figure 3), which drains into the Clear Fork of the Trinity River. The Forest Park-Berry Catchment has a long history of flooding (City of Fort Worth 2015). The origin of the flooding problems in the Forest Park-Berry area goes back to the 20th century when, due to the City's developing business district, the flood plains of the previously natural water ways were reclaimed and replaced by storm drains of the same capacity which later became inadequate as the development escalated. As a result, despite much effort put in over the years, the area remains flood prone. Figure 4 shows the current storm drainage network in the Forest Park-Berry Catchment.

Approach

Table 1 lists the candidate controls considered. In each simulation experiment, the input to the hydrologic and hydraulic models is first specified. Then, the hydrologic-hydraulic simulations are made and the corresponding inundation maps are produced.

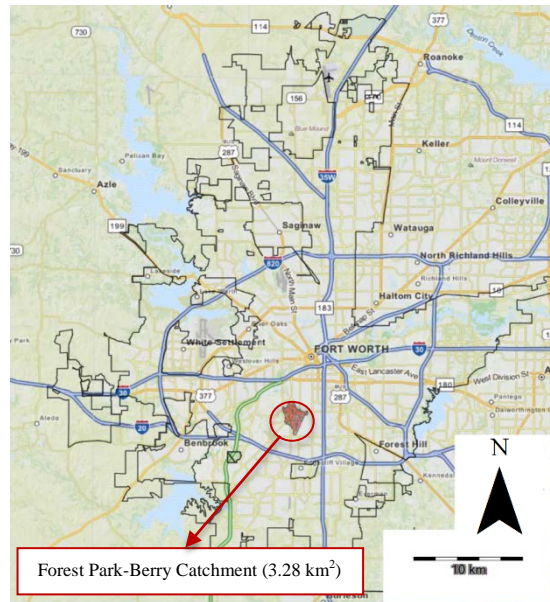


Figure 3 Forest Park-Berry Catchment.

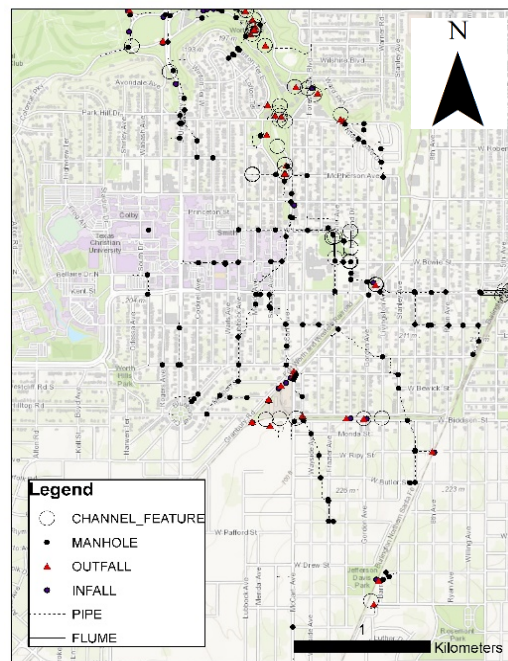


Figure 4 Storm drainage network in the Forest Park-Berry Catchment.

Models Used

Despite recent advances in computing, data science and technology, and remote sensing which led to emergence of new models for urban flooding (Chang et al 2015; Gires et al. 2014), high-resolution urban inundation mapping is still a relatively new area of research. Different approaches exist for modelling urban pluvial flooding (van Dijk et al. 2014). Zhang and Pan (2014) compared some of the most commonly used models in terms of hydrologic and hydraulic modules, model input and output, and applicable flood types. Among them, dual drainage 1D-2D models have been gaining popularity for simulating urban flooding in recent years, due to their computational efficiency compared to full 2D models (Nania et al 2014).

Two types of overland flow occur in urban flooding (Gires and ten Veldhuis 2013):

Direct runoff following abstraction which then enters the storm drainage network (runoff concentration) and

Surcharged runoff from exceeding the storm drainage network's capacity which then joins overland flow (exceedance overland flow). The first is simulated with hydrologic models and the second with hydraulic models. In this study, we used the integrated 1D-2D PCSWMM model which combines semi-distributed hydrologic routing model, 1D hydraulic model for the storm drainage network, and 2D overland flow model. PCSWMM uses the Storm Water Management

Model Version 5 (Rossman 2010) engine for modelling junctions, or nodes, and conduits, or links, of various cross sections and connects them to a 2D overland flow model for 1D-2D dual drainage modelling. PCSWMM also has the capability to ingest radar-based quantitative precipitation estimates (QPE). The choice for the coupled hydrologic-hydraulic modelling approach is based on the need to account for both types of flow in the study basins.

To set up the integrated 1D-2D PCSWMM model, we followed the steps in Figure 7. The subcatchments were delineated by inputting the digital elevation model (DEM) into the Arc Hydro GIS tool (Maidment 2002), and locating outlets and identifying the contributing areas (see Figure 6).

Precipitation is the main forcing for flooding. Spatiotemporal variability of precipitation and accuracy and resolution of QPE are among the most influential factors in inundation mapping particularly for small and highly impervious urban catchments. Gires and ten Veldhuis (2013) summarize the results of a number of studies to conclude that for detailed urban hydraulic modelling, rainfall forcing should have a spatiotemporal resolution higher than 100 to 500 m and 1 to 5 min.

In this study, we used the 1 min-500 m resolution QPE from the Collaborative Adaptive Sensing of the Atmosphere (CASA) X-band weather radar located at the University of Texas at Arlington (UTA). The radar XUTA is one of 5 X-band radars currently in operation in the DFW Demonstration Network (Habibi et al. 2015).

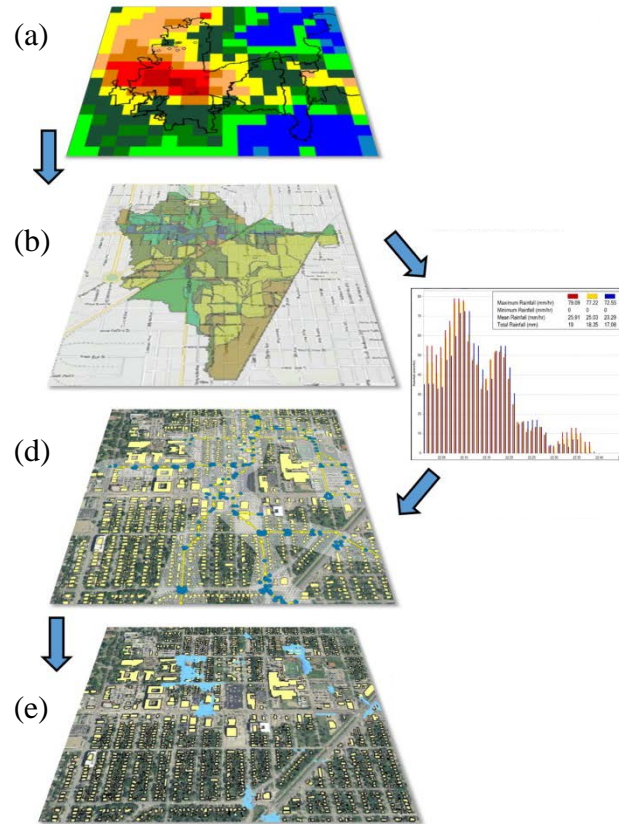


Figure 5 Steps used in hydrologic-hydraulic modelling: a. Rada QPE of the event is imported to PCSWMM.

b. PCSWMM produces hyetographs for each subcatchment.

c. Hyetographs are input into the hydrologic model in PCSWMM.

d. Hydraulic model in PCSWMM simulates flow depth and velocity.

e. The depth, duration, and extent of inundation are mapped in PCSWMM.

A severe flash flooding occurred in the area on June 24, 2014. During this event, more than 70 mm of rain fell in just a few hours (see Figures 7) resulting in

severe inundation in some areas of the city which resulted in more than 40 responses from the Fort Worth emergency services (FloodList 2014).

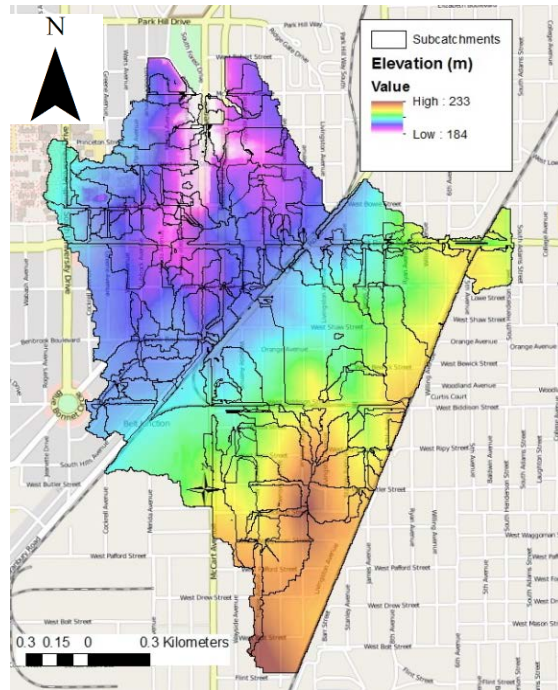


Figure 6 Elevation map and subcatchment delineation.

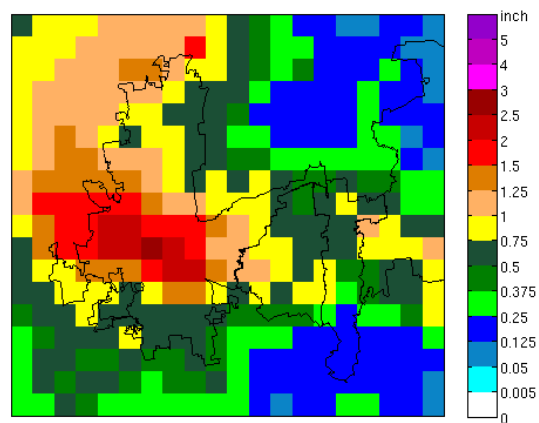


Figure 7 NEXRAD QPE for the June 24, 2014, event (1 inch = 25.4 millimetres).

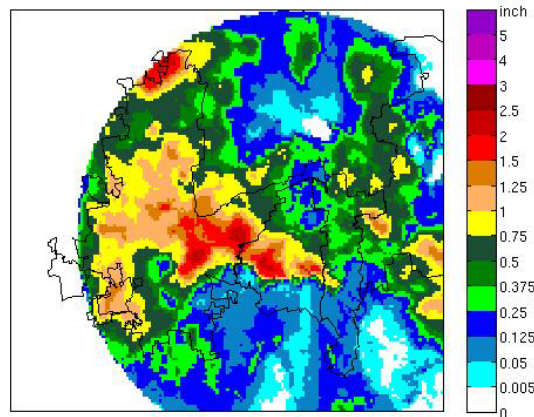


Figure 8 The XUTA-observed rainfall map for June 24, 2014.

Using PCSWMM’s Radar Acquisition and Processing (RAP) tool, the hyetographs were produced for all subcatchments from the CASA QPE for June 24, 2014. The reader is referred to Habibi et al. (2015) for the CASA QPE generation process. Figure 8 shows the 24-hr rainfall map as estimated from XUTA. The black lines in the figure delineate, from left to right, the Cities of Fort Worth, Arlington, Grand Prairie, and parts of Dallas. The hyetographs derived above represent the baseline input in the reference scenario. The input is then modified by $\pm 15\%$ for sensitivity analysis. Three example hyetographs derived from the CASA QPE are shown in Figure 9.

To model the mean areal impervious fraction for each subcatchment, an impervious cover map was used consisting of a building footprint layer, parking lots and streets (Figure 10).

For 2D overland flow modeling, the building footprint layer was added representing obstructions. Other model parameters were specified, wherever

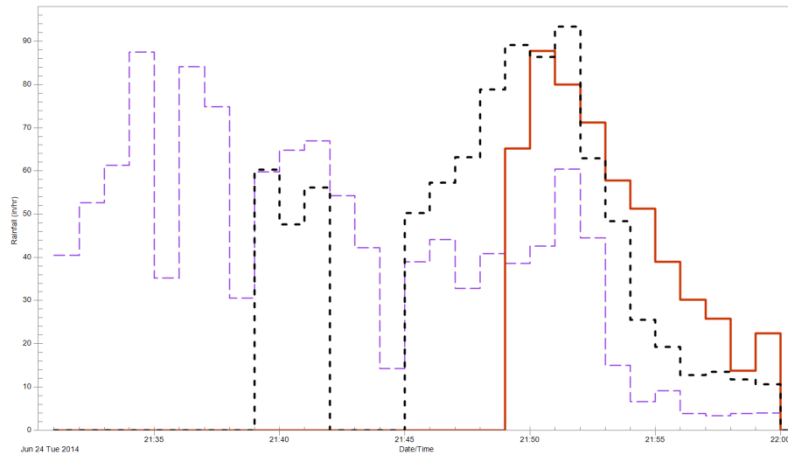


Figure 9 Three examples of derived hyetographs for the June 24, 2014, event. The solid red line is for a downstream subcatchment. The dashed black line is for a subcatchment in the centre of the study area and the dashed blue line is for a subcatchment in upstream part of the study area.

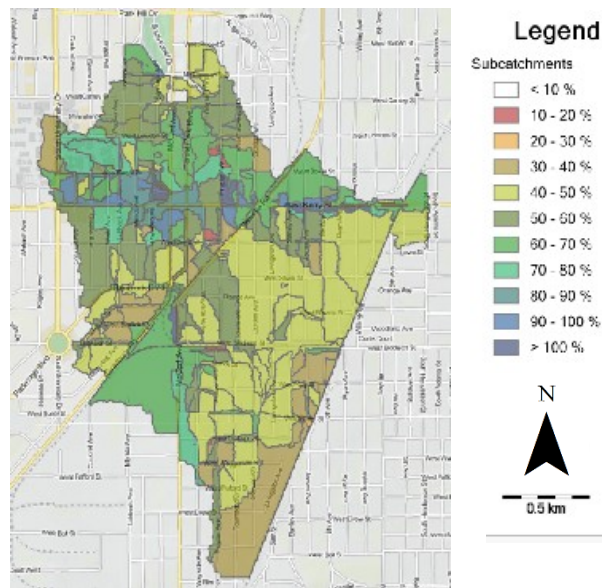


Figure 10 Mean areal impervious fraction for each subcatchment.

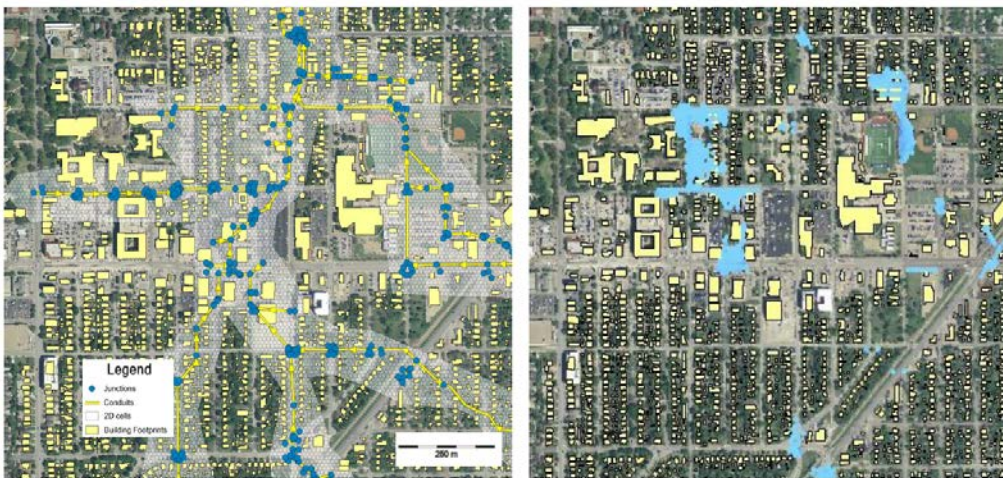
possible, based on the information available from the City of Fort Worth as explained below. The elevations of most inlets and pipes were available. Missing elevations were handled differently case by case depending on the location. If the elevation of an inlet node was not available, the overlain ground surface elevation from the DEM was used. If the underground elevation was missing, a distance-based interpolation technique was used to estimate the elevation from the known neighbouring elevations. Since PCSWMM doesn't allow variable manning roughness values in a 2D mesh boundary, we used a constant manning roughness of 0.015 for all 2D cells. The flow length parameter for each subcatchment was estimated based on the flow accumulation map. For runoff generation, the SCS Curve Number (CN) method was used (Chow et al. 1988). The spatially-varying CNs were initially extracted from the hydrologic models provided by the City of Fort Worth. However, a sensitivity analysis showed little difference in inundation maps due to spatially-varying CN vs. spatially-uniform CN for heavy-to-extreme rainfall cases. Therefore, the average CN of 80 was used in the simulations. Surface storage was neglected, given that they will be quickly filled in very heavy-to-extreme rainfall events modelled here. Table 2 summarizes the model parameters.

In the initial stages of the simulation study, the impact of resolution of subcatchment delineation on runoff was analysed using a 1D model. A large impact was seen. The effect of spatial resolution of subcatchment delineation on

hydrologic simulation has been extensively studied. The state of the art review of urban hydrological modelling in Salvatore et al. (2015) concludes that high spatial resolution is required for resolving the heterogeneity and fast dynamics of urban hydrological processes.

Table 2 Model parameters.

Parameter	Description
Infiltration method	SCS Curve Number
Flow routing method	Dynamic wave (Rossman 2010)
Manning roughness of the pipes	0.013
Manning roughness of 2D mesh	0.05
Manning roughness of impervious surfaces	0.012
Manning roughness of pervious surfaces	0.015
2D domain area	$1.67 \times 10^7 \text{ ft}^2$ ($\sim 1.55 \times 10^6 \text{ m}^2$)
2D mesh type	Hexagonal
2D mesh resolution	35 ft ($\sim 10.67 \text{ m}$)
Number of cells	14268



.Figure 11 Part of the 1D-2D integrated model domain and an example of simulated inundation.

Ghosh and Hellweger (2011), who investigated the scale effect using SWMM, concluded that, coarser subcatchment delineations under-simulate the

peak flows in large storms. Note that the SWMM engine uses semi-distributed modelling and, by construction, runoff from each subcatchment has only a single point of entry into either a junction or a downstream subcatchment. If the subcatchment is so large that it contains multiple inlets, they are ignored except the one identified as the outlet. If, on the other hand, the subcatchment is excessively small, the connectivity of the subcatchments may not be physically realistic due to possible errors in the DEM and storm drain data. Note also that subcatchment delineation is impacted also by the resolution of the DEM used. Lastly, it is very difficult in SWMM-based modelling to break up channels into multiple sections because short conduits can potentially cause numerical instabilities. Therefore, the approach taken in this study was to produce the finest subcatchments that may be derived using the available 5m resolution DEM and the inlet locations. The delineated subcatchments were then visually inspected to identify any clearly erroneous or suspect results. It was found that the erroneous delineations were due to the high resolution of the DEM which resulted in unrealistically small subcatchments at a few locations.

Simulation Experiments, Results and Discussion

The main focus of the study was to assess the impact of variations in precipitation magnitude and percentage of the impervious cover. They are directly associated with climate change and urbanization and hence are of particular interest. We used the June 24, 2014, flash flooding event and the imperviousness

percentage map in Figure 10 as references, and perturbed the precipitation magnitude and imperviousness as summarized in Table 3 to produce a total of nine different simulations. Wobus et al. (2015) used 3 different climate models to project changes in heavy-to-extreme precipitation. While consistent patterns were not found in the model projections of heavy-to-extreme precipitation, they report approximately a 15% change in precipitation amount for the study area. This figure is also comparable to the 16% change in observed precipitation for large amounts for our study area (Figure 2). As such, we chose 15% for the sensitivity analysis.

Table 3 List of model simulations.

		Impervious Cover		
		-15%	Existing	+15%
Precipitation	-15%	Case 1	Case 2	Case 3
	Base	Case 4	Case 5	Case 6
	+15%	Case 7	Case 8	Case 9

The impact of the changes in precipitation amount and imperviousness was assessed by comparing the extent and depth of inundation, and flow velocity. Figure 12 shows the extent of inundation, as measured by the number of wet cells at each time step, for the 9 different cases. For all cases, the maximum inundation extent increases sharply in the first 20 min, less so from 20 to 0 min and very slowly after 30 min. It is interesting to note that the maximum difference among the 9 cases occurs at about 12 min when the inundation extent is fast increasing.

The difference is about 10% of the total inundation extent. It suggests that changes in precipitation amount and imperviousness may significantly alter the wetting dynamics even though the final inundation extent may be similar (see the results at 60 min).

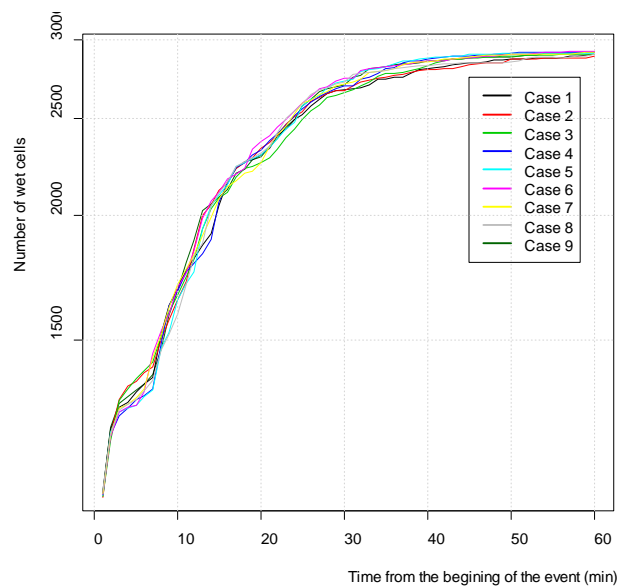


Figure 12 Simulated inundation extent as a function of time elapsed.

The differences among the 9 cases are more discernible in location-specific analyses. Figure 13 shows the maximum inundation depth for the 9 cases. Comparison of Cases 1 through 9 shows that, the modelled inundation is more sensitive to a 15% change in precipitation than that in imperviousness.

Figure 14 shows the relative magnitude of standard deviation of maximum inundation depths among the 9 cases. It is seen that, although the variation of inundation is generally higher in the downstream parts of the study area, there exist some interior locations with very large variations. Since they are all located

along the storm drainage network depicted by red lines in the figure, one may hypothesize that the large variations are due to the limited capacity of the pipes. For example, when a certain pipe is not at full capacity in some cases but becomes surcharged in other cases, one may expect large variations in inundation depth at its inlet cell. In fact, using PCSWMM's design tool, it was found that almost 40% of the pipes become surcharged for the June 24, 2014, extreme event.

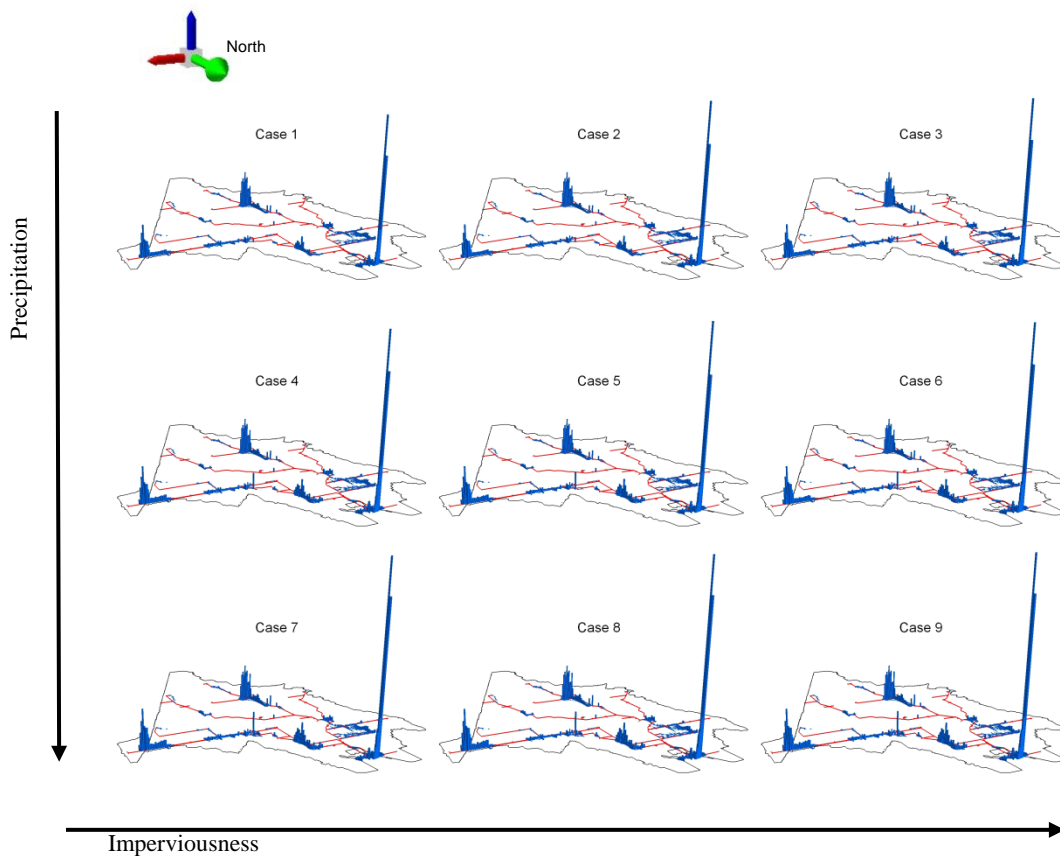


Figure 13 Spatial comparison of maximum inundation depth. The columns have been multiplied by a factor of 300, for better discernibility.

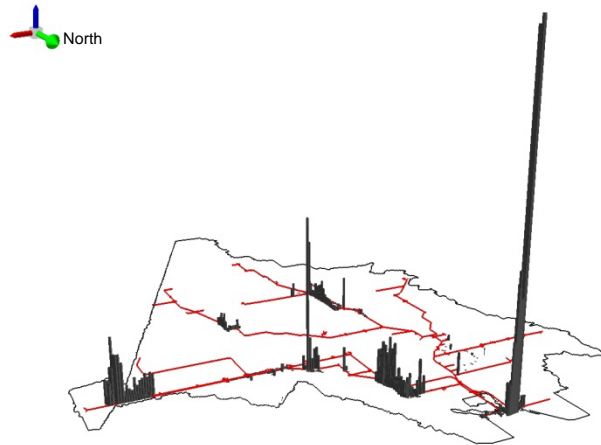


Figure 14 Relative magnitude of standard deviation of maximum inundation depth. The columns have been multiplied by a factor of 3000, for better discernibility.

Figures 15 and 16 show the time series of the location-specific depth and velocity, respectively, for the 2D cell encircled in red in the inset of Figure 15. Figures 15 and 16 show an increasing trend in peak inundation depth and velocity, respectively, with increasing impervious cover and increasing precipitation. The maximum difference in peak depth is about 17% which occurs between Case 1 and Case 9. The figures also show that increased rainfall increases peak discharge more so than increased impervious cover. In addition, the effect of imperviousness decreases when precipitation is more intense.

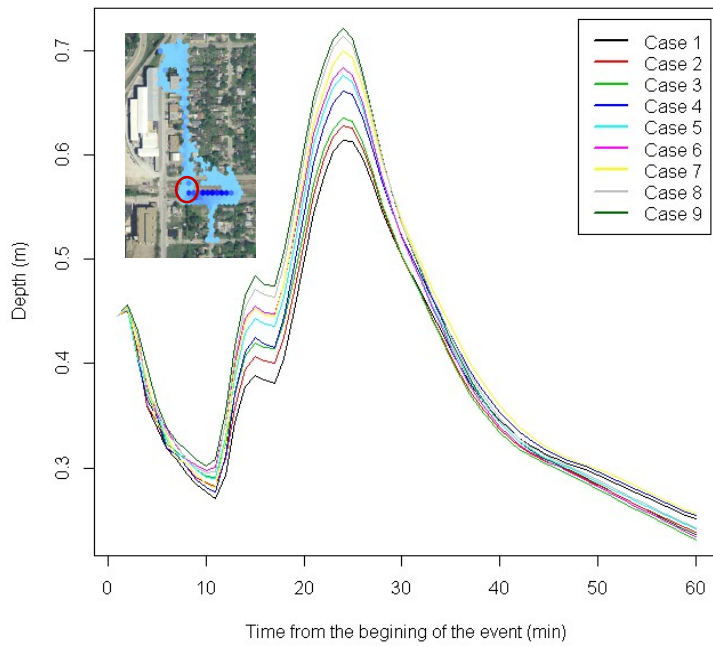


Figure 15 Location-specific comparison of simulated depth time series.

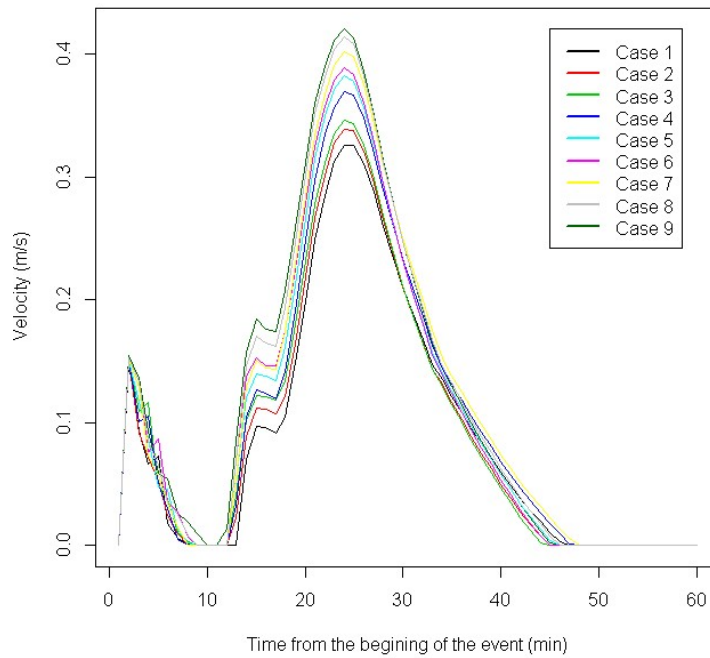


Figure 16 Location specific comparison of simulated velocity time series.

The patterns in the velocity time series in Figure 16 are generally similar to those of peak inundation depth. Note, however, that, at about 10 min into the event, the velocity is reduced to near zero though the depth is non-zero, an indication that ponding may be occurring due possibly to an overwhelmed drainage system before flow resumes. Similar analysis may be performed for different locations of interest. One may also delineate the areas of increased risks by identifying all locations where the maximum depth or velocity exceeds some critical threshold.

While useful, the type of local analyses shown above is not very practical when many locations are involved. Therefore, there is a need for more general, model domain-wide comparisons and characterization of the simulation results. To that end, we derived the empirical cumulative distribution functions (ECDF) of the simulated inundation duration, depth, and velocity (see Figures 17 to 19). The figures consider only the “wet” cells; all cells that remained dry during the event were excluded. Also, because we are interested primarily in higher depths and velocities, only the upper tails are shown in Figures 18 and 19. Figure 17 indicates that, e.g., given that some location gets inundated at all during the 60-min event, there is about 58% chance the inundation lasts for 50 min or more. Similarly, the chances of inundation at the location lasting more than 20, 30, and 40 minutes are approximately 97%, 92%, and 80%, respectively.

The figure indicates that the variations in the inundation duration among the 9 cases can be as large as 7 min (at the exceedance probability of 0.95). It can also be seen in Figure 17 that, the exceedance probability of occurrence of the same inundation duration can vary up to 7%, which occurs at the 46th min, among the 9 cases.

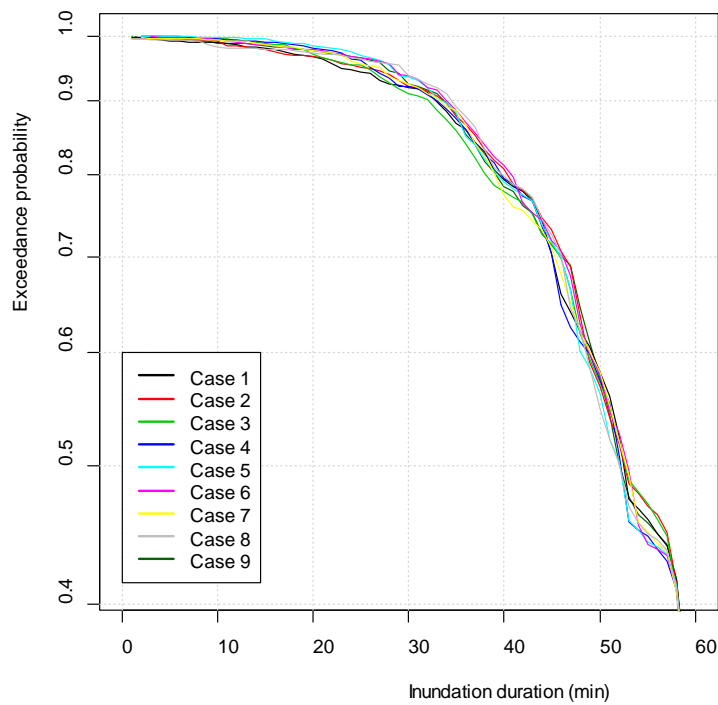


Figure 17 ECDFs of simulated inundation duration.

Figure 18 shows that, e.g., the probability of maximum inundation depth exceeding 20 cm at some location that gets inundated at all during the 60-min event is about 0.01. This probability increases by approximately 0.005 from Case 1 to Case 9. Similarly, the probability of maximum inundation depth exceeding 40

cm varies from 0.004 to 0.007 for Cases 1 through 9. Note that these variations in exceedance probabilities are large, with potentially very significant implications in hydrologic design in urban areas.

Figure 19 is completely analogous to Figure 18 but that it is for maximum flow velocity. Figure 19 indicates that the probability of maximum velocity exceeding 0.8 m/s at some location that gets inundated at all during the 60-min event increases from 0.002 in Case 1 to 0.008 in Case 9. For velocities exceeding 0.5 m/s, the probabilities vary from 0.016 in Case 1 to 0.027 in Case 9.

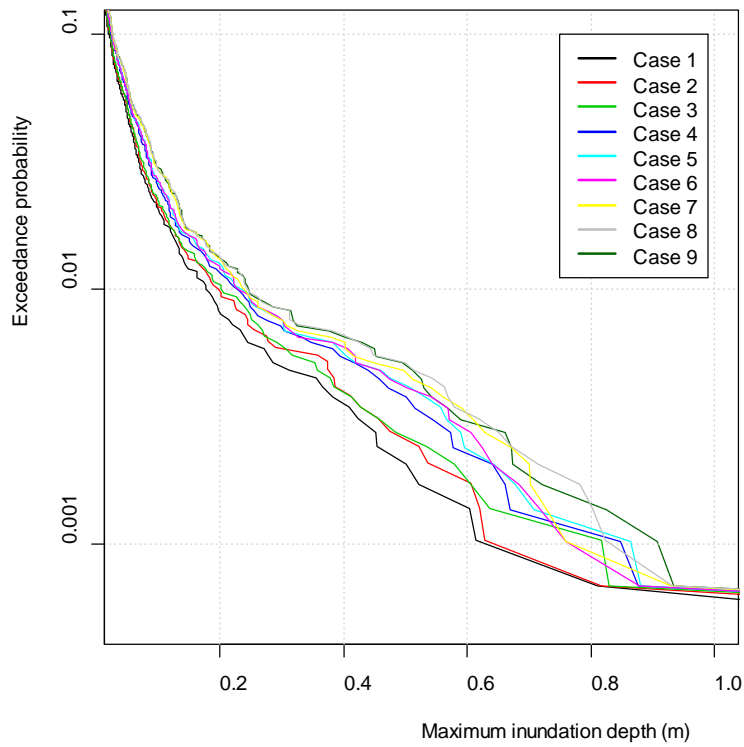


Figure 18 ECDFs of simulated maximum inundation depth.

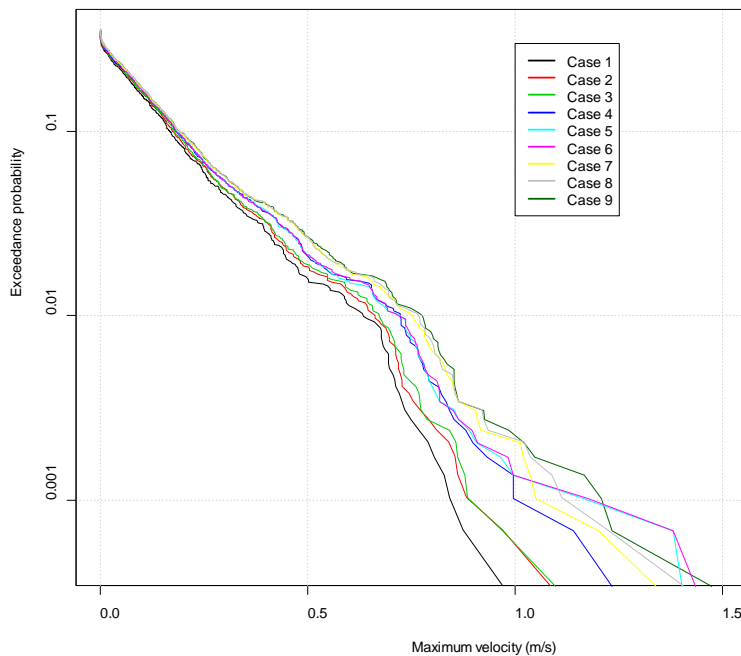


Figure 19 ECDF of simulated maximum flow velocities.

Verification of the model simulation results was carried out qualitatively by comparing with the locations of historical high water reports. The simulated inundation extent for the June 24, 2014, rainfall event used for our simulation experiments, matched reasonably well with the high water reports. Of the seven reports in our study area, four matched with the PCSWMM-modelled inundation areas, two were approximately a block away from the nearest simulated wet cell, and one was missed by a large margin. Due to lack of permission to publish the above reports, in this paper we present the high water reports from a larger event of October 21, 2009, which produced 5.5 to 6 inches of rainfall in a 24-hr period

(see Fig 20). Though the model simulation is not for the same event, one may expect a simulated inundation extent similar to the June 24, 2014, case owing to the fact that this is very small catchment (3.3 km²) and hence spatial variability of rainfall is not very important. Among the six available high-water records for this heavier rainfall event, four are within the modelled inundation extent. The model simulation, however, missed two high-water locations in the eastern part of the catchment. This is likely due to the fact that the 2009 event was more intense and hence flooding was probably more severe than indicated by the June 24th simulation. As illustrated above, lack of observations poses a large challenge in verification of inundation mapping which requires spatially dense and frequently sampled ground truths. We note here that we are deploying real-time water level sensors in the study area and elsewhere in the DFW area and will be gathering crowdsourced observations for near real-time and post-event verification (Hanna 2016).

Conclusions and future research recommendations

This work assesses the impact of variations in hydrologic, hydraulic and hydrometeorological factors that control urban inundation. The study area is a flooding-prone urban catchment in the City of Fort Worth in North Central Texas. This study was focused on assessment of changes in precipitation magnitude and imperviousness.

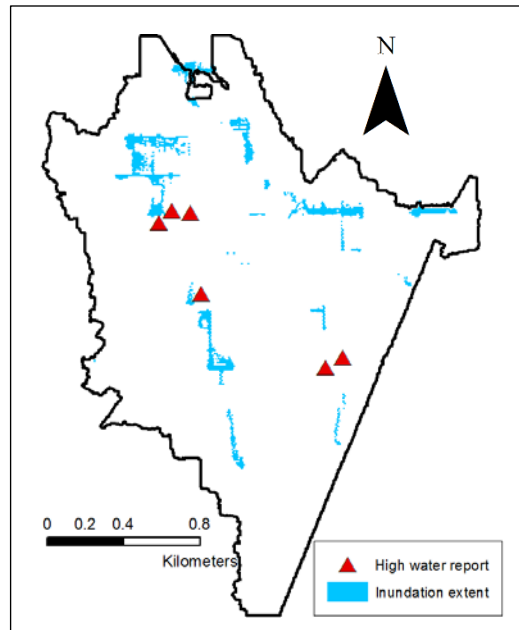


Figure 20 Comparison of June 24, 2014, model simulation with historical high-water reports.

Disclaimer: Flooding incidence data provided by the City of Fort Worth for informational purposes only; The City of Fort Worth assumes no responsibilities for the accuracy of the data.

The results of the nine simulation experiments presented in this work highlight the large impact of changes in precipitation and impervious cover on local and catchment-scale urban flooding. They suggest that, with climate change and continuing urbanization, many areas, and that, for accurate mapping of inundation in urban areas, high-resolution rainfall forcing and physiographic information is essential.

Once demonstrated operation-worthy, we plan to run the integrated 1D-2D model in real time for selected urban catchments in the DFW area as a part of the flash flood warning system under implementation for the area (Habibi et al.

2015). The sensitivity analyses undertaken in this work are part of the effort to assess the feasibility of real-time operation of a 1D-2D model, identify potential alternatives for reduced complexity and computational requirements, increase lead time by the use of rainfall nowcasts (Ruzanski et al 2011; Ruzanski and Chandrasekar 2012) and develop impact-based warning products (Calianno et al 2013).

Due to sparsity of observations, verification of high-resolution prediction is a large challenge. While the model results are generally in agreement with historical reports of inundation (Nazari et al. 2014), they are yet to be verified dynamically. For that, we will be using observations from a network of recently deployed real-time water level sensors and the newly developed crowdsourcing app, iSeeFlood. Higher resolution modelling does not always result in higher accuracy while potentially imparting a false sense of confidence in high resolution output (Dottori et al 2013). To provide a measure of uncertainty associated with inundation mapping, ensemble approaches (Aronica et al. 2012, Gires et al. 2014) or other probabilistic methods (Fu et al. 2011) are necessary. To that end, we plan to explore ensemble inundation mapping as a part of the ongoing effort on integrative sensing and prediction of urban water for sustainable cities (Seo et al. 2015).

Acknowledgements

This material is based upon work supported by the National Science Foundation under Grant No. IIP-1237767 (Brenda Philips, University of Massachusetts Amherst, Principal Investigator (PI)) and CyberSEES-1442735 (Dong-Jun Seo, University of Texas at Arlington, PI), and by the City of Fort Worth. These supports are gratefully acknowledged.

References

- Aronica, G. T., F. Franza, P. D. Bates, and J. C. Neal. 2012. "Probabilistic Evaluation of Flood Hazard in Urban Areas Using Monte Carlo Simulation." *Hydrological Processes* 26 (26): 3962–72.
- Calianno, Martin, Isabelle Ruin, and Jonathan J. Gourley. 2013. "Supplementing Flash Flood Reports with Impact Classifications." *Journal of Hydrology* 477: 1–16.
- Chang, Tsang Jung, Chia Ho Wang, and Albert S. Chen. 2015. "A Novel Approach to Model Dynamic Flow Interactions between Storm Sewer System and Overland Surface for Different Land Covers in Urban Areas." *Journal of Hydrology* 524: 662–79.
- Chow, Ven T., David R. Maidment, and Larry W. Mays. 1988. *Applied hydrology*. 1988.
- City of Fort Worth. 2016. "Forest Park - Berry - Central Arlington Heights".

- Accessed July 6, 2016. <http://fortworthtexas.gov/projects/forestpark/>
- Dottori, F., G. Di Baldassarre, and E. Todini. 2013. "Detailed Data Is Welcome, but with a Pinch of Salt: Accuracy, Precision, and Uncertainty in Flood Inundation Modeling." *Water Resources Research* 49 (9): 6079–85.
- FloodList, June 26, 2014. Accessed April 20, 2015.
<http://floodlist.com/america/usa/storms-flash-floods-texas-june-2014>.
- Ghosh, Indrani, and Ferdi L. Hellweger. 2011. "Effects of spatial resolution in urban hydrologic simulations." *Journal of Hydrologic Engineering* 17(1): 129-137.
- Gires, Abdella Ichiba, and Marie-Claire ten Veldhuis. 2013. "Urban Pluvial Flood Modelling: Current Theory and Practice."
- Gires, Auguste, Agathe Giangola-Murzyn, Jean-Baptiste Abbes, Ioulia Tchiguirinskaia, Daniel Schertzer, and Shaun Lovejoy. 2014. "Impacts of Small Scale Rainfall Variability in Urban Areas: A Case Study with 1D and 1D/2D Hydrological Models in a Multifractal Framework." *Urban Water Journal* 12 (8): 607–17.
- Habibi, Hamideh, Arezoo Rafieei Nasab, Amir Norouzi, Behzad Nazari, Dong-Jun Seo, Ranjan Muttiah, and Clair Davis. 2016. "High Resolution Flash Flood Forecasting for the Dallas-Fort Worth Metroplex." *Journal of Water Management Modeling*.
- Hanna, Bill. 2016. "A flash flood in Fort Worth? UTA researcher has an app for

- that”, Star-Telegram, May 26, <http://www.star-telegram.com/news/local/article80127467.html#storylink=cpy>
- Kezar ,Korri. 2014. “Fort Worth has highest population growth in U.S.; Dallas comes in 24th,” Dallas Business Journal, December 4. <http://www.bizjournals.com/dallas/news/2014/12/04/fort-worth-has-highest-population-growth-in-u-s.html>
- Kunkel, Kenneth E., Thomas R. Karl, David R. Easterling, Kelly Redmond, John Young, Xungang Yin, and Paula Hennon. 2013. “Probable Maximum Precipitation and Climate Change.” *Geophysical Research Letters* 40 (7): 1402–8.
- Kunkel, Kenneth E., Thomas R. Karl, Harold Brooks, James Kossin, Jay H. Lawrimore, Derek Arndt, Lance Bosart, et al. 2013. “Monitoring and Understanding Trends in Extreme Storms: State of Knowledge.” *Bulletin of the American Meteorological Society* 94 (4): 499–514.
- Maidment, David R. 2002. *Arc Hydro: GIS for water resources*. Vol. 1. ESRI, Inc.
- Nanía, Leonardo S, Arturo S Leon, and Marcelo H García. 2014. “Hydrologic-Hydraulic Model for Simulating Dual Drainage and Flooding in Urban Areas : Application to a Catchment in the Metropolitan Area of Chicago.” *Journal of Hydrologic Engineering* 20 (2005): 1–13.
- Nazari, Behzad, Arezoo Rafieeiniasab, Dong- Jun Seo, Sunghee Kim, Ranjan

- Muttiah , and Clair Davis. "Hydraulic modeling for inundation mapping using radar rainfall data-A case study for the City of Fort Worth." *Weather Radar and Hydrology* 5 (2014): 10.
- NWS (National Weather Service). 2015. "Hydrologic Information Center - Flood Loss Data." Accessed April 1, 2015. <http://www.nws.noaa.gov/hic/>.
- O'Brien, Nicole L., and Donald H. Burn. 2014. "A Nonstationary Index-Flood Technique for Estimating Extreme Quantiles for Annual Maximum Streamflow." *Journal of Hydrology* 519: 2040–48.
- Rossman, L. A. 2010. *Storm water management model user's manual, version 5.0*. National Risk Management Research Laboratory, Office of Research and Development, US Environmental Protection Agency.
- Ruzanski, Evan, V. Chandrasekar, and Yanting Wang. 2011. "The CASA Nowcasting System." *Journal of Atmospheric and Oceanic Technology* 28 (5): 640–55.
- Ruzanski, Evan, and V. Chandrasekar. 2012. "An investigation of the short-term predictability of precipitation using high-resolution composite radar observations". *Journal of Applied Meteorology and Climatology* 51 (5): 912-925.
- Salvadore, Elga, Jan Bronders, and Okke Batelaan. 2015. "Hydrological modelling of urbanized catchments: A review and future directions." *Journal of Hydrology* 529: 62-81.

- Seo, Dong Jun, Branko Kerkez, Michael Zink, Nick Fang, Jean Gao, and Xinbao Yu. 2015. "iSPUW: A Vision for Integrated Sensing and Prediction of Urban Water for Sustainable Cities." *In Lecture Notes in Computer Science (Including Subseries Lecture Notes in Artificial Intelligence and Lecture Notes in Bioinformatics)*, 8964:68–78. doi:10.1007/978-3-319-25138-7_7.
- Sharif, Hatim O., Terrance L. Jackson, Md Moazzem Hossain, and David Zane. 2014. "Analysis of flood fatalities in Texas." *Natural Hazards Review* 16(1).
- van Dijk, E., J. Van Der Meulen, J. Kluck, and J. H M Straatman. 2014. "Comparing Modelling Techniques for Analysing Urban Pluvial Flooding." *Water Science and Technology* 69 (2): 305–11.
- Walsh, J, D Wuebbles, and K Hayhoe. 2014. "Chapter 2: *Our Changing Climate.*" *Climate Change Impacts in the United States: The Third National Climate Assessment.*, no. October: 19–67.
- WHO (World Health Organization). 2015. "Global Health Observatory" data. Accessed July 6.
http://www.who.int/gho/urban_health/situation_trends/urban_population_growth_text/en/
- Wobus, Cameron, Lara Reynolds, Russell Jones, Radley Horton, Joel Smith, J. Stephen Fries, Michael Tryby, Tanya Spero, and Chris Nolte. 2015. "Using Dynamically Downscaled Climate Model Outputs to Inform Projections of

Extreme Precipitation Events." Paper presented at *American Geophysical Union (AGU) Fall Meeting, San Francisco, CA, United States, 15-19 Dec. 2015*. NASA Technical Reports Server (NTRS),
<http://ntrs.nasa.gov/search.jsp?R=20160001409>

- Wright, Daniel B., James A. Smith, Gabriele Villarini, and Mary Lynn Baeck. 2013. "Estimating the Frequency of Extreme Rainfall Using Weather Radar and Stochastic Storm Transposition." *Journal of Hydrology* 488: 150–65.
- Zahran, Sammy, Samuel D. Brody, Walter Gillis Peacock, Arnold Vedlitz, and Himanshu Grover. 2008. "Social vulnerability and the natural and built environment: a model of flood casualties in Texas." *Disasters* 32 (4) : 537-560.
- Zhang, Shanghong, and Baozhu Pan. 2014. "An Urban Storm-Inundation Simulation Method Based on GIS.

Chapter 3

QUASI-ANALYTICAL SOLUTION FOR 1-DIMENSIONAL DIFFUSION WAVE EQUATION WITH LATERAL INFLOW USING CONTINUOUS-TIME DISCRETE-SPACE METHODS

Behzad Nazari and Dong-Jun Seo

Abstract

The diffusion wave equation, a simplified form of the Saint-Venant equations, is used extensively in flood routing. To solve the equation, numerous methods have been developed over the years most of which are numerical. Because most numerical methods must meet the Courant–Friedrichs–Lewy (CFL) condition and that the CFL condition is only the necessary condition, their application requires case-specific modeling and analysis to ensure convergence. For many practical routing applications, however, simpler but accurate methods are highly desirable. In this work, we present two new methods for solving the 1-dimensional linear diffusion wave equation for finite domain quasi-analytically. Referred to as the Continuous Time Discrete Space (CTDS) methods, they yield explicit symbolic expressions for time-continuous solutions at discrete points in space. As such, the methods provide a powerful tool for very easily obtaining accurate diffusive wave solutions in lieu of numerical integration when predictions are desired only at specific locations along the channel. The proposed methods are easy to implement and may be used in a variety of routing applications where accurate explicit symbolic solutions are desired for linear advection-diffusion at specific locations.

1. Introduction

The Saint Venant equations, also known as the dynamic wave model, are the governing equations for conservation of mass and momentum for unsteady open channel flow (*Chanson, 2004*). Solving these equations requires large amounts of data to prescribe the fixed boundary conditions (BC) of channel geometry along the reach and elaborate numerical integration to ensure accuracy and convergence (*Szymkiewicz, 2010*). Over the years, simplified forms of the equations have been sought that can be used more easily in practical applications such as operational flood forecasting (*Szymkiewicz, 2010*). Among the most frequently used

simplifications is the diffusive wave approximation which neglects the inertial terms. Though a new more appropriate name “noninertia wave” has been proposed (*Yen and Tsai 2001*), the term “diffusive wave” is still widely used which we adopt here to avoid confusion. The diffusive wave model is attractive for a number of reasons (*Cappelaere, 1997*). It combines the system of equations into a single equation of a single state variable of flow or depth. The model describes translation and attenuation of flood waves with a single advection-diffusion equation for which many different solution techniques are available from multiple fields such as heat transfer (*Ozisik, 1994*), environmental engineering (*Freijer et al., 1998*) and biology (*Mueller et al., 2005*). The model accounts for pressure gradients which have significant effects on propagation of flood waves in mild-sloped channels where the kinematic wave approximation breaks down. Lastly, the model provides a physically-based solution with minimum data requirements. Diffusive wave approximation has been shown to yield satisfactory results in a wide range of applications including operational canal control, real-time flood forecasting, overland flow modeling, modeling of stormwater runoff on impervious surfaces, and flood routing with lateral inflow and backwater effects. The spatial scale of application ranges from small catchments to the Amazon River Basin, and the types of catchments of application include urban, lowland, mountainous, and tropical catchments (*Cheviron and Moussa, 2016*). The recently launched National Water Model (*Gochis et al. 2014*) also uses diffusive wave model to route surface runoff to channels.

Neglecting the inertial terms, one may reduce the Saint Venant equations (*Chanson, 2004*) to:

$$\frac{\partial}{\partial t} Q(x, t) = D \frac{\partial^2}{\partial x^2} Q(x, t) - C \frac{\partial}{\partial x} Q(x, t) + Cq \quad (1)$$

where $Q(x,t)$ is the discharge at location x and time t (cms), x is the distance along the longitudinal direction of flow (m), t is the time (s), q is the constant lateral inflow (cms/m), C is the celerity (m/s) and D is the diffusivity in (m^2/s). C is a measure of the speed of the flood wave and D is a measure of attenuation in the flood wave magnitude as it travels downstream. In general, C and D are not constant but functions of flow, channel geometry, roughness, and slope. *Bajracharya and Barry (1997)* argue that C and D affect flood predictions only marginally. The resulting diffusive wave equation of Eq. (1) with constant C and D is sometimes referred to as the Hayami equation (*Litraco and Fromion, 2009*). In this work, we assume that C and D are constant for derivation of quasi-analytical solutions. In the Discussion Section, we describe how the above assumption may be relaxed in practical applications. The partial differential equation (PDE) in Eq.(1) admits the initial condition (IC) and upstream BC of the following form:

$$\begin{aligned} Q(x, 0) &= qx \\ Q(0, t) &= Q_0(t) \end{aligned} \tag{2}$$

The downstream BC may take on one of the following forms:

$$\frac{\partial Q}{\partial x} \Big|_{x \rightarrow \infty} = q \tag{3a}$$

$$\frac{\partial Q}{\partial x} \Big|_{x \rightarrow L} = q \tag{3b}$$

$$Q(L, t) = Q_L(t) \tag{3c}$$

Eqs. (3a) and (3b) are the Neumann BCs for a semi-infinite channel of $0 < x < \infty$ and for a finite channel of length L (m), respectively. The Dirichlet BC of Eq.(3c) is applicable if the downstream flow is known as a function of time. The choice for the downstream BC has been one of the least well-established aspects of diffusive wave modeling because its prescription has

a limited theoretical basis as explained below. Combining the equations for conservation of mass and momentum into a single diffusive equation requires an additional differentiation step. The resulting higher-order spatial derivative requires an additional BC. Because an integration constant is lost during this additional differentiation, it is not possible to prescribe the BCs uniquely. For this reason, in practice the choice for the most appropriate BC is made problem-specifically based on the intended application.

The diffusive wave equation for finite domains with the Dirichlet BC of Eq. (3c), may be solved via separation of variables (SoV) (*Fan and Li, 2006*), analytical methods (*Moussa, 1996; Moramarco et al., 1999; Chang and Yeh, 2014; Tingsanchali and Manandhar, 1985*) or semi-analytical methods (*Kazezyilmaz-Alhan, 2012, Jia et al., 2013*). The majority of such solution techniques cannot, however, handle the downstream Neumann BC of Eq. (3b). Also, to the best of the authors' knowledge, all existing closed-form solutions for either the Neumann BC of Eq. (3b) or the Dirichlet BC of Eq. (3c) on a finite domain can only be expressed as infinite series (*Fan and Li, 2006; Chen and Liu, 2011*). During the last decades, new solution methods have been developed and applied to the diffusion wave equation. They include various explicit and implicit numerical methods (*Moussa and Bocquillon, 1996; Santillana and Dawson, 2010; Novak et al., 2010; Szymkiewicz, 2010*), Hayami convolution (*Moussa, 1997*), the discrete Hayami convolution method (*Wang et al., 2014*), the fractional-step method (*Moussa and Bocquillon, 2001*), the Green's function approach (*Bull, 2016*), the differential quadrature method (*Hasanvand et al., 2013*), and the mixing cell method (*Singh et al., 1997, Wang et al., 2003a, 2003b*). The majority of the proposed solutions are, however, purely numerical. They are hence subject to numerical diffusion, oscillation, and instability (*Novak et al., 2010*) which become more important with rapid changes in the upstream BCs such as in flash flooding.

While many solution methods exist as described above, no general and practical methods currently exist for solving the diffusive wave equation that can easily handle a variety of downstream BCs. In this work, we propose two new quasi-analytical methods which provide approximate closed-form symbolic solutions for diffusive wave routing, the Laplace-Transformed Continuous-Time Discrete-Space (LTCTDS) method and the Decoupled Continuous-Time Discrete-Space (DCTDS) method. Both methods produce explicit expressions for the diffusive wave equation valid at a set of nodes along the reach of interest subject to constant lateral inflow. Many routing applications in the real world seek routed hydrographs at specific locations, such as the National Weather Service's (NWS) forecast points, within the channel system given the observed or predicted inflows. The proposed methods are very well-suited for such routing applications in diffusive wave conditions (see for example *Tsai 2003*) in lieu of numerical models. The specific new contributions of the paper are as follows.

Two new methods have been developed for explicit quasi-analytical solutions for the diffusion wave equation with a desired number of spatial nodes.

The LTCTDS method follows the general methodology of *Subramanian and White (2000)* to offer approximate, quasi-analytical solutions to partial differential equations with Neumann or Dirichlet BCs on a finite domain at a number of discretized points by explicit-symbolic expressions. The proposed LTCDS method is the first time such a methodology is applied to the 1D linear diffusive wave equation. However, the proposed LTCDS method goes further to offer non-dimensionalized solutions to arbitrary inflow hydrographs with pulse approximation.

The DCTDS method on the other hand, is similar to the methodology *Salkuyeh (2006)*, *Bazán (2008)*, and *Gopaul et al. (2011)* used for solving 1D convection diffusion equations with Dirichlet BCs on a finite domain with a new contribution in the fact that it adds the ability to

model Neumann BCs on a finite domain as well. Other innovative aspects of the DCTDS method are its non-dimensionalized form and the ability to prescribe arbitrary inflow hydrographs with pulse approximation or a family of functionalized inflow hydrographs. Similar to the LTCTDS method, the DCTDS derived approximate solution is explicit, quasi-analytical, and symbolic.

In addition, a generic 5-node unit response function to a constant inflow is also proposed that can be used in general real world applications with minimal computational effort using the principle of superposition. Moreover, all the proposed explicit solutions to linear diffusive wave are analytical and continuous functions of time that do not suffer from numerical instabilities. Generally speaking, analytical solutions make an attractive case for convenient coding, real-time forecasting and control applications, and implementation in large networks (*Moramarco et al.*, 1999; Moussa, 2008). Since the methods presented in this paper are among the only choices for providing explicit solutions to the diffusive wave model with various BCs, they can be good candidates for when the above-mentioned advantages are needed. This paper is organized as follows: In Section 2, the classical solution of the diffusive wave model on a semi-infinite domain of Eq.(1) is given to provide background for the proposed methods. Sections 3 and 4 describe derivations of the LTCTDS and DCTDS methods, respectively. Section 5 provides an example application and discussion. Section 6 conclusions and future research recommendations.

2. Analytical solution for 1-dimensional linear diffusive wave for semi-infinite domain

In this section, we derive the analytical solution for 1-dimensional (1D) diffusive wave for semi-infinite domain. While not new, the solution provides an important reference for both

development and validation of the new methods. The classical solution may be obtained using the Laplace transform method as described. Defining the auxiliary function $f(x, t)$, we write $Q(x, t)$ in Eq.(1) as:

$$Q(x, t) = f(x, t) + q x \quad (4)$$

Eq.(1) is then reduced to the following homogeneous PDE:

$$\frac{\partial}{\partial t} f(x, t) = D \frac{\partial^2}{\partial x^2} f(x, t) - C \frac{\partial}{\partial x} f(x, t) \quad (5)$$

$$f(x, 0) = 0,$$

$$f(0, t) = Q_0(t) \quad (6)$$

$$\frac{\partial f}{\partial x} \Big|_{x \rightarrow \infty} = 0$$

To render the above PDE to an ordinary differential equation (ODE), we define the Laplace transform of $f(x, t)$:

$$u(x) = \mathcal{L}[f(x, t)] = \int_0^{\infty} f(x, t) e^{-s t} dt \quad (7)$$

With Eq.(7), we may rewrite Eq.(5) in terms of x only:

$$D \frac{d^2}{dx^2} u(x) - C \frac{d}{dx} u(x) - s u(x) = 0 \quad (8)$$

where the Laplace domain variable s may be treated as a constant. The ODE described by Eq.

(8) admits the following solution:

$$u(x) = A_1 e^{\frac{(C + \sqrt{C^2 + 4Ds})x}{2D}} + A_2 e^{\frac{(C - \sqrt{C^2 + 4Ds})x}{2D}} \quad (9)$$

where A_1 and A_2 are the integration constants. For a constant inflow of $Q_0(t) = Q_0$, the transformed BCs are:

$$u(0) = \frac{Q_0}{s}, \quad \frac{d}{dx}u(x)|_{x \rightarrow \infty} = 0 \quad (10)$$

Using the above BCs, the constants A_1 and A_2 may be determined as:

$$A_1 = 0, \quad A_2 = \frac{Q_0}{s} \quad (11)$$

The first condition in Eq.(11), $A_1 = 0$, may also be arrived at from physically-based reasoning in that, at the end of a very long channel, the effect of inflow is negligible. A mathematical explanation may also be made using the first term in the right hand side of Eq.(9) in that, if A_1 is nonzero, $u(x)$ diverges as $x \rightarrow \infty$. Given that the response of the system must be finite, one may conclude that A_1 must be zero. This is consistent with the observation made by *Hasanvand et al.* (2013) regarding multiple efforts made by previous researchers to eliminate the need for downstream BCs. In other words, there exists an intrinsic incompatibility within the intended application of diffusive wave routing and the theory of partial differential equations that necessitates the availability of BCs in both ends of the channel. For example, the diffusive wave is essentially used for modelling subcritical flows. However, subcritical flows are controlled from downstream, which is in contrast with the above mentioned explanation for $A_1 = 0$ in an infinite domain. Moreover, with the analytical formulation above, prescribing a known downstream boundary condition at infinity is physically meaningless, although the theory of open channel hydraulics dictates such a condition for subcritical flows.

With the BCs obtained in Eq. (11), we have for $u(x)$:

$$u(x) = \frac{Q_0}{s} e^{\frac{(c - \sqrt{c^2 + 4Ds})x}{2D}} \quad (12)$$

Inverse-transforming the Laplace-domain solution, we arrive at the following solution for Eq.

(5):

$$f(x, t) = Q_0 \left(1 - \frac{1}{2} \operatorname{erfc} \left(\frac{Ct - x}{2\sqrt{Dt}} \right) + \frac{1}{2} e^{\frac{cx}{d}} \operatorname{erfc} \left(\frac{Ct + x}{2\sqrt{Dt}} \right) \right) \quad (13)$$

In the above, erfc denotes the complementary error function:

$$\operatorname{erfc}(\chi) = \frac{2}{\sqrt{\pi}} \int_{\chi}^{\infty} e^{-\tau^2} d\tau \quad (14)$$

By dividing $f(x,t)$ with Q_0 , we may define the following system response function due to a constant unit inflow:

$$r(x, t) = \frac{f(x, t)}{Q_0} = 1 - \frac{1}{2} \operatorname{erfc} \left(\frac{Ct - x}{2\sqrt{Dt}} \right) + \frac{1}{2} e^{\frac{cx}{d}} \operatorname{erfc} \left(\frac{Ct + x}{2\sqrt{Dt}} \right) \quad (15)$$

If the channel reach is so long that the effects of downstream BC may safely be neglected, $r(x, t)$ may be used as the unit response function to a unit step inflow as shown in Fig 1. This result will be used in the following sections to obtain routed flow for an arbitrary inflow via the method of superposition. Finally, replacing $f(x, t)$ in Eq. (15) with $Q(x,t)$ using Eq. (4), we have the solution for the linear diffusive wave equation on an infinite channel with constant upstream and lateral inflows:

$$\begin{aligned} Q(x, t) &= Q_0 r(x, t) + qx \\ &= Q_0 \left(1 - \frac{1}{2} \operatorname{erfc} \left(\frac{Ct - x}{2\sqrt{Dt}} \right) + \frac{1}{2} e^{\frac{cx}{d}} \operatorname{erfc} \left(\frac{Ct + x}{2\sqrt{Dt}} \right) \right) \\ &\quad + qx \end{aligned} \quad (16)$$

The above solution, however, does not hold for a finite channel which necessitates the search for new solution methods which is described below.

3. Continuous-Time Discrete-Space Methods

Many flood routing problems in the real world seek routed hydrographs at specific locations within the channel system in response to arbitrary upstream inflows that are observed or predicted in real-time. In such cases, we may eliminate the space variable x and transform the PDE of Eq. (1) into a system of ODEs in time. To eliminate the space variable x , we use in this work the central finite difference approximation at equidistant nodes. Other forms of finite differencing or arbitrarily spaced nodes are also possible. The resulting system of ODEs at discretization nodes are then solved via two new methods, i.e., the Laplace transform method and the decoupling method which are presented in Sections 3.1 and 3.2, respectively.

3.1 Laplace Transformed Continuous-Time Discrete-Space (LTCTDS) Method

We first non-dimensionalize Eq. (5) by newly defining the following state variables:

$$X = \frac{x}{L}, T = \frac{C t}{L} \quad (17)$$

With Eq.(17), Eq.(5) is rendered to its non-dimensional equivalent as follows:

$$\begin{aligned} \frac{\partial}{\partial T} f(X, T) &= \frac{1}{Pe} \frac{\partial^2}{\partial X^2} f(X, T) - \frac{\partial}{\partial X} f(X, T) \\ f(X, 0) &= 0 \\ f(0, T) &= Q_0(T) \\ \frac{\partial f}{\partial X} \Big|_{X \rightarrow 1} &= 0 \end{aligned} \quad (18)$$

The main advantage of this non-dimensional form is that we have scaled the length to be $0 < X < 1$. In addition, this form is easier to manipulate since three parameters (C, D, and L) have been combined and represented in the compact form of

$$\text{Pe} = \frac{CL}{D} \quad (19)$$

where Pe denotes the Peclet number. The Peclet number, which has been extensively studied (Szymkiewicz, 2010), is a dimensionless ratio of the advective component to the diffusive component in the advection-diffusion process. Applying the Laplace transform (Subramanian and White, 2000) to Eq. (18) and rearranging the terms, we have:

$$\frac{1}{\text{Pe}} \frac{d^2}{dX^2} u(X) - \frac{d}{dX} u(X) - s u(X) = 0 \quad (20)$$

where $u(X) = \mathcal{L}[f(x, t)]$ as defined in Eq. (7). Discretizing Eq.(20) via central finite differencing with spatial resolution of $h = 1/N$ for N equidistant nodes, we may approximate Eq.(20) as:

$$\frac{u_{i-1} - 2u_i + u_{i+1}}{\text{Pe} h^2} - \frac{u_{i+1} - u_{i-1}}{2h} - su_i = 0 \quad (21)$$

For example, for a 5-point discretization Eq. (21) and the transformed BCs of $u_0 = 1/s$ and

$\frac{d}{dx} u_5 = 0$ form the following system of linear equations:

$$\begin{bmatrix} -4 - \frac{2\text{Pe} s}{25} & 2 - \frac{\text{Pe}}{5} & 0 & 0 & 0 \\ 2 + \frac{\text{Pe}}{5} & -4 - \frac{2\text{Pe} s}{25} & 2 - \frac{\text{Pe}}{5} & 0 & 0 \\ 0 & 2 + \frac{\text{Pe}}{5} & -4 - \frac{2\text{Pe} s}{25} & 2 - \frac{\text{Pe}}{5} & 0 \\ 0 & 0 & 2 + \frac{\text{Pe}}{5} & -4 - \frac{2\text{Pe} s}{25} & 2 - \frac{\text{Pe}}{5} \\ 0 & 0 & 1 & -4 & 3 \end{bmatrix} \begin{bmatrix} u_1 \\ u_2 \\ u_3 \\ u_4 \\ u_5 \end{bmatrix} = \begin{bmatrix} -\frac{10 + \text{Pe}}{5s} \\ 0 \\ 0 \\ 0 \\ 0 \end{bmatrix} \quad (22)$$

In order to obtain a closed-form solution for Eq.(22), we use symbolic algebra. Symbolic algebra is a process during which the variables are kept in their symbolic form while undergoing algebraic manipulation. The results are expressed in terms of symbols that can be valid for all the numerical values within each symbol's domain which usually encompasses infinite possibilities. On the other hand, if the symbols are assigned numeric values from the beginning, arithmetic computations must be repeated for each value and the results are valid only for those finite numbers of assigned values that were prescribed. In addition, symbolic solutions require less processing and memory demand due to the fact that the processes involved in evaluating mathematical expressions are more efficient than solving systems of equations. There are multiple readily available software packages such as Mathematica, Maple, and Matlab for symbolic algebra. The resulting exact symbolic solution describes the response of the linear diffusive wave model at five uniformly-spaced discretized points in Laplace domain:

$$\begin{bmatrix} u_1 \\ u_2 \\ u_3 \\ u_4 \\ u_5 \end{bmatrix} = \begin{bmatrix} 5(\text{Pe} + 10)(\text{Pe}^3(12s^3 + 40s^2 + 175s + 250) + 50\text{Pe}^2(28s^2 + 70s + 125) + 12500\text{Pe}(3s + 4) + 125000) \\ \frac{2\eta s}{25(\text{Pe} + 10)^2(\text{Pe}^2(3s^2 + 10s + 25) + 25\text{Pe}(8s + 15) + 1250)} \\ \frac{\eta s}{125(\text{Pe} + 10)^3(\text{Pe}(3s + 10) + 50)} \\ \frac{2\eta s}{625(\text{Pe} + 5)(\text{Pe} + 10)^3} \\ \frac{\eta s}{125(\text{Pe} + 10)^3(\text{Pe}(s - 10) - 50)} \\ - \frac{\eta s}{2\eta s} \end{bmatrix} \quad (23)$$

where

$$\begin{aligned}
\eta = & 3125000 + 62500\text{Pe}(25 + 24s) + 6250\text{Pe}^2(45 + 32s + 16s^2) \\
& + 125\text{Pe}^3(175 + 160s + 44s^2 + 16s^3) + \text{Pe}^4(625 + 500s \\
& + 250s^2 + 40s^3 + 12s^4)
\end{aligned} \tag{24}$$

Eq. (23) may be back-transformed into the time domain using inverse Laplace transform by taking advantage of the fact that the rational polynomials of Laplace domain in Eq. (23) have closed-form inverse Laplace solutions. The resulting explicit solution is of particular interest for the last point, u_5 , or the most downstream location:

$$\begin{aligned}
f(X = 1, T) = & 1 \\
& + \frac{1}{24\text{Pe}^3} \left(\frac{k(m_4)e^{m_4T}}{m_{14}m_{24}m_{34}} - \frac{k(m_3)e^{m_3T}}{m_{13}m_{23}m_{34}} + \frac{k(m_2)e^{m_2T}}{m_{12}m_{23}m_{24}} \right. \\
& \left. - \frac{k(m_1)e^{m_1T}}{m_{12}m_{13}m_{14}} \right)
\end{aligned} \tag{25}$$

In Eq.(25), $m_1, m_2, m_3,$ and m_4 denote the roots of $\Omega(m) = 0$, $m_{ij} = m_i - m_j$, and $k(m)$ and $\Omega(m)$ are given by:

$$\begin{aligned}
K(m) = & \text{Pe}^3 \Psi(m) + 250\text{Pe}^2 \omega(m) + 12500\text{Pe} \theta(m) + 3125000 \\
\Omega(m) = & 3125000 + 1562500\text{Pe} + 281250\text{Pe}^2 + 21875\text{Pe}^3 + 625\text{Pe}^4
\end{aligned} \tag{26a}$$

$$\begin{aligned}
& + (1500000\text{Pe} + 200000\text{Pe}^2 + 20000\text{Pe}^3 + 500\text{Pe}^4)m \\
& + (100000\text{Pe}^2 + 5500\text{Pe}^3 + 250\text{Pe}^4)m^2 + (2000\text{Pe}^3 \\
& + 40\text{Pe}^4)m^3 + 12\text{Pe}^4m^4
\end{aligned} \tag{26b}$$

In Eqs.(26), $\Psi(m)$, $\omega(m)$, and $\theta(m)$ are given by:

$$\Psi(m) = 24m^3 + 80m^2 + 500m + 1125 \tag{27a}$$

$$\omega(m) = 16m^2 + 44m + 175 \tag{27b}$$

$$\theta(m) = 16m + 35 \tag{27c}$$

For $Pe \geq 10$, the roots of Eq. (26b) become imaginary (see Fig 2). As such, Eq. (25) is valid only for $Pe < 10$. Similar results can be obtained for any spatial discretization. For any value of the Pe number, at least $\lceil Pe/2 \rceil + 1$ nodes, where $\lceil \cdot \rceil$ denotes the ceiling operator, are required to produce a real-valued response function for a single application of the LTCTDS method. Because Pe is directly proportional to the length of the channel, for larger values of the Pe number it is necessary to subdivide the channel and apply the LTCTDS method to each subreach successively from up- to downstream to ensure that the Pe number stays within the valid range. In practice, the above constraint does not pose a limitation as the response functions obtained via symbolic algebra can be programmed only once and run in real-time repeatedly each time using the appropriate IC and BCs.

To route the inflow hydrograph of any shape using the unit response function derived above, we use a linear systems approach similar to the unit hydrograph theory (*Chow et al.*, 1988) or the linear operator method (*Singh et al.*, 1997; *Kazezyilmaz-Alhan*, 2012). Any inflow hydrograph $Q_0(t)$ within some time window may be approximated by a series of pulses to a desired level of resolution. Any observational data would in fact consist of a series of pulses due to the finite temporal sampling intervals. One may hence express any inflow hydrograph as:

$$Q_0(t) = I_0 r(t) + (I_1 - I_0) r(t - \Delta t) + (I_2 - I_1) r(t - 2\Delta t) \dots \quad (28)$$

where I_i is the magnitude of the i -th pulse, $r(t)$ is the response to a unit step function, and Δt is the time step. Because the total response to a series of pulses is equal to the superposition of the responses to each individual pulses owing to the linear nature of the linear diffusive wave equation, one may calculate the response to any $Q_0(t)$ using only the unit response function $r(t)$ in a manner completely analogous to *Chow et al.*(1988) or the linear operator method of *Singh et al.* (1997). To illustrate, Fig 3 shows the unit response functions $r(t)$ obtained from the

quasi-analytical solution of the LTCTDS method for a 10-node discretization. Fig 4 shows how the principles of proportionality and superposition may be applied to any such unit response functions. Note in Fig 4 that, the response of the system to a unit pulse of duration $\Delta t = 100$ can be obtained by the first two terms of the right-hand side of Eq. (28) by summing the unit step function at $t=0$ and the negative unit step function at $t=100$.

To test the LTCTDS method, a synthetic inflow hydrograph (see Fig 5) is prescribed as the upstream BC. For comparison, the diffusive wave equation with the same inflow BC was solved numerically using the method of lines (Wolfram Research, Inc., 2017) (see Fig 6). The results show a strong agreement between the numerical solution and the quasi-analytical solution from the LTCTDS method (Fig 7). Note that the y-axis is in logarithmic scale, and that those regions where the differences are near-zero (i.e., perfect agreement) have been cut off to highlight only the noticeable differences. It is interesting to note that the differences are the smallest when the peak flow passes the downstream sections between $t=200$ (s) and $t=300$ (s), and that the largest differences are associated with the sharp edges in the first few upstream sections. The largest differences are due largely to the inaccuracies associated with numerical integration when there are sharp edges in the inflow BC where the gradients may be discontinuous. In purely numerical approaches, treatment of such edges requires refinement of the computational mesh. The quasi-analytical response functions, on the other hand, do not suffer from such limitations. Fig 8 shows an example comparison among the 5-node LTCTDS solution, the 10-node LTCTDS solution and the numerical solution for the most downstream location. At other nodes within the channel, similar accuracies could be obtained using the 5-node LTCTDS solution by adjusting the Pe number for shorter channel lengths. The figure indicates that the LTCTDS method is able to produce high-quality solutions even with relatively coarse spatial

discretization. Fig 9 shows the effect of the Peclet number on the 5-node LTCTDS-derived unit response function. Larger advective effects (and hence larger Pe numbers) results in the wave front traveling downstream faster whereas larger diffusivity (and hence smaller Pe numbers) result in larger degrees of attenuation of the peak. Fig 9 also shows a slight drawback of the solution in Eq. (25). For small values of dimensionless time of $T < 0.00017Pe^3 - 0.00423Pe^2 + 0.04690Pe + 0.00243$, the unit response function becomes slightly negative. Because this solution is for the downstream end of the channel, the response function is almost certainly zero over the time interval above. Therefore, this very minor artifact can easily be addressed in practice by forcing any negative responses to be zero.

For a large number of nodes, the symbolic derivation of the inverse Laplace transform may become unstable. Even if the inversion is simplified by specifying the Peclet number numerically, numerical errors start to appear in the unit response function for small T and grow larger as N increases. This is because, as the level of discretization increases, the NxN matrix in the lefthand side of Eq.(22) becomes numerically nearly singular as the model states between two adjacent locations become nearly identical. Because a finer spatial mesh discretization is required for larger Peclet numbers, the above loss of accuracy limits the universal applicability of LTCTDS method. Although there exist numerical methods for approximating the symbolic solution of inverse Laplace transform (*Kazeyilmaz-Alhan 2012*), an additional numerical inversion step may negate any additional gains from explicit symbolic methods. In such cases, symbolic approaches may not offer any significant advantages over purely numerical methods or even analytical solutions of partial sums of infinite series derived from SoV-based methods for semi-infinite domain. The further interested reader is referred to *Hassanzadeh and Pooladi-Darvishi (2007)* and *Wang and Zhan (2015)* which include comparison of several different

numerical Laplace inversion methods applied to advection-diffusion equations. The DCTDS method described below is developed to address the above shortcomings of the LTCTDS method.

3.2 Decoupled Continuous-Time Discrete-Space (DCTDS) Method

As in the LTCTDS method, we first discretize the PDE into a system of ODEs.

Approximating the spatial derivative in Eq.(18) via central finite differencing over a grid of N internal points with the $(N+1)$ th point representing the most downstream location, we have:

$$\frac{d^2}{dX^2} f_i(T) = \frac{f_{i+1}(T) - 2f_i(T) + f_{i-1}(T)}{h^2} \quad (29)$$

where $f_i(T) = f(X_i, T)$ and $h=1/(N+1)$. Using the 3-term backward scheme (*Subramanian and White, 2000*) for the derivative for the last node, we have:

$$f_{N-1}(T) - 4f_N(T) + 3f_{N+1}(T) = 0 \quad (30)$$

After some manipulation, Eq. (18) may be written in the following matrix form:

$$\frac{d}{dT} \mathbf{f} = \frac{1}{\text{Pe} h^2} (\mathbf{A} \mathbf{f} + \mathbf{f}_0) \quad (31)$$

where \mathbf{f} is the transpose of the vector $(f_1(T), f_2(T), \dots, f_N(T))$, and the $N \times N$ matrix \mathbf{A} and the $N \times 1$ vector \mathbf{f}_0 are given by:

$$\mathbf{A} = \begin{bmatrix} -2 & 1 - \frac{h\text{Pe}}{2} & 0 & \dots & 0 & 0 & 0 \\ 1 + \frac{h\text{Pe}}{2} & -2 & 1 - \frac{h\text{Pe}}{2} & \ddots & 0 & 0 & 0 \\ \vdots & \ddots & \ddots & \ddots & \vdots & \vdots & \vdots \\ 0 & 0 & 0 & \dots & 1 + \frac{h\text{Pe}}{2} & -2 & 1 - \frac{h\text{Pe}}{2} \\ 0 & 0 & 0 & \dots & 0 & \frac{2(1+h\text{Pe})}{3} & -\frac{2(1+h\text{Pe})}{3} \end{bmatrix}_{N \times N} \quad (32a)$$

$$\mathbf{f}_0 = \begin{bmatrix} f_{1,0} \\ f_{2,0} \\ \vdots \\ f_{N,0} \end{bmatrix}_{N \times 1} = \begin{bmatrix} \left(1 + \frac{hPe}{2}\right) Q_0(T) \\ 0 \\ \vdots \\ 0 \end{bmatrix}_{N \times 1} \quad (32b)$$

Eq. (31) represents a coupled system of differential equations which in general can only be solved numerically. In this work, we use eigenvalue decomposition of \mathbf{A} to orthogonalize, or decouple, the system of equations for analytical solution. As Eqs. (29) and (30) show, every component of the system of differential equations of Eq. (31) includes more than one unknown elements of vector \mathbf{f} . However, if the system can be simplified to a diagonalized form, the differential equations become decoupled so that each one contains only one unknown f_i . In order to diagonalize the system of equations, the matrix \mathbf{A} may be eigenvalue-decomposed as:

$$\mathbf{A} = \mathbf{PZP}^{-1} \quad (33)$$

Eq.(31) may then be written as:

$$\frac{d}{dt} \mathbf{f} = \frac{1}{Pe h^2} (\mathbf{PZP}^{-1} \mathbf{f} + \mathbf{f}_0) \quad (34)$$

In the above, \mathbf{Z} is the diagonal matrix of eigenvalues and \mathbf{P} is the column-wise augmented matrix of the corresponding eigenvectors (Meyer, 2000):

$$\mathbf{Z} = \begin{bmatrix} \lambda_1 & 0 & 0 & \cdots & 0 \\ 0 & \lambda_2 & 0 & \ddots & 0 \\ \vdots & \ddots & \ddots & \ddots & \vdots \\ 0 & 0 & 0 & 0 & \lambda_N \end{bmatrix} \quad (35)$$

$$\mathbf{P} = [\mathbf{P}_1 | \mathbf{P}_2 \cdots \mathbf{P}_{N-1} | \mathbf{P}_N] \quad (36)$$

Owing to the fact that \mathbf{A} is symmetric and tri-diagonal, we may obtain the eigenvalues analytically using the Chebyshev polynomials of the second type (Kulkarni *et al.*, 1999):

$$U_m(x) = \frac{\sin((m+1)\cos^{-1}x)}{\sin(\cos^{-1}x)} \text{ for } |x| \leq 1 \quad (37)$$

where $U_m(x)$ is the second type Chebyshev polynomial of order m . Using *Kulkarni et al.*(1999), one may obtain the characteristic equation of matrix \mathbf{A} :

$$\frac{U_{N-1}\left(-\frac{2}{\sqrt{4-\frac{Pe^2}{(1+N)^2}}}-\frac{\lambda}{2}\right)}{U_{N-2}\left(-\frac{2}{\sqrt{4-\frac{Pe^2}{(1+N)^2}}}-\frac{\lambda}{2}\right)} = -\frac{4(1+N)\left(1+\frac{Pe}{1+N}\right)\sqrt{4-\frac{Pe^2}{(1+n)^2}}}{(2+2N+Pe)\left(28+\frac{4Pe}{1+N}+3\sqrt{4-\frac{Pe^2}{(1+N)^2}}\lambda\right)} \quad (38)$$

The eigenvalues of \mathbf{A} are given by the ordered roots of Eq. (38). It is worth mentioning that the

roots of the function $U_{N-2}\left(-\frac{2}{\sqrt{4-\frac{Pe^2}{(1+N)^2}}}-\frac{\lambda}{2}\right)$ which have analytical expressions prescribe the

feasible ranges for root finding algorithms. Fig 10 shows three examples of root finding for determination of the eigenvalues with different combinations of Pe and N . An additional advantage of using Eq. (38) is that it provides the theoretical bound for minimum N to ensure real-valued solution, i.e., $N > \frac{Pe}{2} - 1$. Since \mathbf{A} is non-singular, there always exists a matrix \mathbf{P} that satisfies:

$$\mathbf{f} = \mathbf{P}\mathbf{v} \quad (39)$$

By substituting Eq. (39) in Eq. (34), we then have:

$$\mathbf{P}\frac{d}{dT}\mathbf{v} = \frac{1}{Pe h^2}(\mathbf{PZ}\mathbf{v} + \mathbf{f}_0) \quad (40)$$

Pre-multiplying \mathbf{P}^{-1} to both sides of Eq. (40), we have:

$$\frac{d}{dT} \mathbf{v} = \frac{1}{\text{Pe } h^2} (\mathbf{Z} \mathbf{v} + \mathbf{v}_0) \quad (41)$$

where

$$\mathbf{v}_0 = \mathbf{P}^{-1} \mathbf{f}_0 \quad (42)$$

Because \mathbf{Z} is diagonal, the system of N first-order differential equations may be decoupled into the n simple ODEs of the following form:

$$\frac{d}{dT} v_i(T) = \frac{1}{\text{Pe } h^2} (\lambda_i v_i(T) + w_i Q_0(T)) \quad (43)$$

Furthermore, for a constant uniform inflow it may be shown that:

$$\frac{d}{dT} v_i(T) = \frac{1}{\text{Pe } h^2} (\lambda_i v_i(T) + w_i) \quad (44)$$

where w_i is a constant. Eq. (44) has the following analytical solution:

$$v_i(T) = \frac{w_i (e^{\frac{T \lambda_i}{\text{Pe } h^2}} - 1)}{\lambda_i} \quad (45)$$

Using $\mathbf{f} = \mathbf{P} \mathbf{v}$ and substituting $f(x,t)$ back in Eq. (4), we may obtain the set of response functions to a constant inflow at all internal nodes. The solution at the most downstream point, which is often the most important for flood routing, is given solving Eq. (30) for f_{N+1} and by:

$$Q_L(t) = qL - \frac{f\left(x_{N-1}, \frac{C t}{L}\right)}{3} + \frac{4f\left(x_N, \frac{C t}{L}\right)}{3} \quad (46)$$

The solution for the diffusion wave equation at the $N+1$ discretized points to a series of arbitrary pulsed inflows may be obtained using the principle of superposition as described in the previous subsection. As expected, the response functions are summations of $N+1$ exponential terms.

In the above, the DCTDS method is described in the context of routing a unit inflow hydrograph. The same method may also be used to route more complex inflow hydrographs.

For example, many studies (*Szymkiewicz, 2010; Hasanvand et al., 2013; Perumal and Sahoo, 2007*) have used generic functions as inflow hydrographs such as a Pearson Type-III distribution:

$$Q_0(T) = Q_0(T = 0) + (Q_{Tp} - Q_0(T = 0)) \left(\frac{T}{Tp} \right) e^{1 - \left(\frac{T}{Tp} \right)} \quad (47)$$

where Q_{Tp} is the peak flow and Tp is the dimensionless time-to-peak. For the above inflow hydrograph, the solution to Eq. (43) is given by:

$$v_i(T) = - \frac{w_i e^{1 - \left(\frac{T}{Tp} \right)}}{(h^2 Pe + Tp \lambda_i)^2} \left(h^2 Pe \left(T + Tp \left(1 - p e^{\left(\left(\frac{T}{Tp} \right) + \frac{T \lambda_i}{h^2 Pe} \right)} \right) \right) + T \lambda_i Tp \right) \quad (48)$$

As an example application, we now consider an inflow hydrograph of $Q_0(t) = 5 + 95 \left(\frac{t}{600} \right) e^{1 - \left(\frac{t}{600} \right)}$ where t is time (s) and the flow (cms) increases from the initial value of 5 (cms) to a peak flow of 100 (cms) at $t=600$ (s). Following the properties of the hypothetical channel analyzed in *Szymkiewicz (2010)*, we assume $C=1.88$ m/s and $D= 2100$ m²/s and the length of the channel to be 10 km. After non-dimensionalizing the hydrograph using Eq. (17), solving with a 15-node DCTDS method, and finally back-transforming to the dimensional form, we obtain the explicit solution shown in Fig 11. The figure shows a very close agreement with the numerical solution obtained via the method of lines with a maximum difference of about 0.634 (cms) (see Fig 12). In Appendix, we provide analytical solutions of the Eq. (43) for different types of inflow hydrographs using the DCTDS methodology. They includes solutions for generic inflow of the functional forms of $T^r e^{kT}$, $e^{k T^2+j}$, $T e^{k T^2+j}$, $T^2 e^{k T^2+j}$, $\sin(kT)$, and $\cos(kT)$. Note that many other functions may be constructed using these generic functions following approximations using Taylor series expansion, Fourier transform, Legendre polynomials, and Chebyshev polynomials (*Hamming, 2012; Komzsik, 2006*).

3.3 Dirichlet boundary condition downstream

The development above deals with the Neumann BCs at the downstream point. The CTDS methods can still be used when the downstream BC is a known function of time. An analytical Laplace-based solution is already available when the downstream depth is available (*Cimorelli et al.*, 2014). Here we describe an alternative solution using DCTDS. In this case, the problem becomes one of boundary-value advection-diffusion in which the matrix \mathbf{A} is a standard tri-diagonal matrix whose diagonal eigenvalue matrix is given by the following (Meyer, 2000):

$$\lambda_i = -2 + 2\cos\left(\frac{i\pi}{N+1}\right) \quad (49)$$

where λ_i denotes the i -th eigenvalue, $i=1, \dots, N$. The i -th column, \mathbf{P}_i , of the eigenvalue vector, \mathbf{P} , is given by:

$$\mathbf{P}_i = \begin{bmatrix} \sin\left(\frac{i\pi}{N+1}\right) \\ \sin\left(\frac{2i\pi}{N+1}\right) \\ \vdots \\ \sin\left(\frac{Ni\pi}{N+1}\right) \end{bmatrix} \quad (50)$$

In practice, a known downstream BC is often available for depth-based diffusive wave with backwater consideration:

$$\begin{aligned} \frac{\partial}{\partial T} y(X, T) &= \frac{1}{\text{Pe}} \frac{\partial^2}{\partial X^2} y(X, T) - \frac{\partial}{\partial X} y(X, T) \\ y(X, 0) &= y_{t0}(X) \\ y(0, T) &= y_0(T) \\ y(1, T) &= y_L(T) \end{aligned} \quad (51)$$

where y denotes the depth and the rest of the symbols have already been defined. The solution process is analogous to that above except for:

$$\mathbf{f}_0 = \begin{bmatrix} f_{1,0} \\ f_{2,0} \\ \vdots \\ f_{N-1,0} \\ f_{N,0} \end{bmatrix} = \begin{bmatrix} y_{t_0}(X_1) + y_0(T) \\ y_{t_0}(X_2) \\ \vdots \\ y_{t_0}(X_{N-1}) \\ y_{t_0}(X_N) + y_L(T) \end{bmatrix} \quad (52)$$

Owing to the availability of the closed-form expressions in Eqs. (49) and (50), the DCTDS method provides a parsimonious and accurate solution to the diffusive wave model with Dirichlet BCs. For example, there may exist tidal backwater waves that follow a sine or cosine pattern. Using the methodology described above and the ODE solutions in Appendix, one may easily obtain quasi-analytical expressions for the temporal evolution of flood waves at specific forecast points of interest.

4. Application and discussion

The two new methods introduced in this paper provide the users with additional tools for diffusive wave routing. Depending on the problem, one method may be better-suited than the others. For very short channel reaches typical of urban catchments, the analytical solution of Eq.(14) may not be appropriate due to the semi-infinite length assumption. In this section, we compare the two CTDS methods and the analytical solution for semi-infinite domain for a real-world flooding event that occurred in Aug 1968 in a 112 km reach of the Yuanling- Wangjiahe River, China (*Singh et al., 1997*). For this event, diffusive wave routing is considered to be appropriate (*Singh et al., 1997, Wang et al., 2003a, 2003b*) and the parameters C and D were already estimated to be 3.327 m/s and 16,935 m²/s, respectively (*Singh et al. 1997*). Estimation of C and D has been a subject of many previous studies (*Cappelaere 1997, Knight and Shamseldin 2005*) and may be carried out in a number of different ways. One may use their

theoretical description (Szymkiewicz 2010; Moussa and Bocquillon 2001) and the most recently observed inflow similar to the “freezing” approach of Koussis (1983). If available, one may use long-term observations to calibrate, parametrize and summarize the parameter values in look-up tables or approximation functions (Singh *et al.* 1997). Fig 13 shows the inflow hydrograph, the three outflow hydrographs predicted by the three solutions and the verifying observed outflow. In this example, lateral inflow is considered negligible. Fig 13 also indicates that the DCTDS and LTCTDS methods produce nearly identical results, but that they are very close to the analytical solution. This is a long channel and hence the assumption of semi-infinite length may be considered reasonable. The error in predicting the peak values may be due to a combination of the assumption of constant C and D and ignoring the lateral inflow. That the observed hydrograph has a larger volume than the model solutions suggests that there may exist small lateral inflow. In fact, integrating the area under the curves of observed inflow and outflow hydrographs shows a 9,558,000 m³ discrepancy, that could be partly due to at least a small amount of lateral inflow. Our experiment showed that even a very small lateral inflow, which is very likely to exist in such a long reach during a large event, may modify the routed hydrographs closer to the observed flows. In fact, as Fig 14 shows, an envelope created by the range of values of C from 2.7 to 4.2 m/s, D from 16000 to 16,935 m²/s, and q from 0.001 to 0.0015 m³/s/m captures encompasses all the observed flows. Therefore, appropriate values of these parameters have the ability to model the observed hydrographs.

To apply the CTDS methods, it is necessary to specify a priori the number of nodes to be used in discretizing the channel. Because the optimal resolution of spatial mesh depends on the Peclet number, it is important to evaluate the combined effects of the number nodes and the Peclet number on the accuracy of the results. For this assessment, we compared the unit

response functions derived from the CTDS methods with that derived from numerical simulation via the method of lines. Figs 15 and 16 show the differences between the numerical solution and the CTDS solution for various combinations of N and Pe . The figures indicate that, for smaller values of Pe and N , the response functions derived from DCTDS and LTCTDS are nearly identical. For a combination of relatively large N and small to moderate Pe , however, the LTCTDS method quickly deteriorates (see Fig 15 for $Pe=5$ and 11) as explained in Subsection 3.1. The DCTDS method, on the other hand, does not suffer from this limitation and produces solutions that are nearly identical to the numerical solutions (see Fig 16). As such, the DCTDS method offers a distinct advantage over purely numerical methods in that the former provides closed-form solutions that can be very easily evaluated without numerical integration.

The Muskingum-Cunge (MC) method is one of the most widely used simplified methods in flood routing (Szymkiewicz, 2010). The MC method is theoretically equivalent to linear diffusive wave model and hence offers a useful and practical point of comparison with the CTDS methods. For numerical integration, the MC method employs two free parameters, the spatial step and the temporal step (USACE 1991). The accuracy of the MC method depends on the Courant number and the choice of travel time and cross sectional weighting parameters. Barry and Bajracharya (1995) investigated which combination of spatial and temporal steps may yield the best solution. They found that a simple explicit scheme is the best method to solve the complete diffusion wave equation starting from the kinematic wave equation, and that third-order accuracy is attained if the optimal Courant number is 12. While simpler than dynamic wave routing, the MC method still requires careful selection of the spatial and temporal steps, the numerical integration scheme and initialization. The DCTDS method, on the other hand, provides near-exact closed-form solutions for the unit response function for

arbitrary combinations of C and D from which the forecast hydrograph can very easily be constructed via the principle of superposition. As noted above, the parameters, C and D, depend on flow, channel geometry, roughness, and slope. For channels in which significant variations in C and D may exist due to longitudinal variations in channel geometry, roughness and/or slope, it will be necessary to sectionalize the channel so that different combinations of values for C and D may be used for different sections. To account for dependence of C and D on the magnitude of flow, one may prescribe different values of C and D depending on the magnitude of each pulse in the inflow hydrograph. The above approach would amount to a diffusive wave version of layered routing which is commonly practiced in operational flood forecasting with the lag-K, Muskingum and other routing techniques (NWS, 2005). Additional research and evaluation are needed, however, to develop a robust objective procedure for layered diffusive wave routing using the CTDS methods.

Lastly, while the computational savings may not be significant for small-scale applications of the proposed methods, one may expect significant savings if routing has to be performed for a large network of channels (*Moramarco et al.*, 1999; *Liu et al.*, 2003; *Choudhury*, 2007) or a dense network of small channels in large urban areas (*Habibi et al.*, 2016). The simplicity and computational ease of the CTDS methods also mean that they can be easily implemented on site on single-board computers such as Raspberry Pi modules for real-time forecasting. Table 1 provides a general comparison among different methods, their applicability and capabilities.

5. Conclusions and future research recommendations

Diffusive wave routing is an important methodology for predicting the movement of flood waves in open channels. Unlike dynamic wave routing, diffusive wave routing does not require large amounts of data. Unlike kinematic wave routing, diffusive wave routing accounts for

pressure gradients which are important for mildly-sloped channel. Most solution techniques for diffusive wave routing that are currently available, however, are purely numerical. To satisfy the CFL condition and to ensure convergence, numerical integration has to be carried out in general problem-specifically. This work proposes two new methods for 1D diffusive wave routing which do not require numerical integration. Referred to as the LCTDS method, the new method renders the original PDE into a system of ODEs via the Laplace transform which are then solved via symbolic algebra following finite difference approximation of the ODEs. If the number of nodes used is large, the accuracy of the LCTDS method may deteriorate due to numerical singularity. The DCTDS method addresses the above shortcoming by orthogonalizing the PDE via eigenvalue decomposition. The new methods provide closed-form symbolic solutions for 1D diffusive routing for a set of nodes in a finite domain due to a unit pulse of inflow and a constant lateral inflow. The complete hydrographs at downstream locations may be obtained via the principle of superposition and proportionality from a fixed-interval pulse representation of the inflow hydrograph.

The proposed solutions in addition to classical analytical solution offer a wide range of tools for practical flood routing. In addition, unlike conventional numerical models, the symbolic-explicit nature of the proposed solutions provides modelers with algorithmic flexibility in implementing them. Because the new methods assume constant C and D , they may not be directly applicable if the parameters vary in time due, e.g., changes in the magnitude of the flood wave. For “layered” 1D diffusive wave routing which uses flow magnitude-dependent parameters as commonly practiced with the existing routing methods, additional research and evaluation are needed to develop a robust objective procedure. Owing to the closed-form solutions, the proposed methods are expected to provide significant computational savings for

routing through large channel systems. The simplicity and the computational ease of the CTDS methods also mean that they can be easily implemented on site on single-board computers such as Raspberry Pi modules in various real-time applications.

6. Acknowledgements

This material is based upon work supported in part by the National Science Foundation under Grant CyberSEES-1442735 (Dong-Jun Seo, University of Texas at Arlington, PI) This support is gratefully acknowledged.

7. Appendix

Several different generic hydrographs and their analytical ODE solutions associated with the DCTDS method is presented below:

A.1. If $Q_0(T) = T^r \text{Exp}(k T)$ then

$$v_i(T) = \frac{w_i e^{\frac{T\lambda_i}{h^2 \text{Pe}}} \left(h^2 \text{Pe} T^r \Gamma\left(1 + r, -kT + \frac{T\lambda_i}{h^2 \text{Pe}}\right) + \Gamma(1 + r, 0)(h^2 k \text{Pe} - \lambda_i) \left(-kT + \frac{T\lambda_i}{h^2 \text{Pe}}\right)^r \right)}{h^2 \text{Pe}(h^2 k \text{Pe} - \lambda_i) \left(-kT + \frac{T\lambda_i}{h^2 \text{Pe}}\right)^r} \quad (\text{A1})$$

Where $\Gamma(a, x)$ is the incomplete Gamma function defined as

$$\Gamma(a, x) = \int_x^\infty t^{a-1} e^{-t} dt \quad (\text{A2})$$

A.2. If $Q_0(T) = \text{Exp}(k T^2 + j T)$ then

$$\begin{aligned}
v_i(T) &= \frac{\sqrt{\pi} w_i e^{\frac{4h^2 \text{Pe} T \lambda_i - (\lambda_i - h^2 j \text{Pe})^2}{4h^4 \text{Pe}^2}} \left(\text{erfi} \left(\frac{h^2 j \text{Pe} - \lambda_i}{2h^2 \sqrt{k} \text{Pe}} \right) - \text{erfi} \left(\frac{h^2 \text{Pe}(j + 2kT) - \lambda_i}{2h^2 \sqrt{k} \text{Pe}} \right) \right)}{2h^2 \sqrt{k} \text{Pe}} \quad (\text{A3})
\end{aligned}$$

A.3. If $Q_0(T) = T \text{Exp}(k T^2 + j T)$ then

$$\begin{aligned}
v_i(T) &= - \frac{w_i e^{\frac{4h^2 \text{Pe} T \lambda_i - (\lambda_i - h^2 j \text{Pe})^2}{4h^4 \text{Pe}^2}}}{4h^4 k^{3/2} \text{Pe}^2} \left(\sqrt{\pi} \lambda_i \left(\text{erfi} \left(\frac{h^2 j \text{Pe} - \lambda_i}{2h^2 \sqrt{k} \text{Pe}} \right) \right. \right. \\
&\quad \left. \left. - \text{erfi} \left(\frac{h^2 \text{Pe}(j + 2kT) - \lambda_i}{2h^2 \sqrt{k} \text{Pe}} \right) \right) \right. \\
&\quad \left. + h^2 \text{Pe} \left(-\sqrt{\pi} j \text{erfi} \left(\frac{h^2 j \text{Pe} - \lambda_i}{2h^2 \sqrt{k} \text{Pe}} \right) + \sqrt{\pi} j \text{erfi} \left(\frac{h^2 \text{Pe}(j + 2kT) - \lambda_i}{2h^2 \sqrt{k} \text{Pe}} \right) \right. \right. \\
&\quad \left. \left. + 2\sqrt{k} \left(e^{\frac{(\lambda_i - h^2 j \text{Pe})^2}{4h^4 k \text{Pe}^2}} - e^{\frac{(\lambda_i - h^2 \text{Pe}(j + 2kT))^2}{4h^4 k \text{Pe}^2}} \right) \right) \right) \quad (\text{A4})
\end{aligned}$$

where $\text{erfi}(x)$ is the imaginary error function defined as

$$\text{erfi}(x) = \frac{2}{\sqrt{\pi}} \int_0^x e^{t^2} dt \quad (\text{A5})$$

A.4. If $Q_0(T) = T^2 \text{Exp}(k T^2 + j T)$

$$\begin{aligned}
v_i(T) = & \frac{e^{-\frac{h^4 j^2 \text{Pe}^2 + \lambda_i^2}{4h^4 k \text{Pe}^2}} w_i}{8h^6 k^{5/2} \text{Pe}^3} \left(e^{\frac{(j+2kT)\lambda_i}{2h^2 k \text{Pe}}} \sqrt{\pi} \text{erfi} \left(\frac{h^2 j \text{Pe} - \lambda_i}{2h^2 \sqrt{k} \text{Pe}} \right) (-h^4(j^2 - 2k)\text{Pe}^2 \right. \\
& + 2h^2 j \text{Pe} \lambda_i - \lambda_i^2) \\
& - e^{\frac{(j+2kT)\lambda_i}{2h^2 k \text{Pe}}} \sqrt{\pi} \text{erfi} \left(\frac{h^2 \text{Pe}(j + 2kT) - \lambda_i}{2h^2 \sqrt{k} \text{Pe}} \right) (-h^4(j^2 - 2k)\text{Pe}^2 \\
& + 2h^2 j \text{Pe} \lambda_i - \lambda_i^2) \\
& + 2e^{\frac{h^4 j^2 \text{Pe}^2 + \lambda_i^2}{4h^4 k \text{Pe}^2}} h^2 \sqrt{k} \text{Pe} \left(e^{\frac{T\lambda_i}{h^2 \text{Pe}}} (h^2 j \text{Pe} - \lambda_i) \right. \\
& \left. \left. + e^{T(j+kT)} (-h^2 \text{Pe}(j - 2kT) + \lambda_i) \right) \right) \quad (\text{A6})
\end{aligned}$$

A.5. If $Q_0(T) = \sin(k T)$

$$v_i(T) = - \frac{w_i \left(h^2 k \text{Pe} \left(\cos(k T) - e^{\frac{T\lambda_i}{h^2 \text{Pe}}} \right) + \lambda_i \sin(k T) \right)}{h^4 k^2 \text{Pe}^2 + \lambda_i^2} \quad (\text{A7})$$

A.6. If $Q_0(T) = \cos(k T)$

$$v_i(T) = \frac{w_i \left(\lambda_i \left(e^{\frac{T\lambda_i}{h^2 \text{Pe}}} - \cos(k T) \right) + h^2 k \text{Pe} \sin(k T) \right)}{h^4 k^2 \text{Pe}^2 + \lambda_i^2} \quad (\text{A8})$$

References

- Bajracharya, K., Barry, D. A. (1997). Accuracy criteria for linearised diffusion wave flood routing. *Journal of Hydrology*, 195(1-4), 200-217.
- Barry, D. A., K. Bajracharya (1995). On the Muskingum-Cunge flood routing method. *Environment International*, 21(5): 485-490.
- Bazán, F. S. (2008). Chebyshev pseudospectral method for computing numerical solution of convection–diffusion equation. *Applied Mathematics and Computation*, 200(2), 537-546.
- Bull, J. R. (2016). A fast direct solver for the advection-diffusion equation using low-rank approximation of the Green's function. *arXiv preprint arXiv:1612.09273*.
- Cappelaere, B. (1997). Accurate diffusive wave routing. *Journal of Hydraulic Engineering*, 123(3), 174-181.
- Chang, C. M., Yeh, H. D. (2014). Variability of stream flow discharge in response to self-similar random fields of temporal fluctuations in lateral inflow rate. *Journal of Hydrology*, 517, 246-249.
- Chanson, H. (2004). *Environmental hydraulics for open channel flows*. Butterworth-Heinemann.

- Chen, J. S., Liu, C. W. (2011). Generalized analytical solution for advection-dispersion equation in finite spatial domain with arbitrary time-dependent inlet boundary condition. *Hydrology and Earth System Sciences*, 15(8), 2471.
- Cheviron, B., Moussa, R. (2016). Determinants of modelling choices for 1-D free surface flow and morphodynamics in hydrology and hydraulics: a review. *Hydrology and Earth System Sciences*, 20(9), 3799-3830.
- Choudhury, P. (2007). Multiple inflows Muskingum routing model. *Journal of Hydrologic Engineering*, 12(5), 473-481.
- Chow, V. T., Maidment, D. R., Mays, L. W. (1988). *Applied hydrology*.
- Cimorelli, L., Cozzolino, L., Della Morte, R., Pianese, D. (2014). Analytical solutions of the linearized parabolic wave accounting for downstream boundary condition and uniform lateral inflows. *Advances in Water Resources*, 63, 57-76.
- Dan, D., Mueller, C., Chen, K., Glazier, J. A. (2005). Solving the advection-diffusion equations in biological contexts using the cellular Potts model. *Physical Review E*, 72(4), 041909.
- Fan, P., Li, J. C. (2006). Diffusive wave solutions for open channel flows with uniform and concentrated lateral inflow. *Advances in water resources*, 29(7), 1000-1019.

- Fischer, H. B. (1968). *Methods for Predicting Dispersion Coefficients in Natural Streams: With Applications to Lower Reaches of the Green and Duwamish Rivers, Washington* (Vol. 582). US Government Printing Office.
- Freijer, J. I., Veling, E. J. M., Hassanizadeh, S. M. (1998). Analytical solutions of the convection–dispersion equation applied to transport of pesticides in soil columns. *Environmental modelling & software*, 13(2), 139-149.
- Gochis, D.J., Yu, W., Yates, D.N., 2014. The WRF-Hydro model technical description and user’s guide, version 2.0. NCAR Technical Document Available at: https://www.ral.ucar.edu/projects/wrf_hydro.
- Gopaul, A., Cheeneebash, J., & Baurhoo, K. (2011). A Comparison of Recent Methods for solving a model 1D Convection Diffusion Equation. *World Academy of Science, Engineering and Technology, International Journal of Mathematical, Computational, Physical, Electrical and Computer Engineering*, 5(9), 1444-1448.
- Habibi, H., Nasab, A. R., Norouzi, A., Nazari, B., Seo, D. J., Muttiah, R., Davis, C. (2016). High Resolution Flash Flood Forecasting for the Dallas-Fort Worth Metroplex. *Journal of Water Management Modeling*.
- Hamming, R. (2012). *Numerical methods for scientists and engineers*. Courier Corporation.
- Hasanvand, K., Hashemi, M. R., Abedini, M. J. (2013). Development of an Accurate Time Integration Technique for the Assessment of Q-Based versus

- h-Based Formulations of the Diffusion Wave Equation for Flow Routing. *Journal of Hydraulic Engineering*, 139(10), 1079-1088.
- Hassanzadeh, H., Pooladi-Darvish, M. (2007). Comparison of different numerical Laplace inversion methods for engineering applications. *Applied mathematics and computation*, 189(2), 1966-1981.
- Jia, X., Zeng, F., Gu, Y. (2013). Semi-analytical solutions to one-dimensional advection–diffusion equations with variable diffusion coefficient and variable flow velocity. *Applied Mathematics and Computation*, 221, 268-281.
- Kazezyilmaz-Alhan, C. M. (2012). An improved solution for diffusion waves to overland flow. *Applied Mathematical Modelling*, 36(9), 4165-4172.
- Knight, D., Shamseldin, A. (Eds.). (2005). *River basin modelling for flood risk mitigation*. CRC Press.
- Komzsik, L. (2006). *Approximation techniques for engineers*. CRC press.
- Koussis, A. D. (1983). Unified theory for flood and pollution routing. *Journal of hydraulic engineering*, 109(12), 1652-1664.
- Kulkarni, D., Schmidt, D., Tsui, S. K. (1999). Eigenvalues of tridiagonal pseudo-Toeplitz matrices. *Linear Algebra and its Applications*, 297(1-3), 63-80.
- Litrico, X., Fromion, V. (2009). Modeling of Open Channel Flow. *Modeling and Control of Hydrosystems*, 17-41.

- Liu, Y. B., Gebremeskel, S., De Smedt, F., Hoffmann, L., Pfister, L. (2003). A diffusive transport approach for flow routing in GIS-based flood modeling. *Journal of Hydrology*, 283(1), 91-106.
- Meyer, C. D. (2000). *Matrix analysis and applied linear algebra* (Vol. 2). Siam.
- Moramarco, T., Fan, Y., Bras, R. L. (1999). Analytical solution for channel routing with uniform lateral inflow. *Journal of Hydraulic Engineering*, 125(7), 707-713.
- Moussa, R. (1996). Analytical Hayami solution for the diffusive wave flood routing problem with lateral inflow. *Hydrological processes*, 10(9), 1209-1227.
- Moussa, R., Bocquillon, C. (1996). Algorithms for solving the diffusive wave flood routing equation. *Hydrological Processes*, 10(1), 105-123.
- Moussa, R. (1997). Geomorphological transfer function calculated from digital elevation models for distributed hydrological modelling. *Hydrological processes*, 11(5), 429-449.
- Moussa, R., Bocquillon, C. (2001). Fractional-step method solution of diffusive wave equation. *Journal of Hydrologic Engineering*, 6(1), 11-19.
- Moussa, R. (2008). Effect of channel network topology, basin segmentation and rainfall spatial distribution on the geomorphologic instantaneous unit hydrograph transfer function. *Hydrological Processes*, 22(3), 395-419.

- National Weather Service (2005). NWSRFS User Manual Documentation, NWS Office of Hydrologic Development, Silver Spring, MD.
- Novak, P., Guinot, V., Jeffrey, A., Reeve, D. E. (2010). *Hydraulic modelling—an introduction: principles, methods and applications*. CRC Press.
- Ozisik, N. (1994). *Finite difference methods in heat transfer*. CRC press.
- Perumal, M., Sahoo, B. (2007). Applicability criteria of the variable parameter Muskingum stage and discharge routing methods. *Water resources research*, 43(5).
- Santillana, M., Dawson, C. (2010). A numerical approach to study the properties of solutions of the diffusive wave approximation of the shallow water equations. *Computational Geosciences*, 14(1), 31-53.
- Salkuyeh, D. K. (2006). On the finite difference approximation to the convection–diffusion equation. *Applied mathematics and computation*, 179(1), 79-86.
- Singh, V. P., Wang, G. T., Adrian, D. D. (1997). Flood routing based on diffusion wave equation using mixing cell method. *Hydrological processes*, 11(14), 1881-1894.
- Singh, V. P., Wang, G. T., Adrian, D. D. (1997). Flood routing based on diffusion wave equation using mixing cell method. *Hydrological processes*, 11(14), 1881-1894.

- Sivapalan, M., Bates, B. C., Larsen, J. E. (1997). A generalized, non-linear, diffusion wave equation: theoretical development and application. *Journal of Hydrology*, 192(1-4), 1-16.
- Subramanian, V. R., White, R. E. (2000). Symbolic solutions for boundary value problems using Maple. *Computers & Chemical Engineering*, 24(11), 2405-2416.
- Szymkiewicz, R. (2010). *Numerical modeling in open channel hydraulics* (Vol. 83). Springer Science & Business Media.
- Tingsanchali, T., Manandhar, S. K. (1985). Analytical diffusion model for flood routing. *Journal of hydraulic engineering*, 111(3), 435-454.
- Toprak, Z. F., Cigizoglu, H. K. (2008). Predicting longitudinal dispersion coefficient in natural streams by artificial intelligence methods. *Hydrological Processes*, 22(20), 4106-4129.
- Tsai, C. W. (2003). Applicability of kinematic, noninertia, and quasi-steady dynamic wave models to unsteady flow routing. *Journal of Hydraulic Engineering*, 129(8), 613-627.
- US Army Corps of Engineers (1991). A Muskingum-Cunge channel flow routing method for drainage networks. TP-135. US Army Corps of Engineers, Institute for Water Resources, Hydrologic Engineering Center, Davis, CA.

- Wang, G. T., Chen, S., Boll, J. (2003). A semianalytical solution of the Saint-Venant equations for channel flood routing. *Water Resources Research*, 39(4).
- Wang, G. T., Chen, S., Boll, J., Singh, V. P. (2003). Nonlinear convection-diffusion equation with mixing-cell method for channel flood routing. *Journal of Hydrologic Engineering*, 8(5), 259-265.
- Wang, L., Wu, J. Q., Elliot, W. J., Fiedler, F. R., Lapin, S. (2014). Linear diffusion-wave channel routing using a discrete Hayami convolution method. *Journal of Hydrology*, 509, 282-294.
- Wang, Q., Zhan, H. (2015). On different numerical inverse Laplace methods for solute transport problems. *Advances in Water Resources*, 75, 80-92.
- Wolfram Research, Inc: The Numerical Method of Lines. Retrieved April 16, 2017, from <https://reference.wolfram.com/language/tutorial/NDSolveMethodOfLines.html>
- Yen, B. C., Tsai, C. S. (2001). On noninertia wave versus diffusion wave in flood routing. *Journal of Hydrology*, 244(1), 97-104

Figures

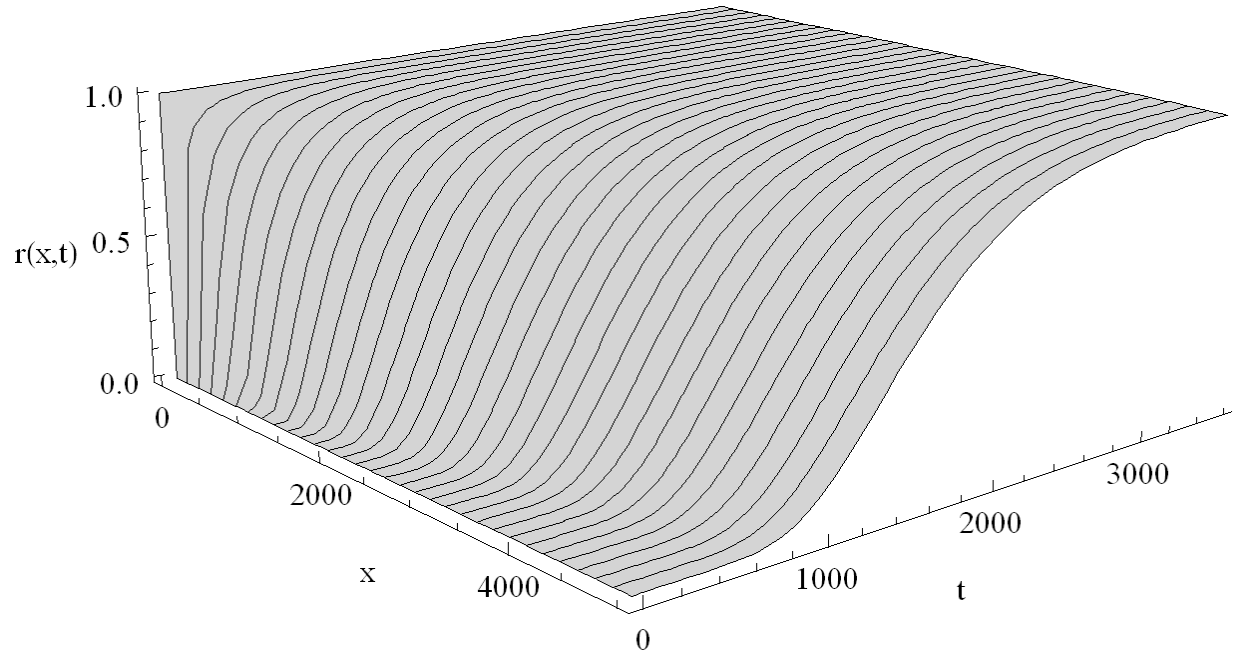


Figure 1 The unit response function for a semi-infinite channel with $C=3$ units and $D= 1000$ units.

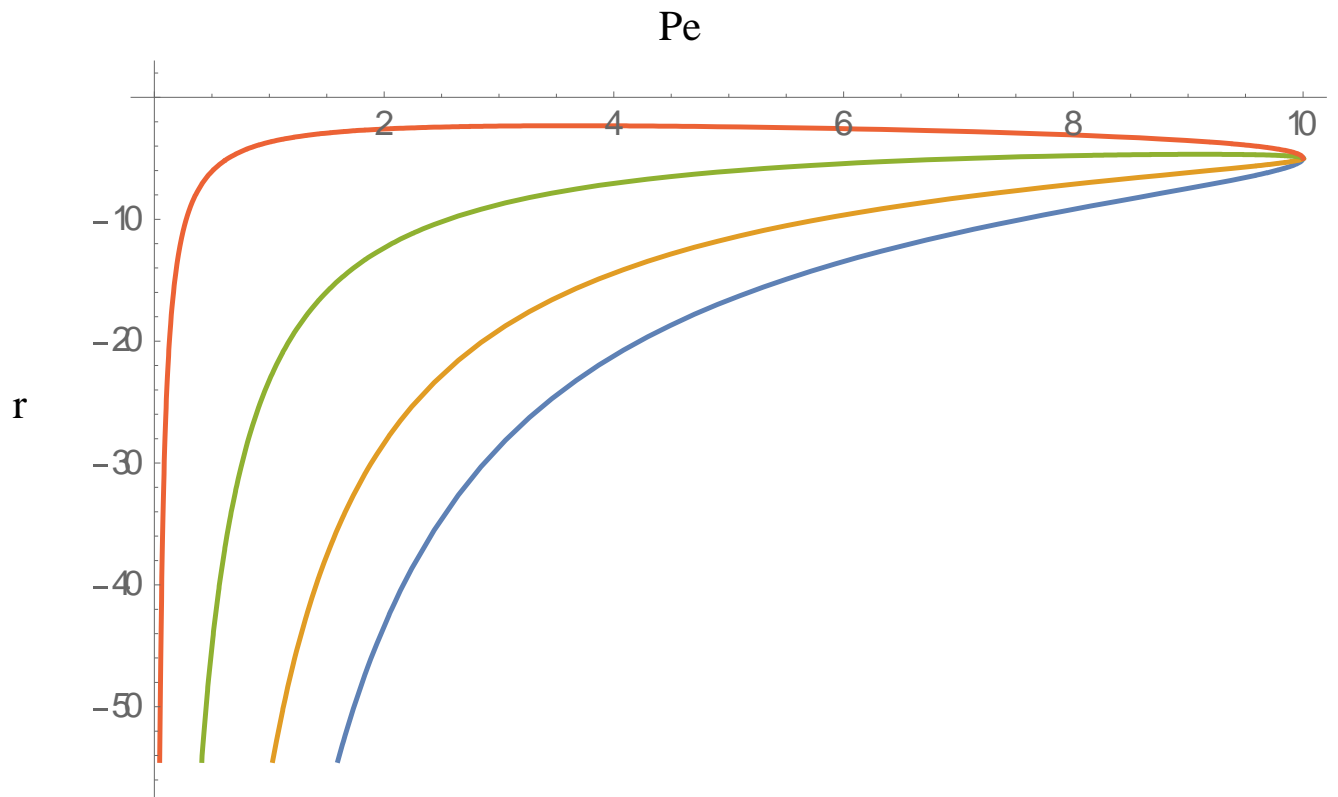


Figure 2 Roots of $\Omega(r) = 0$ for a different values of Peclet number

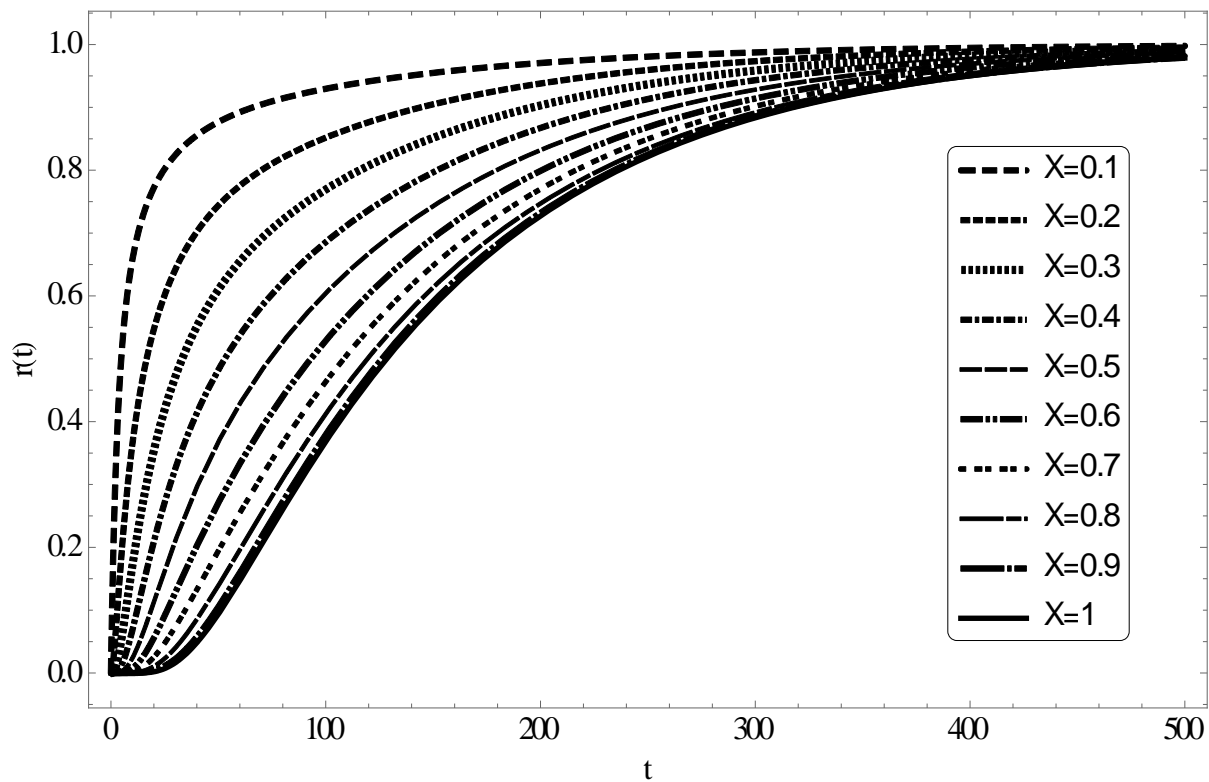


Figure 3 10-node LTCTDS derived unit response functions for $C=2.88$, $D=2000$, $q=0$, and $L=1000$.

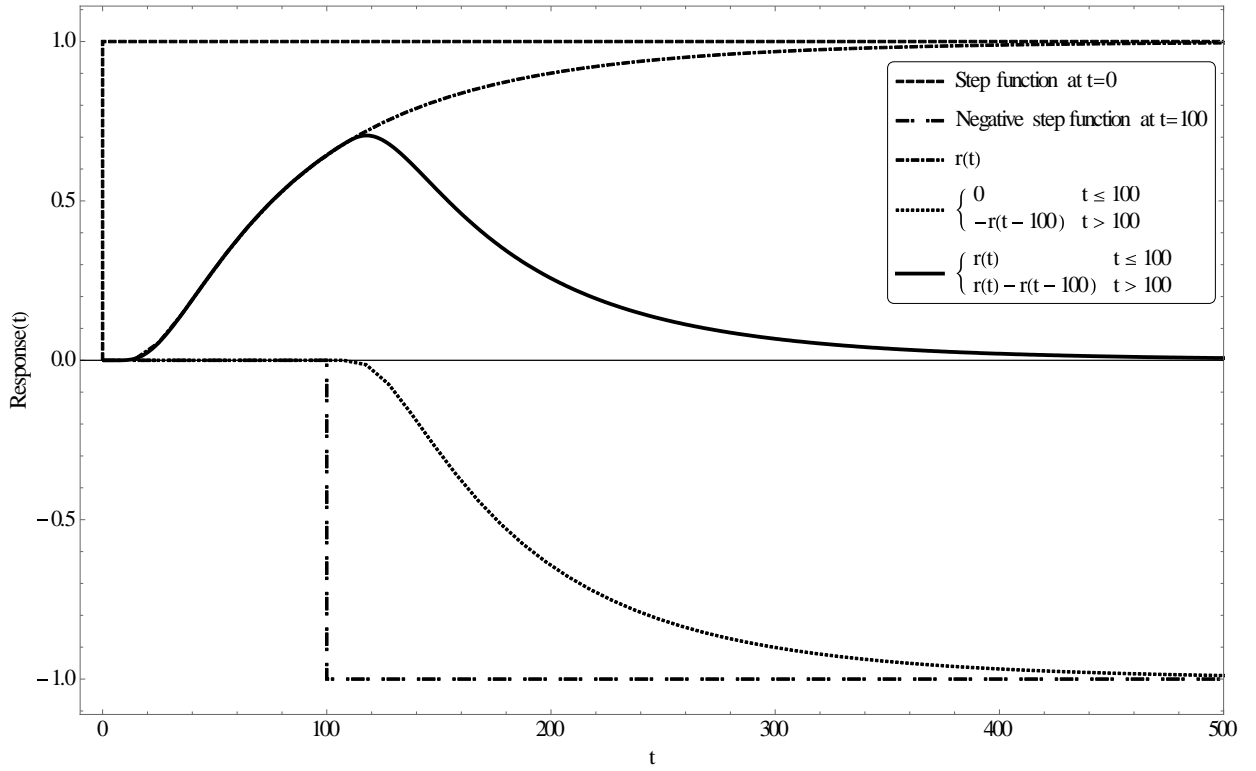


Figure 4 Illustration of system response to a pulse.

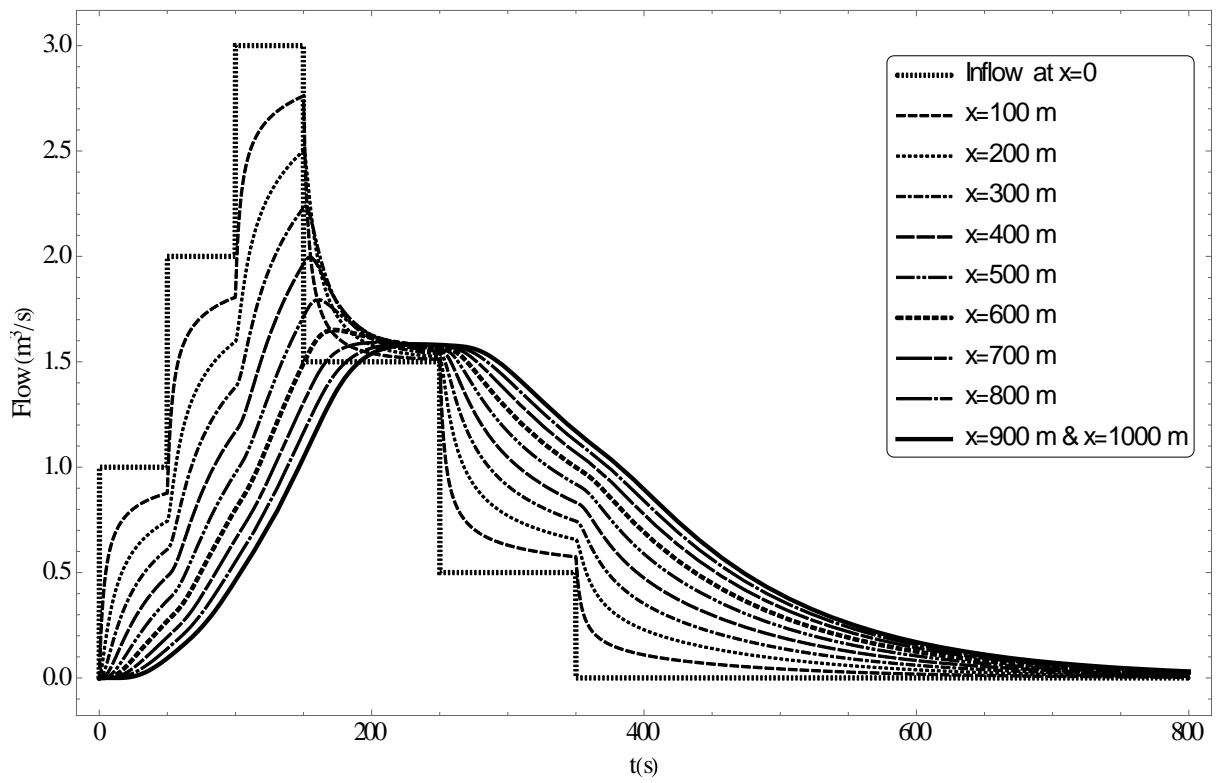


Figure 5 Results of 10-node LTCTDS derived response functions for a synthetic inflow with $C=2.88$, $D=2000$, $q=0$, and $L=1000$

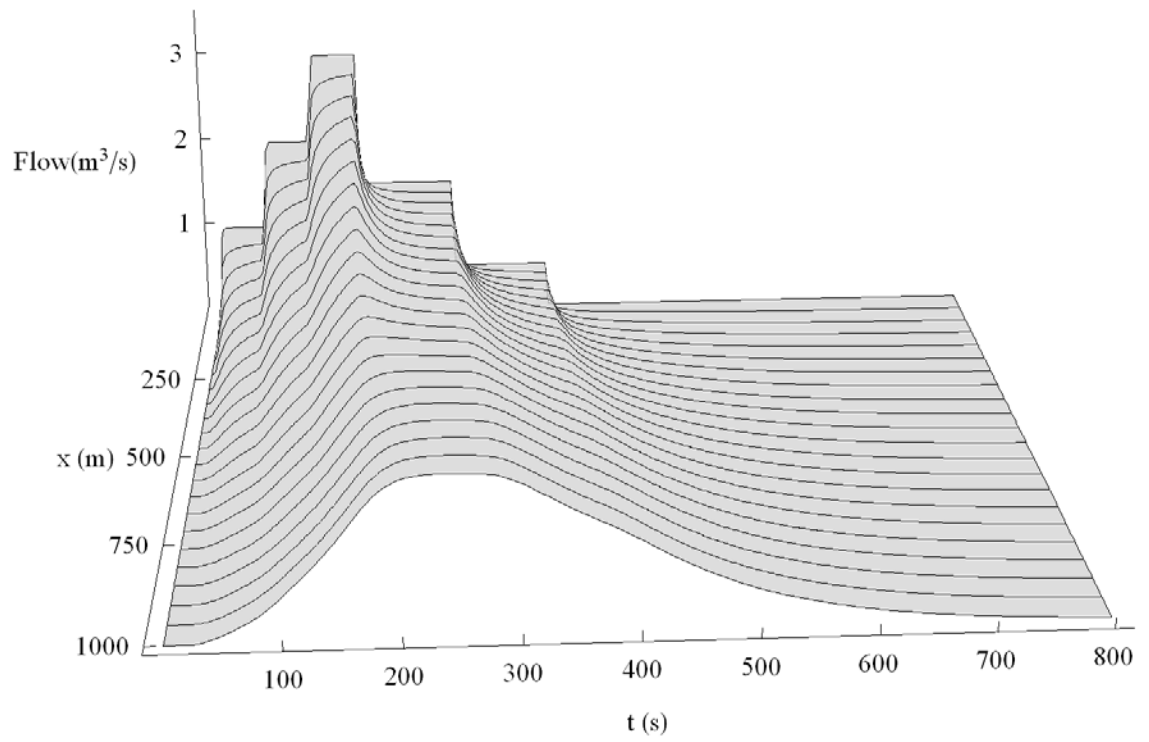


Figure 6 Numerical solution of the synthetic case study

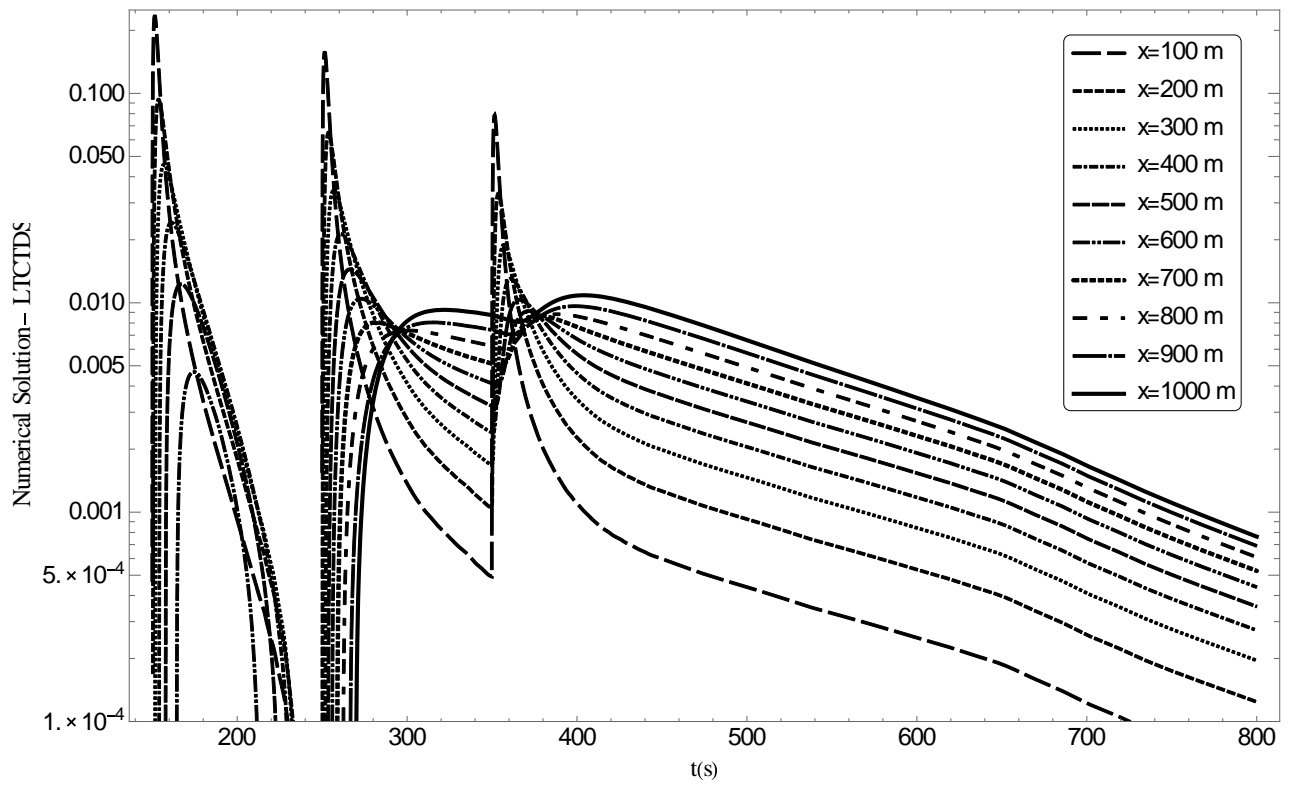


Figure 7 The difference between numerical solution and LTCTDS method.

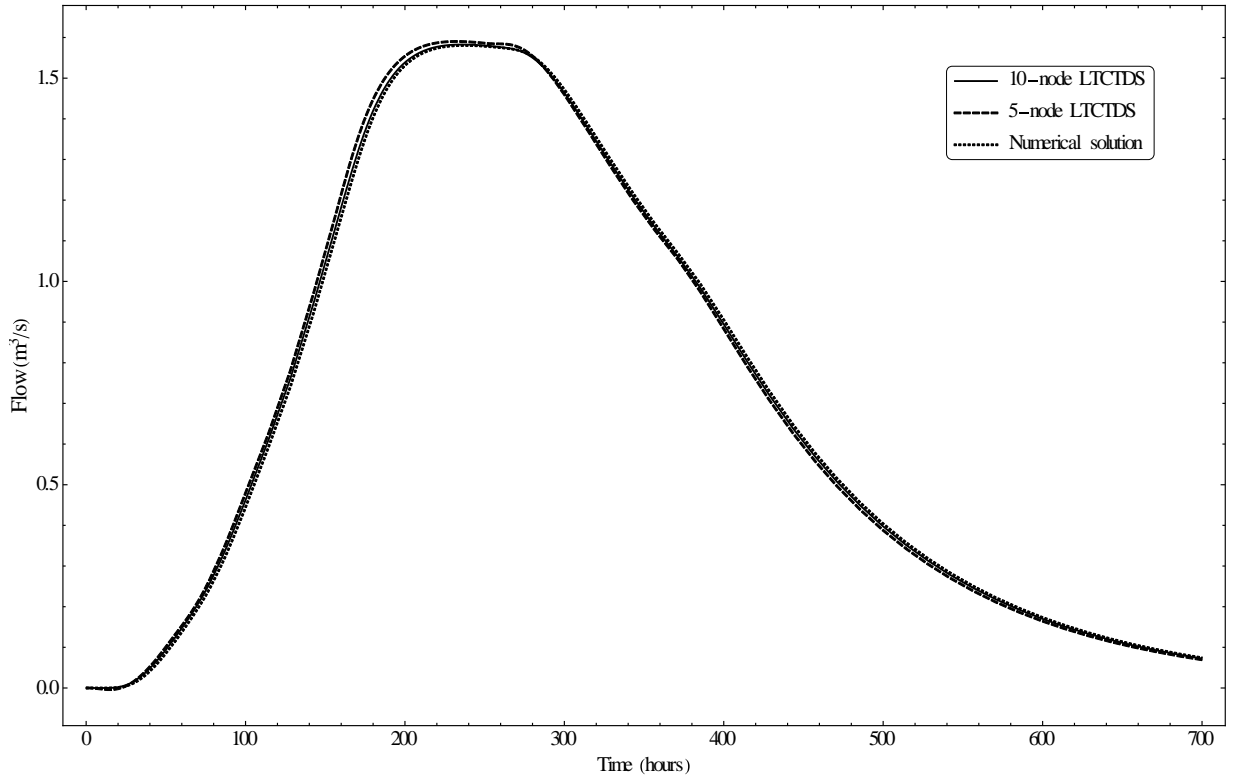


Figure 8 The difference between numerical solution, 10-node LTCTDS, and 5-node LTCTDS at the downstream section of the synthetic inflow example

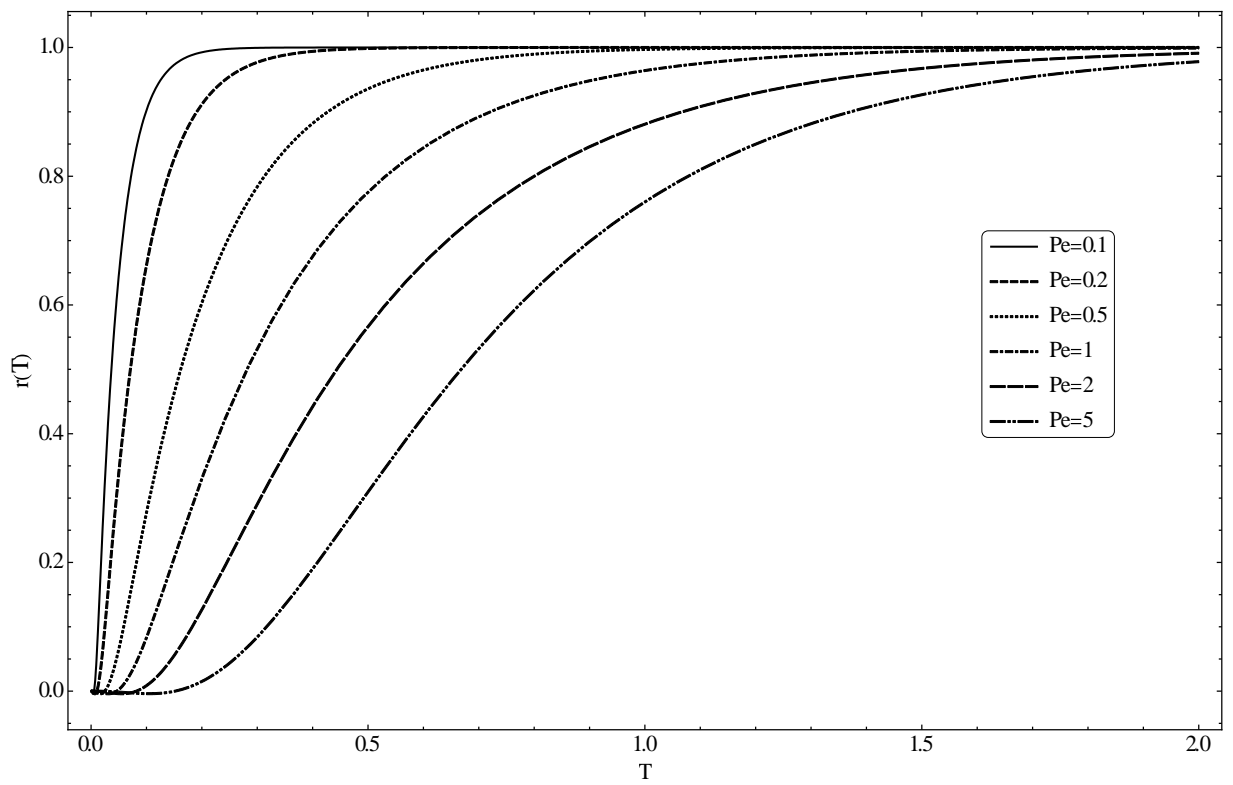


Figure 9 The effect of Peclet number on the 5-node LTCTDS derived unit response function

Pe = 1

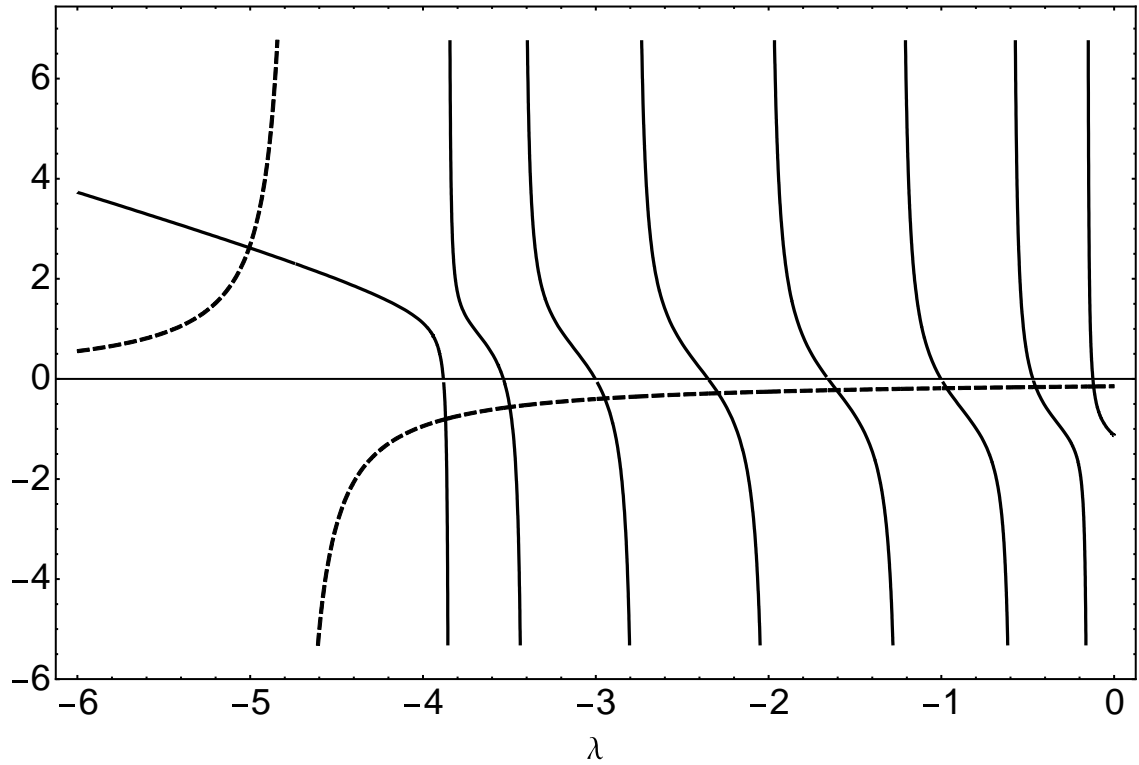
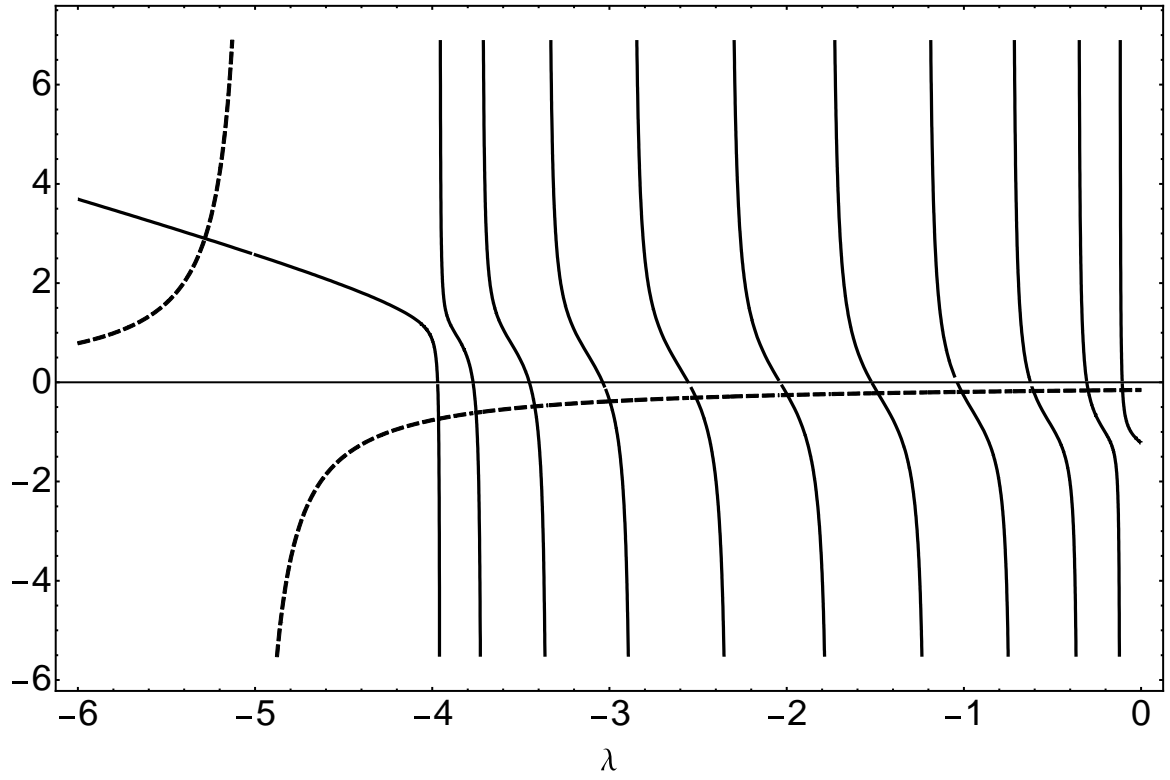


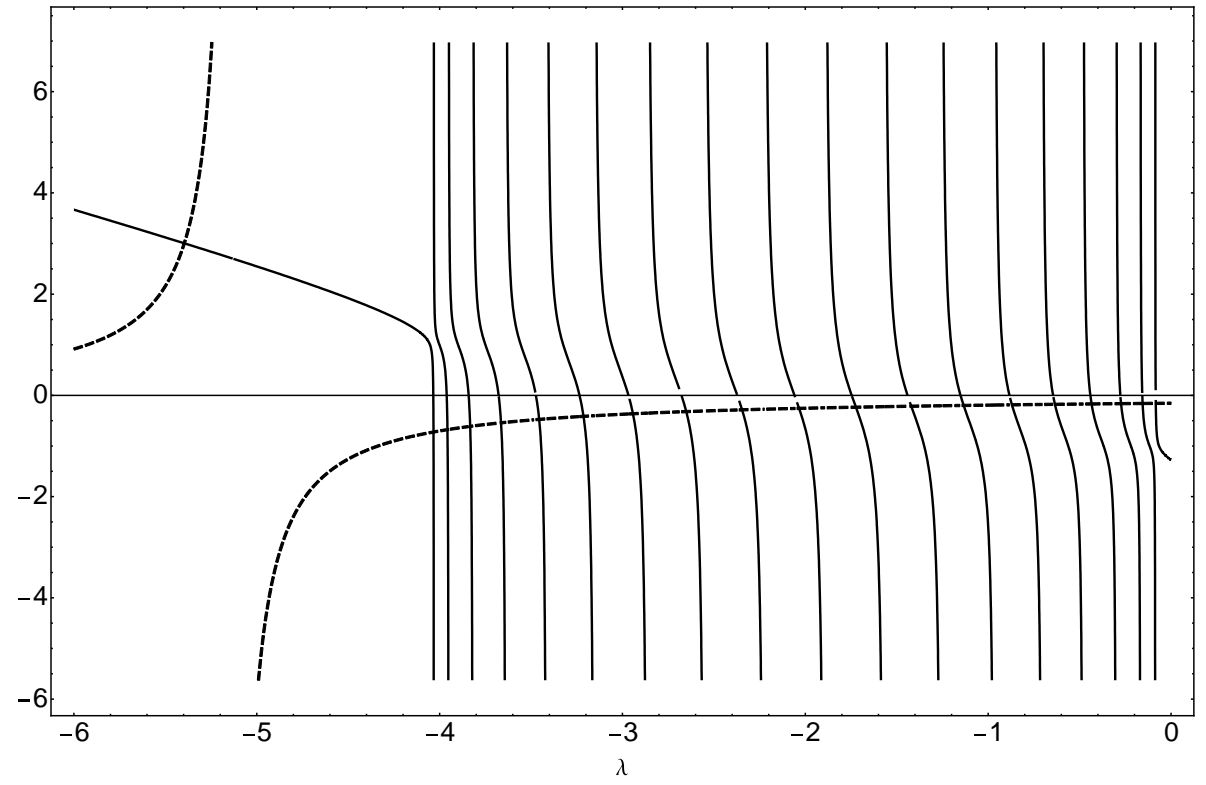
Figure 10 The eigenvalues of Matrix A can be determined by finding the intersections of the curves defined by the left hand side of the Eq. (44) depicted by solid lines and the curves defined by the right hand side of the Eq. (44) depicted by the dashed line are for a) $Pe=1$ and $N=9$

Pe=5



b) Pe=5 and N=12

Pe = 10



c) Pe=10 and N=20

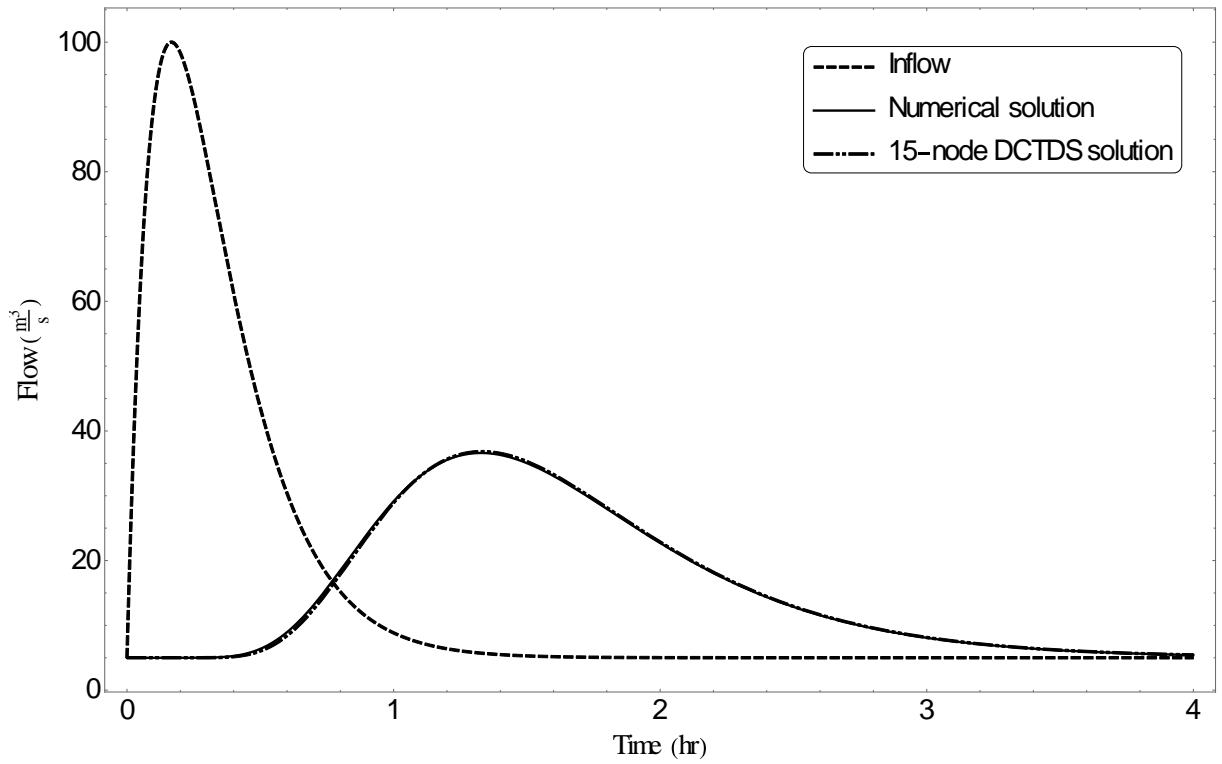


Figure 11 Comparison of the results of the 15-node DCTDS derived routed flood against the numerical solution. The hypothetical inflow defined by $Q_0(t) = 5 + 95 \left(\frac{t}{600}\right) e^{1-\left(\frac{t}{600}\right)}$ was used for this example.

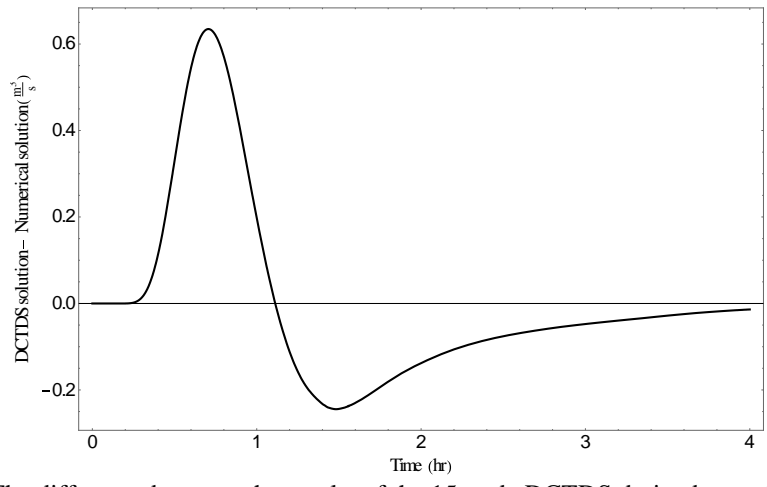


Figure 12 The difference between the results of the 15-node DCTDS derived routed flood and the numerical solution.

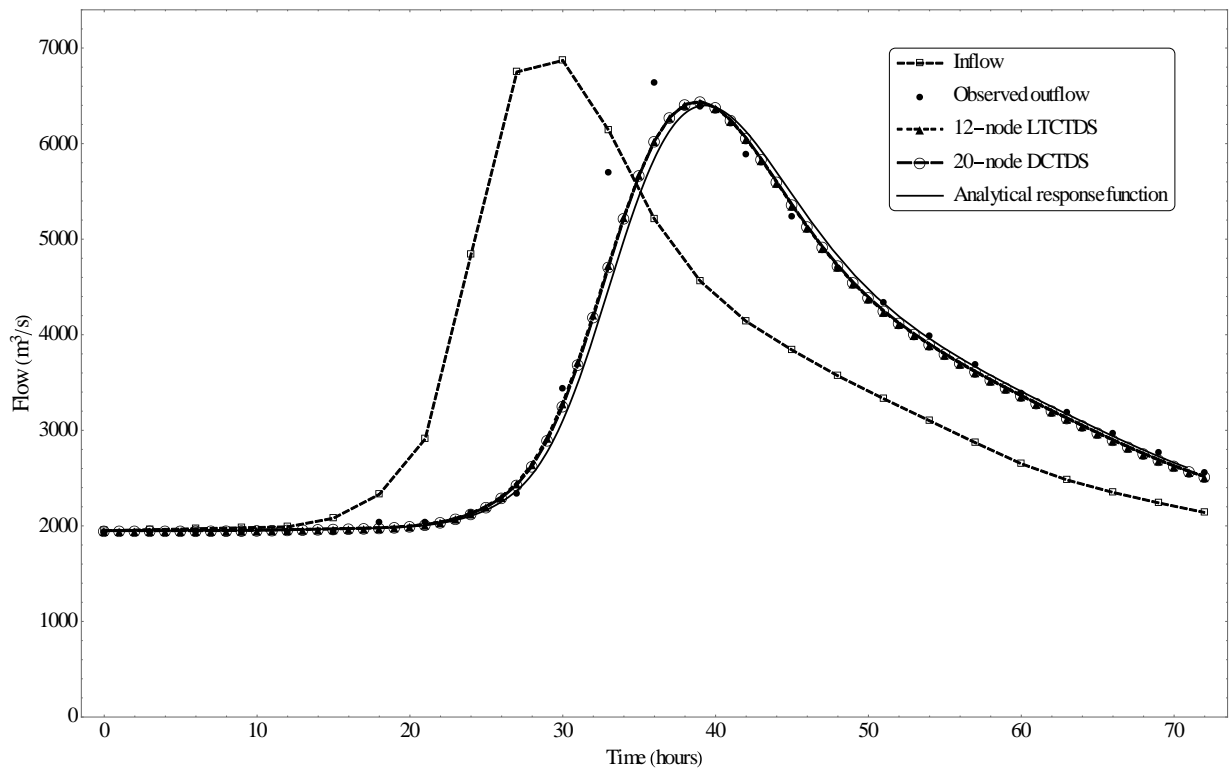


Figure 6 Application of the proposed methods for routing a flooding event that occurred in Yuanling- Wangjiahe River reach.

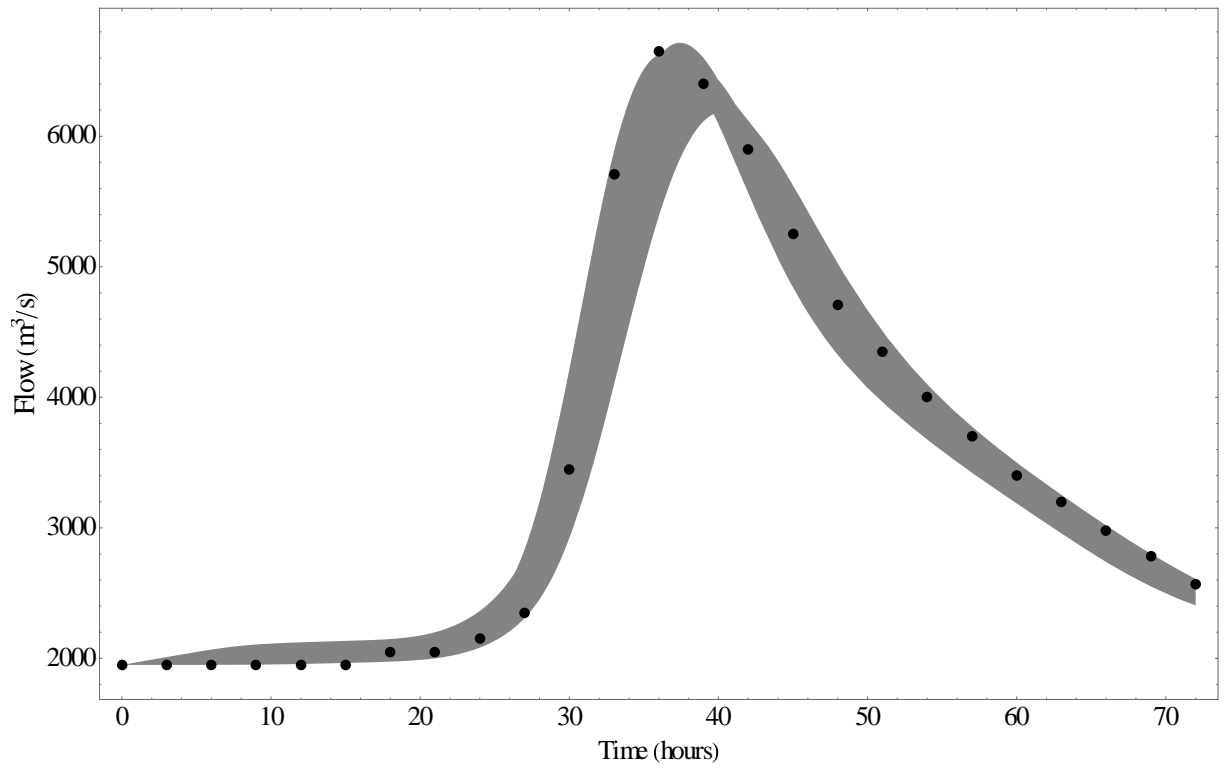


Figure 14 Envelope of downstream discharges produced by variation of C, D, and q

Pe=0.5

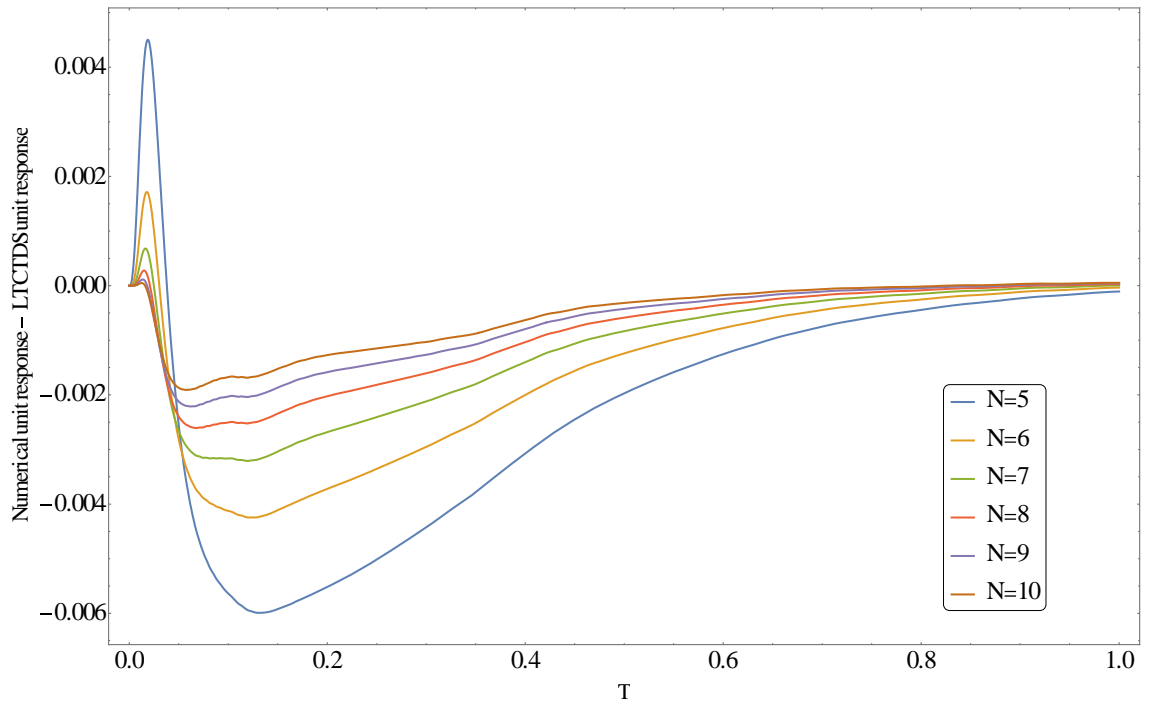


Figure 15 Sensitivity of the LTCTDS derived unit response function to N and Pe

Pe=1

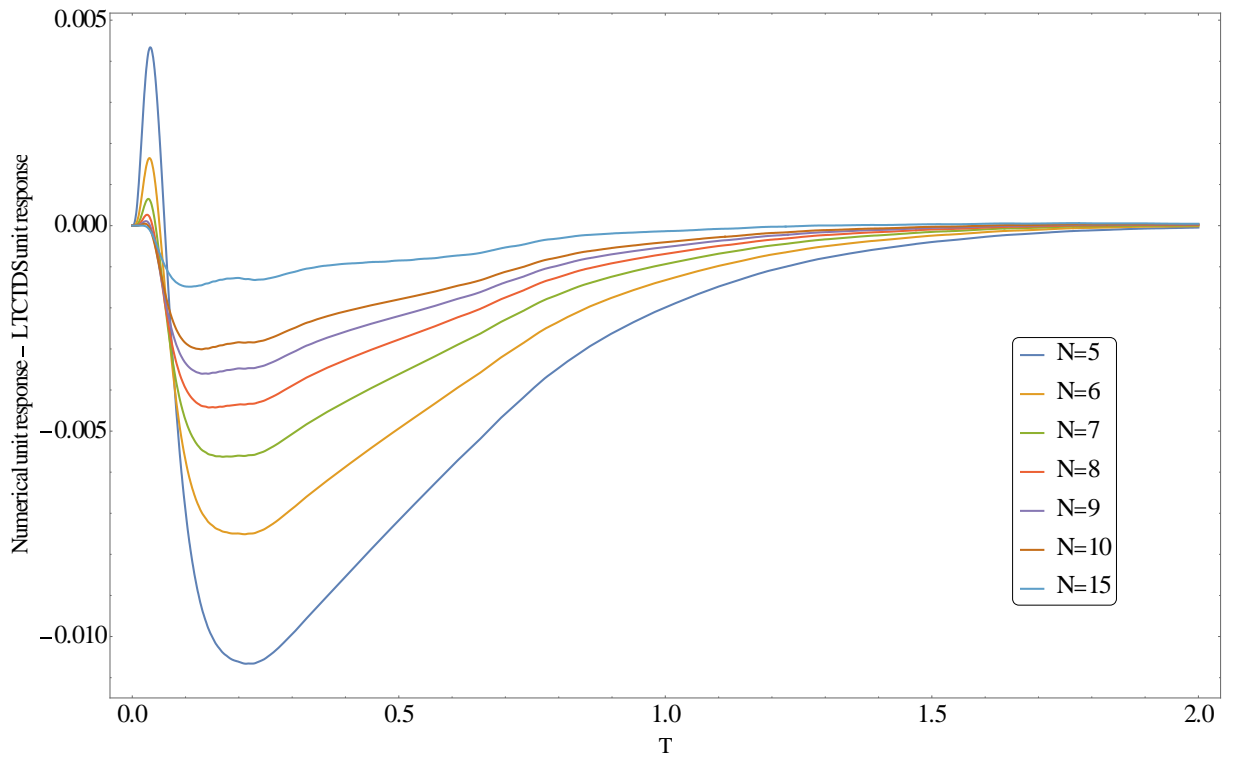


Figure 15 Sensitivity of the LTCTDS derived unit response function to N and Pe

Pe=5

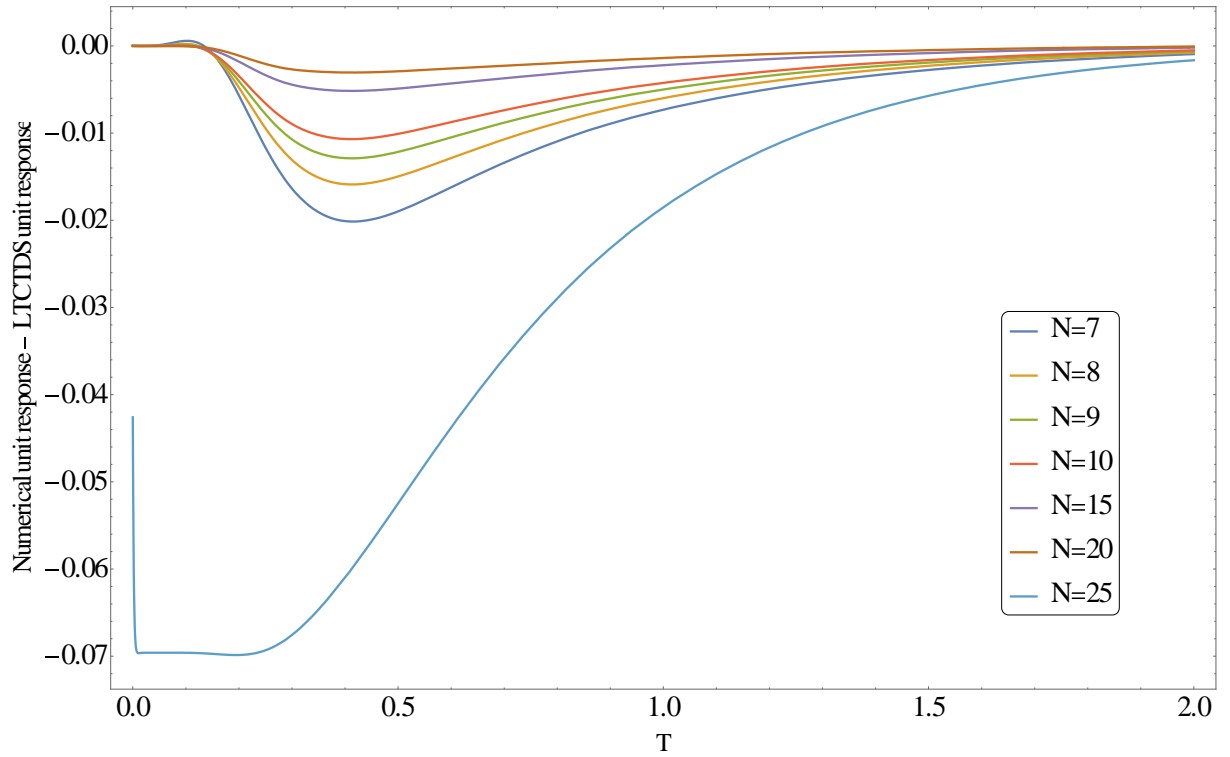


Figure 15 Sensitivity of the LTCTDS derived unit response function to N and Pe

Pe=11

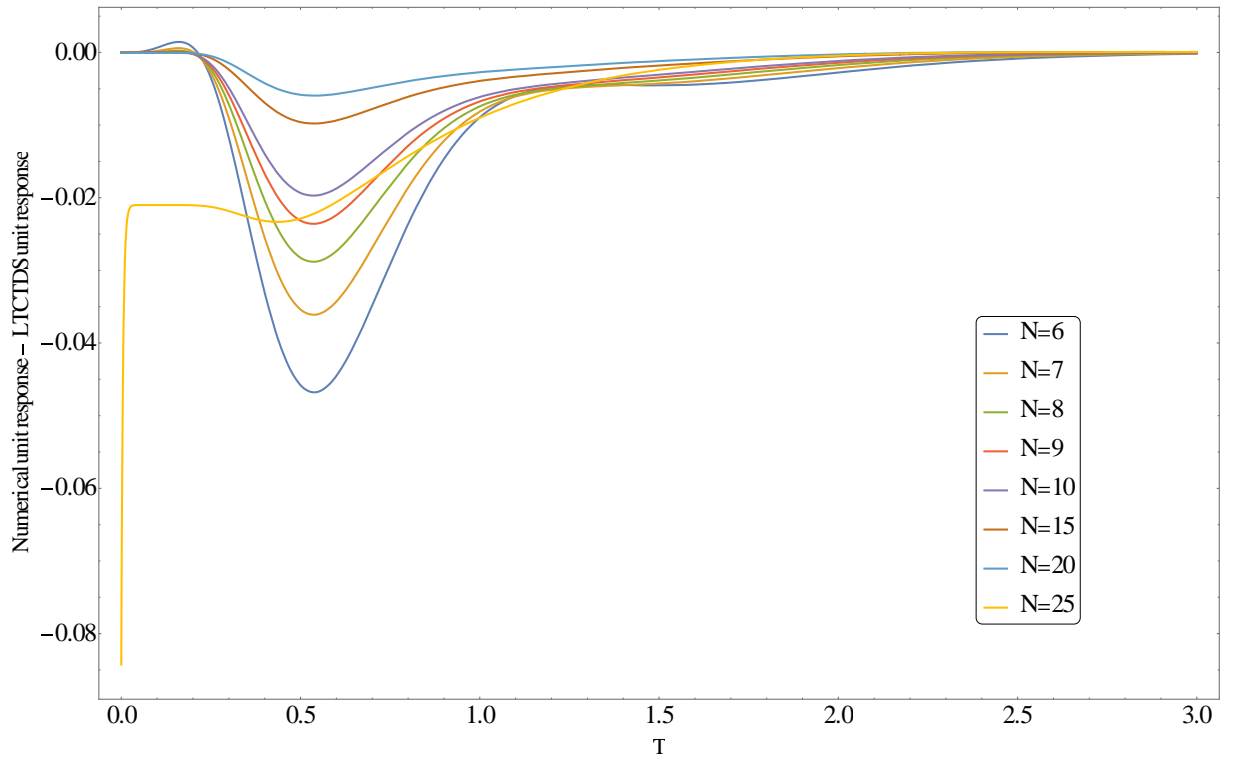


Figure 15 Sensitivity of the LTCTDS derived unit response function to N and Pe

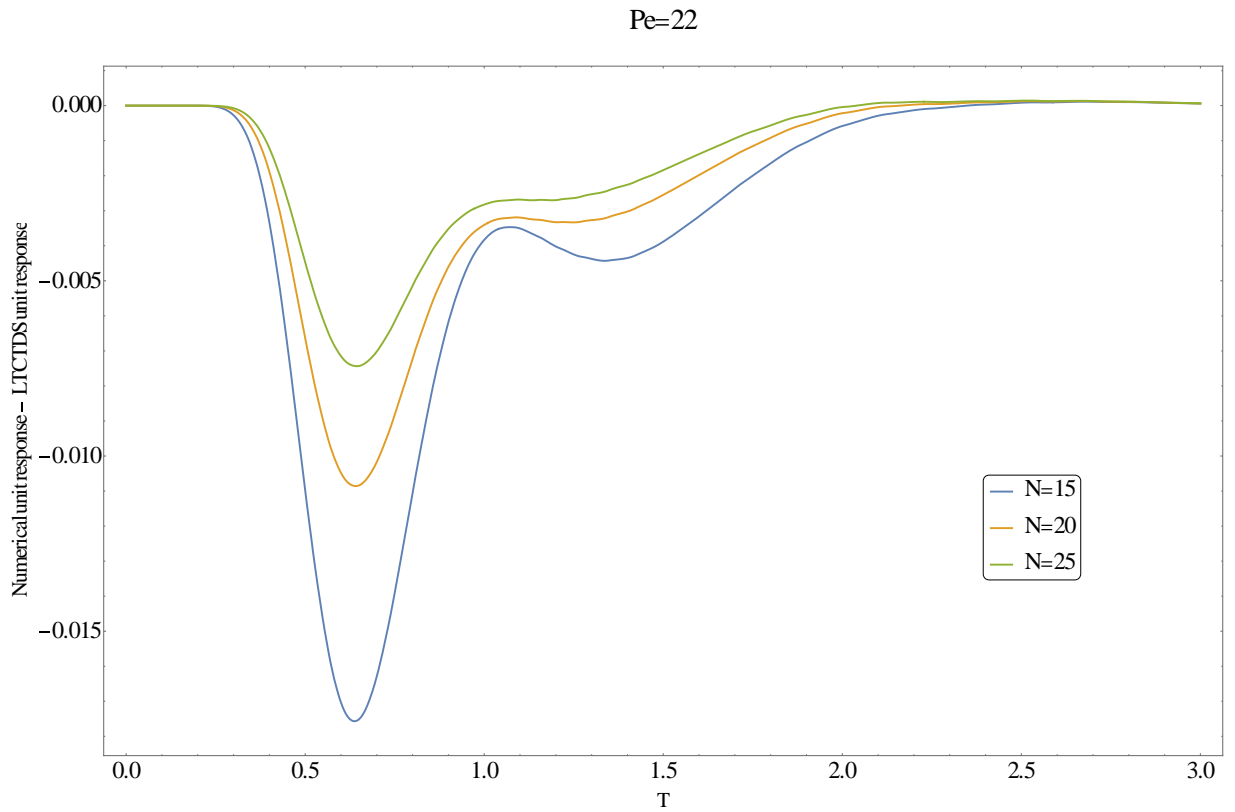


Figure 15 Sensitivity of the LTCTDS derived unit response function to N and Pe

Pe=0.5

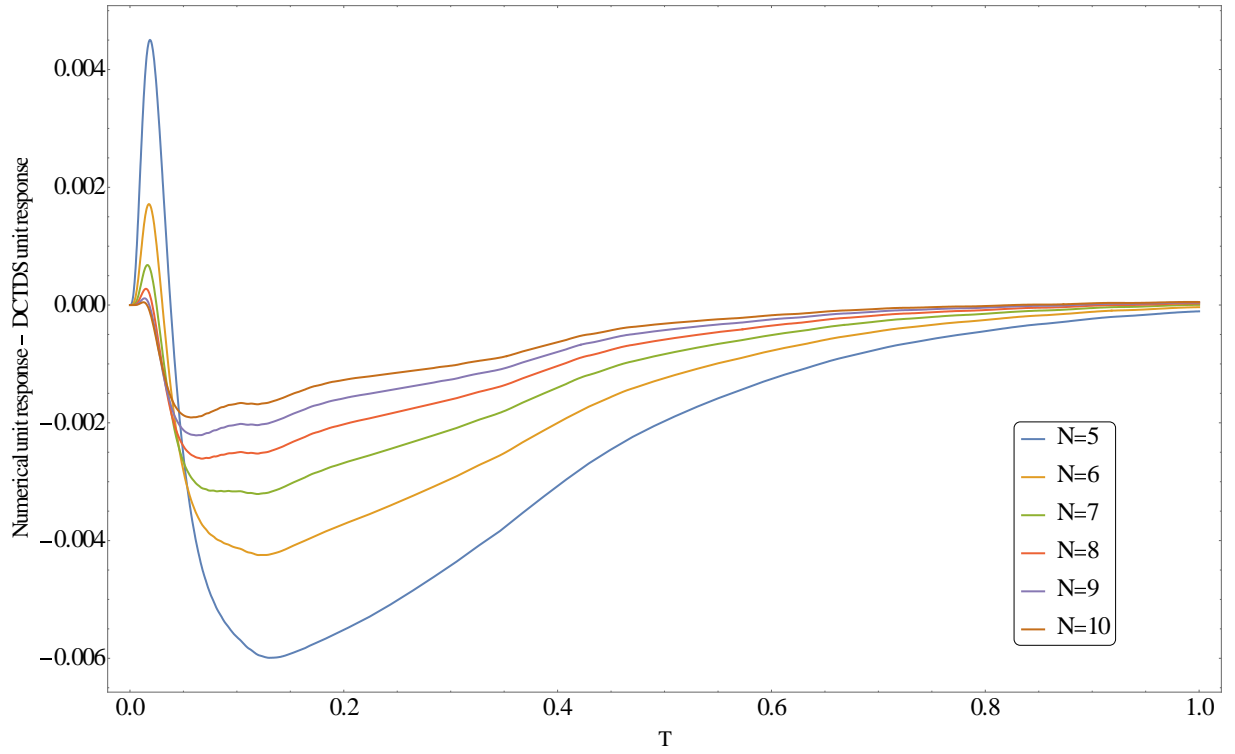


Figure 16 Sensitivity of the DCTDS derived unit response function to N and Pe

Pe=1

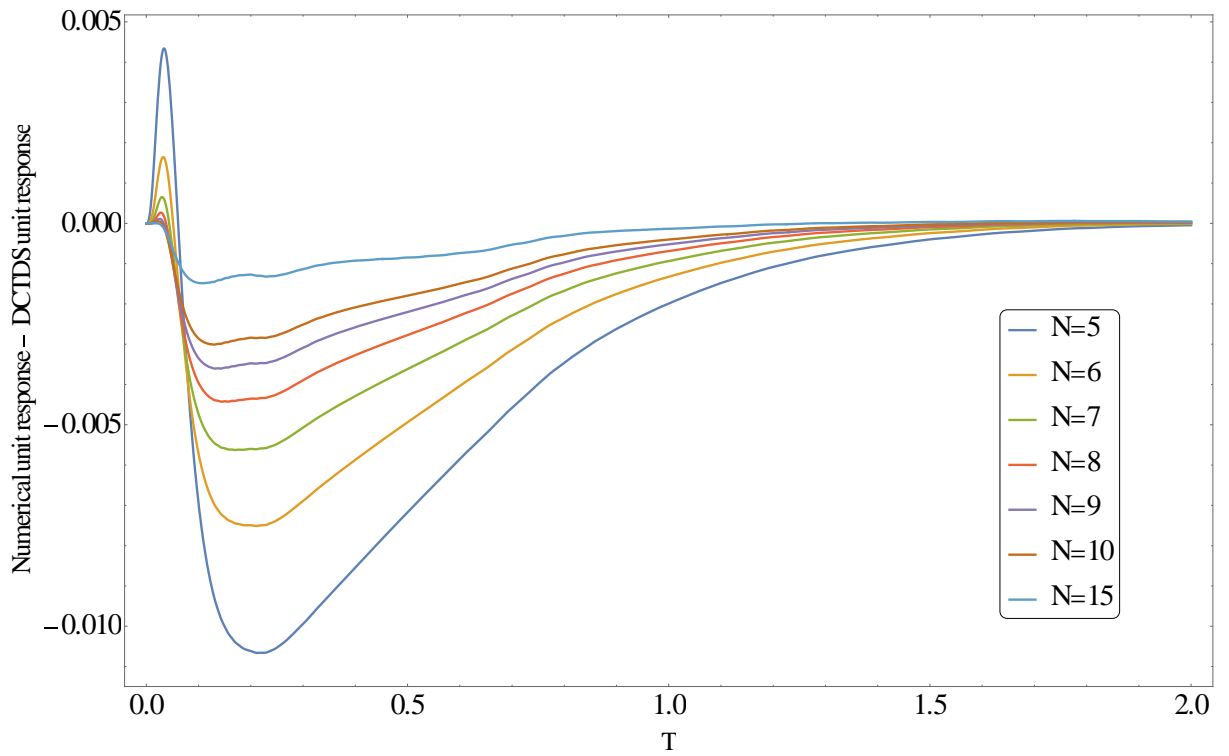


Figure 16 Sensitivity of the DCTDS derived unit response function to N and Pe

Pe=5

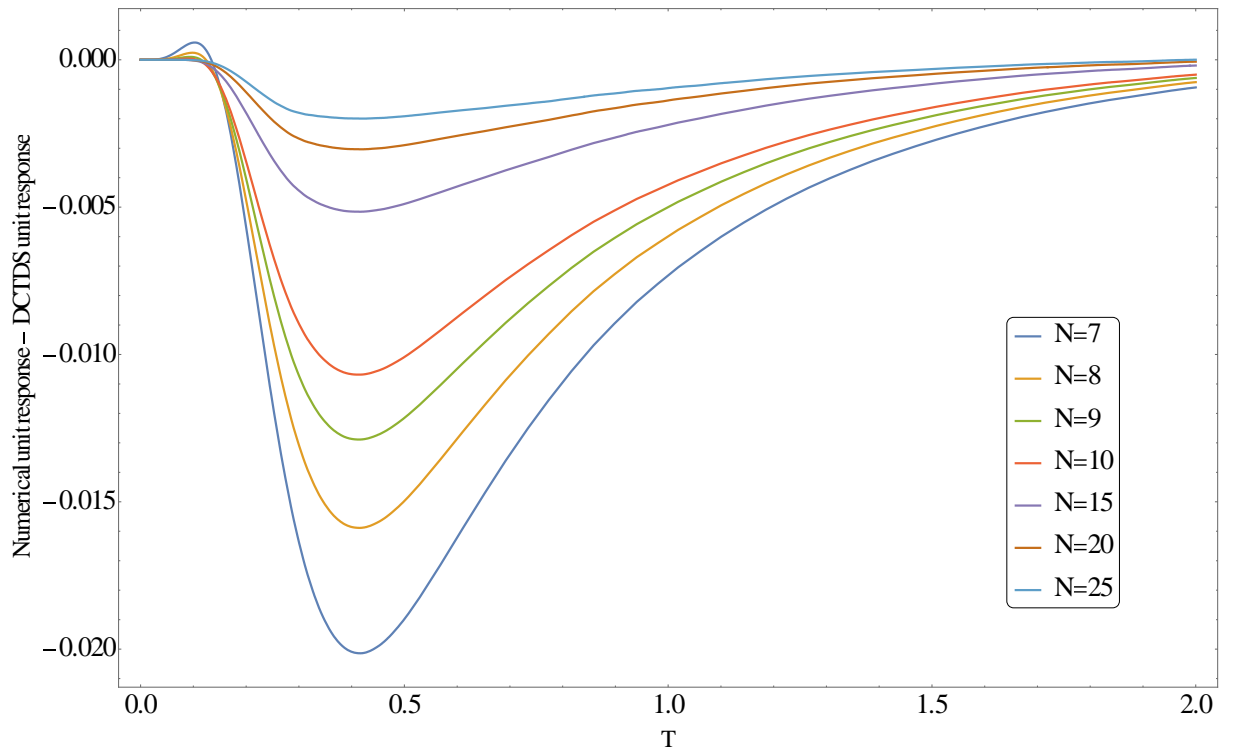


Figure 16 Sensitivity of the DCTDS derived unit response function to N and Pe

Pe=11

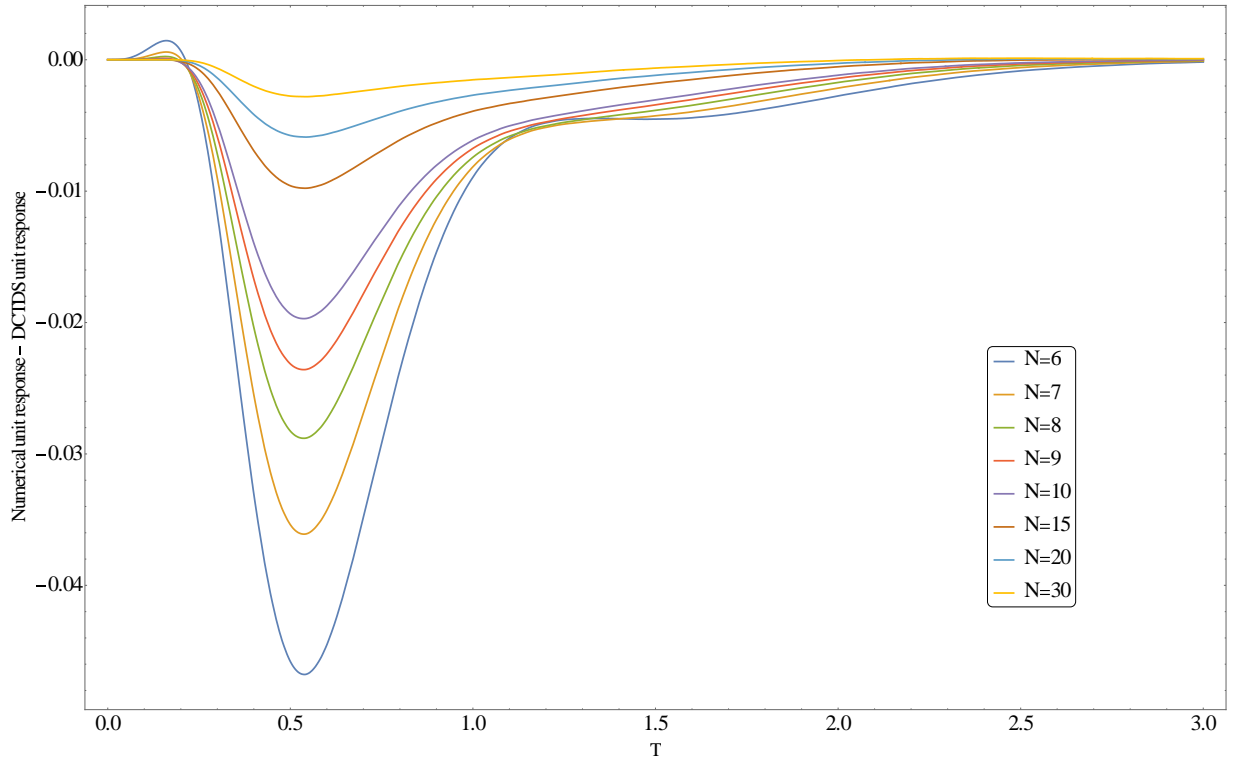


Figure 16 Sensitivity of the DCTDS derived unit response function to N and Pe

Pe=22

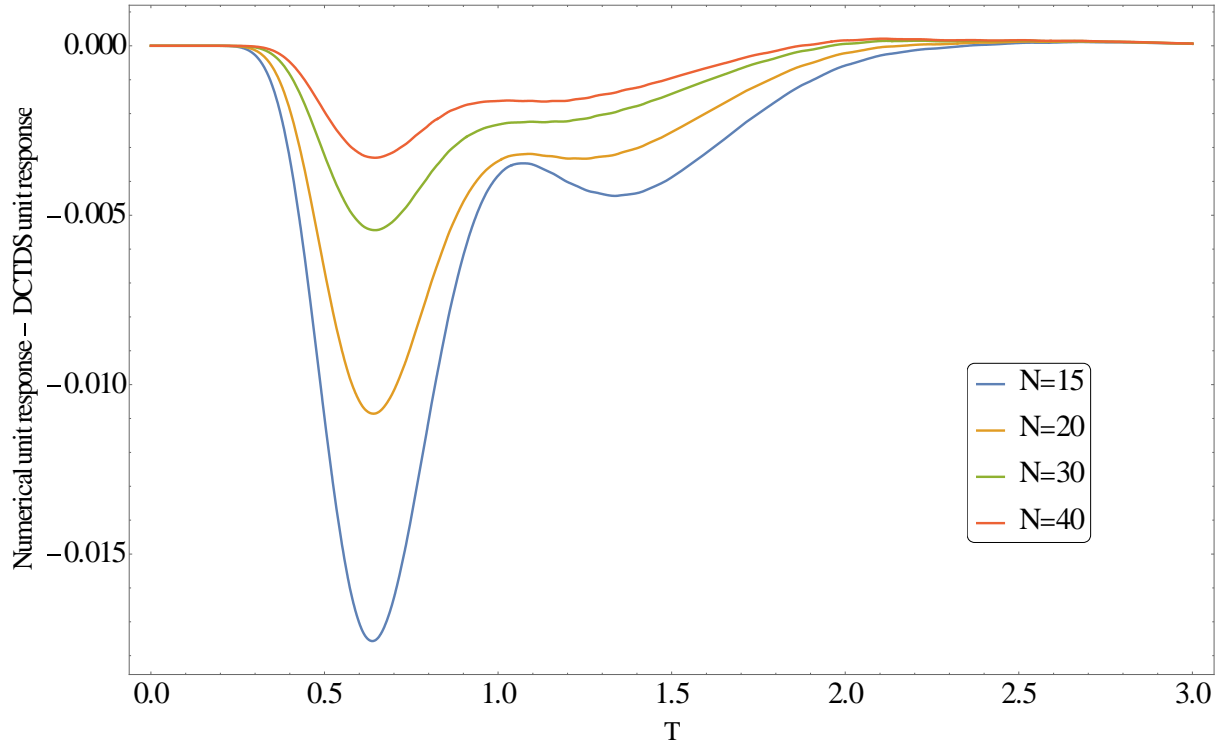


Figure 16 Sensitivity of the DCTDS derived unit response function to N and Pe

Table 1 Comparison of capabilities of different methods in solving diffusive wave equation

	LTCTDS	DCTDS	Numerical solutions	Analytical solution (semi-infinite)
Applicability in short channels	Yes	Yes	Yes	No
Applicability in long channels	Yes *	Yes *	Yes	No
Explicit expressions for solution	Yes	Yes	No	Yes
Capable of prescribing various boundary conditions	Yes	Yes	Yes	No
Ease of prescribing variable C and D	No	No	Yes	No
Ease of prescribing quasi-variable C and D	Yes**	Yes**	Yes	No
Stability (numerical artifacts, Courant condition, etc.)	Yes	Yes	No	Yes

* for very long channels, multiple sub-divisions might be needed

** at every time step, C and D can be updated according to the new inflow values

Chapter 4

ANALYTICAL SOLUTION FOR NONLINEAR RESERVOIR ROUTING WITH POWER-LAW STORAGE FUNCTION

Behzad Nazari and Dong-Jun Seo

Abstract

A new direct solution for nonlinear reservoir routing with a general power-law storage function is presented. The resulting implicit solution is expressed in terms of the incomplete Beta function and is valid for inflow hydrographs that may be approximated by a series of pulses of finite duration. A separate solution for zero inflow representing recession is also presented. The new solution extends the previous results reported in the literature which provide direct solutions only for certain exponents in the power-law storage function. In addition to the wide spectrum of applications that require modeling of nonlinear reservoirs or open channels, the direct solution may also be used for physically-based semi-distributed routing of hillslope flow following simplification of the flow paths as a dendritic network of nonlinear reservoirs. This paper presents the solutions and illustrative examples of application.

1 Introduction

Hydraulic modelling involves solving the governing equations for conservation of mass and momentum, i.e., the Saint Venant equations (*Chanson, 2004*) and is the most accurate method for flood routing in theory (*Kim and Georgakakos, 2014*). However, hydraulic routing models require large amounts of data to prescribe the fixed boundary conditions (BC) of channel geometry along the

reach and elaborate numerical integration to ensure accuracy and convergence (Szymkiewicz, 2010).

On the other hand, hydrologic routing models, despite being less theoretically detailed (McCuen (1989)), are usually more feasible for large scale systems in practice (Kim and Georgakakos, 2014). There exist many choices of hydrologic routing models depending on their underlying theoretical framework, availability of data, accuracy requirements, computational efficiency, etc. Kim and Georgakakos (2014) provide a review of the hydrologic routing methods including linear reservoir, Muskingum method, Lag and K method, Muskingum-Cunge method, and nonlinear cascade reservoirs. Storage-based channel or reservoir routing models are among the oldest and most widely used conceptual models in hydrology (Nourani *et al.*, 2009). Fread and Hsu (1993) discuss the errors associated with using storage routing methods in operational flood routing. In storage routing methods, the continuity equation for hydrologic routing is described by the following differential equation (Xiong and Melching, 2005):

$$\frac{d}{dt}S(t) = I(t) - O(t) \quad (1)$$

where $I(t)$, $O(t)$, and $S(t)$ denote the inflow, outflow and storage at time t , respectively. In most real-world applications, the storage and outflow are not known jointly and hence an additional equation is needed to solve Eq. (1). This closing equation usually relates storage and discharge and is referred to as the

storage–outflow relationship (Chow *et al.*, 1988) or storage function (Sugiyama *et al.*, 1997). Numerous studies (see Boyd *et al.*, 1979; Basha, 1994; Basha, 1995; Tallaksen, 1995; Sugiyama *et al.*, 1997; and Basha, 2000 just to name several) have postulated that the storage function can in general be expressed as the following power-law function:

$$S = kQ^m \quad (2)$$

where S and Q denote the storage and outflow, respectively, and k and m denote the storage coefficient and exponent, respectively. In stating Eq.(2), we assume that the storage function is time-invariant and hence S is a proper function of Q . If $m=1$, the storage function becomes linear which renders Eq.(1) a linear reservoir routing problem. Linear storage models are simple and easy to parametrize. However, most hydrological systems do not show a linear storage behavior in practice (Kim and Georgakakos, 2014; Niazkar and Afzali, 2017). To overcome this limitation, Nash (1957) and many others have developed various hydrological models by adopting the concept of cascading such linear reservoirs (Chow *et al.*, 1988) also known as multilinear methods (Perumal, 1992; Camacho and Lees, 1999; Sahoo, 2013).

If $m \neq 1$, the problem becomes one of nonlinear reservoir routing. Basha (1995) offers an approximate solution for nonlinear routing by using perturbation expansion around the parameter m . Glynn and Glynn (1996) presented another diffusion approximation for a network of nonlinear reservoirs with power-law

release rules. To the best of the authors' knowledge, however, no exact solutions to the above problem have been reported to date in the literature. In fact, *Hughes and Murrell* (1986) claimed that for non-zero inflows, no analytical solution to this problem exists unless m is $1/2$ or 1 . They presented several numerical solution methods and postulated that the accuracy of solution depends on the magnitude of time interval in the numerical integration.

In this work, we present an exact implicit solution for nonlinear routing of Eq. (1) with the power-law storage function of Eq. (2). Because it is exact, the solution is not subject to possible instabilities due, e.g., to too large time steps as in numerical methods, and hence provides a significant addition to the suite of methods available for reservoir and channel routing. When parametrized, the proposed solution can be useful in practical modeling, design, forecasting and control problems when applied to single reservoirs, cascade of reservoirs, and network of channels. In fact, with an extension of the transfer function analogy (*Chow et al.*, 1988; *McCuen*, 1989) of hydrological processes, the proposed methodology can be applied to any system with elements that can be approximated by power-type storage functions. The outflow from each component will be the inflow of the next element.

A very useful consequence of such a system analysis approach is its application in nonlinear channel routing in networks. In fact, the hillslopes can be considered as such networks, even in ungagged basins.

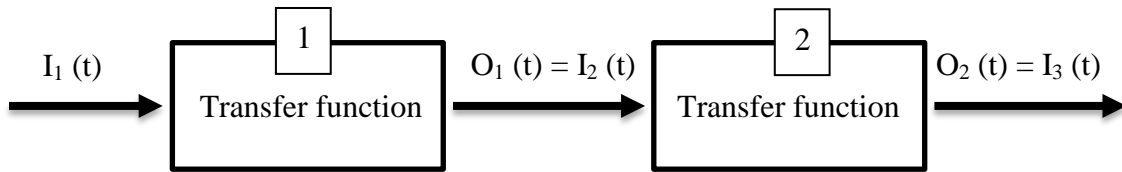


Figure 1 A general cascade approach for modelling hydrological systems.

In this work, we will improve a methodology based on coupling of mass and momentum conservation equations that has been widely used for distributed nonlinear flood routing in networks (see Gupta *and* Waymire, 1998; Reggiani *et al.*, 2001; Menabde and Sivapalan, 2001; Gupta, 2004; Mantilla and Gupta, 2005; Mantilla *et al.*, 2006; Mandapaka *et al.*, 2009; Small *et al.*, 2013; Ayalew *et al.*, 2014; Choi *et al.*, 2015 among many others). In the present work, a general formulation for determining the parameters of power-type storage function using hydraulic properties of channels is developed. This step enables the modelers to apply the proposed exact implicit solution to the dynamic routing equation. The presented routing method can be parametrized either by using statistical methods (similar to the Muskingum method) or hydraulic properties of the channels (similar to the Muskingum-Cunge method) with an additional advantage of offering an exact solution to the governing nonlinear and nonhomogeneous ordinary differential equation.

This paper is organized as follows: In section 2, the implicit exact solution of the nonlinear routing problem described by Eqs. (1) and (2) will be presented. In sections 3, general equations for determining the parameters of power-type

storage functions in several typical routing problems will be presented . Sections 4 demonstrate example applications of the proposed method for several routing problems, and finally, conclusions and recommendations for future works will be discussed in section 5.

2 Exact solution for routing problem with a power-type storage function

Using the chain rule, one may rearrange Eq. (1) as:

$$\frac{dQ}{dt} = \frac{I(t) - Q(t)}{\frac{dS}{dQ}} \quad (3)$$

If the storage function is of the power-law type of Eq. (2), there exist real-valued parameters a and b that satisfy:

$$\frac{1}{\frac{dS}{dQ}} = aQ^b \quad (4)$$

Combining Eqs. (3) and (4) gives the following nonhomogeneous nonlinear ordinary differential equation:

$$\frac{d}{dt} Q(t) = aQ(t)^b(I(t) - Q(t)) \quad (5)$$

2.1 Non-zero inflow

For a sufficiently short time interval over which the inflow may be assumed constant, or $I(t) = r$, and $r \neq 0$, Eq.(5) may be rearranged to the following form via separation of variables:

$$\frac{dQ}{Q^b(r-Q)} = a dt \quad (6)$$

Denoting the initial condition (IC) of Eq. (6) as $Q(t_0) = Q_0$ and integrating both sides, we have:

$$\int_{Q_0}^Q \frac{dQ}{Q^b(r-Q)} = a \int_{t_0}^t dt \quad (7)$$

After integrating the left hand side of Eq. (7) using Mathematica software package 10.3 (Wolfram Research, Inc., 2015) and manual manipulation of the obtained expressions, the following exact implicit solution was obtained:

$$\begin{aligned} Q_0^{1-b} {}_2F_1\left(1, 1-b; 2-b; \frac{Q_0}{r}\right) - Q^{1-b} {}_2F_1\left(1, 1-b; 2-b; \frac{Q}{r}\right) \\ = a(b-1)r(t-t_0) \end{aligned} \quad (8)$$

In the above ${}_2F_1$ is the hypergeometric function defined as (Weisstein, 2002b; Gradshteyn and Ryzhik, 2014):

$$\begin{aligned} {}_2F_1(x_1, x_2; x_3; x_4) \\ = \frac{\Gamma(x_3)}{\Gamma(x_2)\Gamma(x_3-x_2)} \int_0^1 \frac{s^{x_2-1}(1-s)^{x_3-x_2-1}}{(1-x_4s)^{x_1}} ds \end{aligned} \quad (9)$$

In Eq.(9), $\Gamma(x)$ is the Gamma function defined as (Weisstein, 2002a):

$$\Gamma(x) = \int_0^\infty s^{x-1} e^{-s} ds \quad (10)$$

On the other hand, the incomplete Beta function (see Figs 2 and 3) is defined as (Weisstein, 2003):

$$B_x(u, v) = \int_0^x s^{u-1}(1-s)^{v-1} ds \quad (11)$$

which has the following relationship with the hypergeometric function ${}_2F_1$ (Weisstein, 2003)

$$B_x(u, v) = \frac{x^u}{u} {}_2F_1(u, 1-v; u+1; x) \quad (12)$$

Accordingly, using Mathematica, Eq. (8) can be further simplified to the following implicit solution for $Q(t)$:

$$B_{\frac{Q}{r}}(1-b, 0) - B_{\frac{Q_0}{r}}(1-b, 0) = a r^b (t - t_0) \quad (13)$$

Eq. (13) may be used to obtain Q for different values of t as long as the inflow is constant. For the next pulse of inflow, r_{i+1} , Eq. (13) may be reinitialized by using Q obtained from the previous inflow r_i . Solving for Q in Eq.(13) amounts to nonlinear root finding for which a combination of look-up tables for evaluation of the incomplete Beta functions and iterative root finding may be used. In this work, Eq.(13) was solved using the Mathematica. Note that, if $\frac{Q}{r} > 1$, which occurs when the discharge is larger than the inflow, each incomplete Beta function in the right-hand side of Eq.(13) includes an imaginary term of $-\pi i$ which gets cancelled out. Fig 2 shows the incomplete Beta function for various values of b in the real domain of $0 < x < 1$ and Fig 3 shows the real component of the incomplete Beta function for various values of b for $1 < x$.

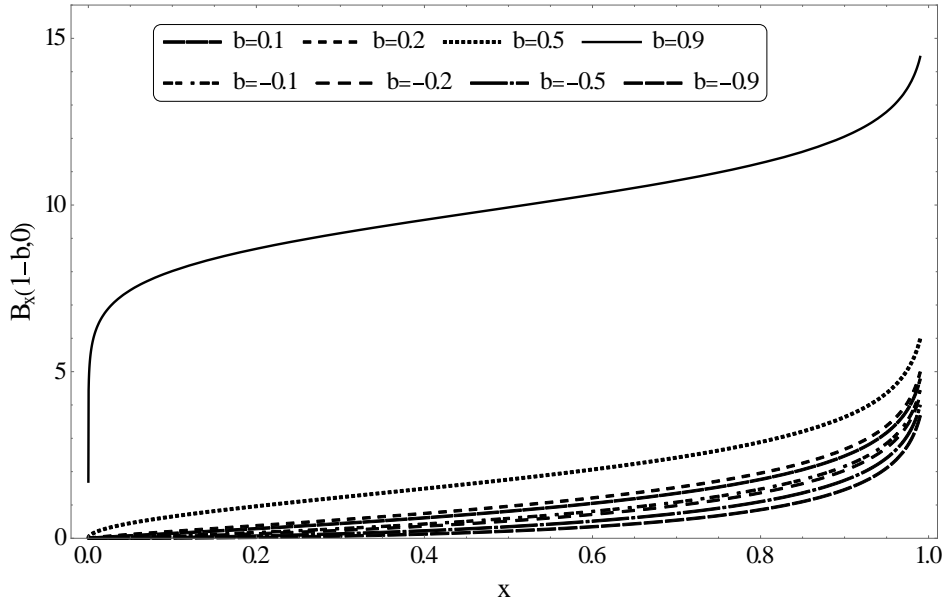


Figure 2 The incomplete Beta function for different values of b in its real domain.

These two figures highlight the singularity of the incomplete Beta function at $x=1$, has a physically sense explanation. This singularity corresponds to outflow being equal to a constant inflow, i.e., $\frac{Q}{r} = 1$, which is the trivial solution to the dynamic routing equation with zero storage. Interestingly, this conclusion can be reached with the assumption of power-type storage function as well, due to the fact that power functions never become zero. In addition, Figs 2 & 3 show that the transition between $\frac{Q}{r} < 1$ and $\frac{Q}{r} > 1$ cannot be done in a single time step due to the discontinuity of the incomplete Beta function at $\frac{Q}{r} = 1$.

2.2 Zero inflow

If inflow becomes zero, the analytic solution above is no longer applicable.

Instead, one may simplify Eq. (5) to:

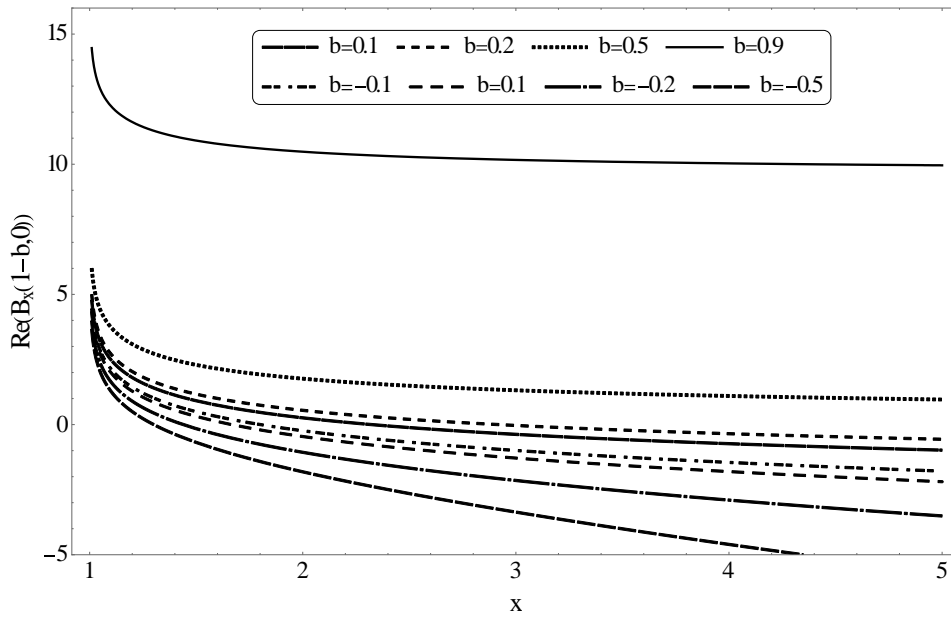


Figure 3 The real component of the incomplete Beta function for different values of b for $x > 1$.

$\text{Re}(z)$ denotes the real component of a complex argument z .

$$\frac{d}{dt} Q(t) = -aQ(t)^{b+1} \quad (14)$$

Eq.(13) may be rearranged as below following separation of variables:

$$\frac{dQ}{Q^{b+1}} = -a dt \quad (15)$$

Integrating both sides of Eq. (15) and inserting the initial conditions, one arrives at the following exact solution for $Q(t)$:

$$Q(t) = \left(\frac{1}{Q_0^b} + a b (t - t_0) \right)^{-\frac{1}{b}} \quad (16)$$

Eq. (16) represents the recession curve for nonlinear reservoir with a power-law storage function.

2.3 Solution for a single pulse inflow

In order to demonstrate the effect of different values of a and b , a single pulse inflow with the duration of 10 s is prescribed. As Fig 4 shows, the variation of a and b offer a wide range of hydrograph shapes that shows the versatility of power-type storage functions in flood routing applications. As expected, it can be seen in Fig 4 that larger values of a correspond to larger storage which corresponds to larger attenuation and lag of flood peaks. On the other hand, b dictates the shape of outflow hydrographs and makes the proposed solution significantly more flexible than previous studies that used either the linear reservoir approach or nonlinear reservoirs with fixed values of b . In Fig 4, it can also be seen that the proposed method has the ability to admit negative values of b .

3 Theoretical determination of storage function parameters for simple cases

3.1 A reservoir with an overflow spillway

If a reservoir has an overflow spillway, its outflow follows the weir equation

(Butler and Davies, 2004):

$$Q = \frac{2}{3} C_d W \sqrt{2g} H^{1.5} \quad (17)$$

where C_d is the coefficient of discharge, W is the width of spillway in meters, g is the gravitational acceleration of 9.81 m/s^2 and H is the head over spillway in meters.

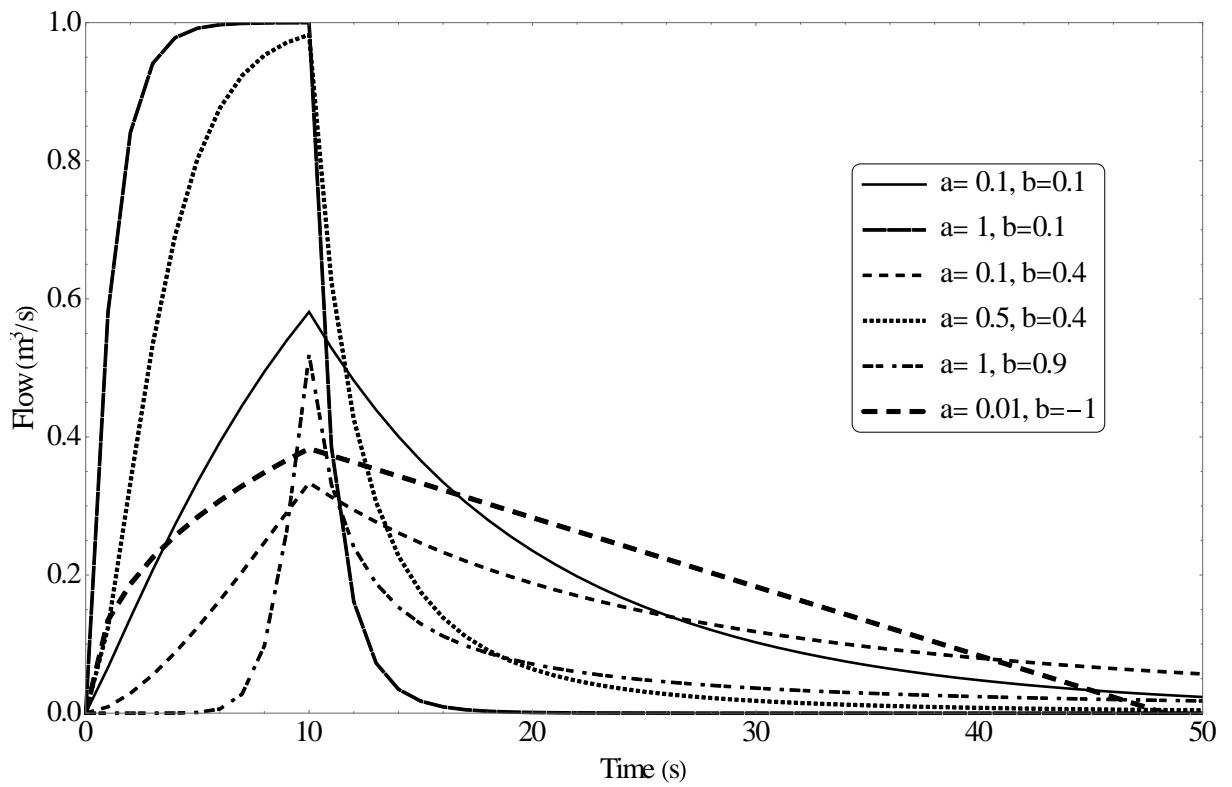


Figure 4 The effect of different values of a and b on the routed hydrograph in response to a 10s unit pulse.

Assuming that the storage in the reservoir follows a power function

$$S = S_b + jH^k \quad (18)$$

where S_b is volume of reservoir below the spillway and j and k are the parameters that approximate the volume of the reservoir above the spillway with a power function. Solving Eq. (17) for H and substituting in Eq. (18) gives the storage as a function of discharge:

$$S = S_b + j \left(\frac{Q}{\frac{2}{3} C_d W \sqrt{2g}} \right)^{\frac{2k}{3}} \quad (19)$$

Since S_b is independent of discharge, Eq. (4) is still valid with

$$a = \frac{3}{2kj} \left(\frac{2}{3} C_d W \sqrt{2g} \right)^{\frac{2k}{3}} \quad (20)$$

and

$$b = 1 - \frac{2k}{3} \quad (21)$$

3.2 A reservoir with an orifice spillway

Flow out of a reservoir through an orifice spillway follows the orifice equation (*Butler and Davies, 2004*):

$$Q = C_d A_o \sqrt{2gH} \quad (22)$$

where C_d is the coefficient of discharge, A_o is the area of the spillway in m^2 , and

H is the head over spillway in meters. If the storage in the reservoir can be

approximated by Eq. (18), solving Eq. (22) for H and substituting in Eq. (18)

gives the storage as a function of discharge:

$$S = S_b + j \left(\frac{Q}{C_d A_o \sqrt{2g}} \right)^{2k} \quad (23)$$

Since S_b is independent of discharge, Eq. (4) is still valid with

$$a = \frac{1}{2kj} (C_d A_o \sqrt{2g})^{2k} \quad (24)$$

and

$$b = 1 - 2k \quad (25)$$

3.3 Nonlinear channel routing

In this section, the hydraulic properties of channels are used to construct the power-law storage function which is then used in the proposed nonlinear routing method for channel routing. A general flow resistance equation for wide channels that combines the geometric properties of the channel cross section and flow properties usually takes the following form (Menabde and Sivapalan, 2001; Yen, 2002):

$$v = c_0 y^\alpha S_0^\beta \quad (26)$$

where v is velocity, y is the depth, and S_0 is the slope. c_0 , α , and β are the parameters of flow resistance equation. For example, in Manning equation $c_0 = 1/n$, $\alpha=2/3$, and $\beta=1/2$, in Chezy equation $c_0 = C$, $\alpha=1/2$ and $\beta=1/2$, and in Darcy-Weisback equation $c_0 = \sqrt{\frac{8g}{f}}$, $\alpha=1/2$ and $\beta=1/2$ where n is Manning's roughness, C is Chezy's roughness, and f is Darcy-Weisback's roughness. The cross-sectional area may be approximated by a power law:

$$A = c_1 y^\omega \quad (27)$$

where c_1 and ω are the parameters of a power law cross section. For example, for a rectangular cross section c_1 is the width of the channel and $\omega=1$.

From the continuity equation, the discharge is given by:

$$Q = A v = c_0 c_1 y^{\alpha+\omega} S_0^\beta \quad (28)$$

Solving Eq. (28) for the depth gives:

$$y = \left(\frac{Q}{c_0 c_1 S_0^\beta} \right)^{\frac{1}{\alpha+\omega}} \quad (29)$$

Assuming that the change in depth over the channel is not very large and the unsteadiness of flood wave has a wavelength larger than the channel length l , the storage, S , is given by (McCuen , 1989):

$$S = Al = c_1 l y^\omega \quad (30)$$

Substituting Eq. (29) in Eq. (30) and expanding gives:

$$S = l c_0^{\frac{-\omega}{\alpha+\omega}} c_1^{\frac{\alpha}{\alpha+\omega}} S_0^{\frac{-\beta\omega}{\alpha+\omega}} Q^{\frac{\omega}{\alpha+\omega}} \quad (31)$$

Using Eq. (31), one may express a and b of Eq. (4) as follows:

$$a = \frac{\alpha + \omega}{\omega l} c_0^{\frac{\omega}{\alpha+\omega}} c_1^{\frac{-\alpha}{\alpha+\omega}} S_0^{\frac{\beta\omega}{\alpha+\omega}} \quad (32)$$

and

$$b = \frac{\alpha}{\alpha + \omega} \quad (33)$$

While the parameters defined here are determined by specific flow resistance equations such as the Manning, Chezy, or Darcy-Weisbach equation, the proposed formulation allows prescribing a and b empirically based on actual

observations. When the physiographic information necessary to prescribe the parameters a and b is not available for hillslope flows, they may be determined using the fractal relationships if self-similarity holds for the hillslope networks (*Menabde and Sivapalan, 2001*).

4 Applications

In this section, we provide several example applications of the exact solutions derived above. The first and second examples show the application of the proposed method in routing an arbitrary inflow hydrograph through a reservoir with an overflow spillway and an orifice spillway, respectively. The third and fourth examples pertain to routing problem in a single channel and the fifth example shows how to route arbitrary inflow hydrographs through a system of 5 channels.

4.1 Example 1: A reservoir with an overflow spillway

Assume a pond with the storage-head function of $S=165 H^{2.5}$ and a 1m wide spillway with $C_d=0.85$. When the pond is full and water level is at the crest of the spillway, an inflow of $I(t) = 0.0453 e^{-0.0167 t}$ enters the pond. Using Eqs. (20) and (21), one can determine $a= 0.0168$ and $b= -0.6667$. If Eq. (13) is solved with a time interval of $\Delta t= 10$ s, the routed hydrograph of Fig 5 is obtained.

4.2 Example 2: A reservoir with an orifice spillway

Assume a tank with a 5m in 5m base with storage-head function of $S=25 H$ and a 24 inch orifice (0.6096 m) with $C_d=0.6$ in the bottom of the tank. Water is pumped into the tank with the inflow function shown in Fig 6. Using Eqs. (24) and (25), one can determine $a= 0.012 5$ and $b= -1$. If Eq. (13) is solved with a time interval of $\Delta t= 10$ s, the routed hydrograph of Fig 6 is obtained. This example shows that negative values of b can be used within the framework of the proposed method. In fact, the negative curvature of the recession limb in Fig 6 is because of the negative value of b .

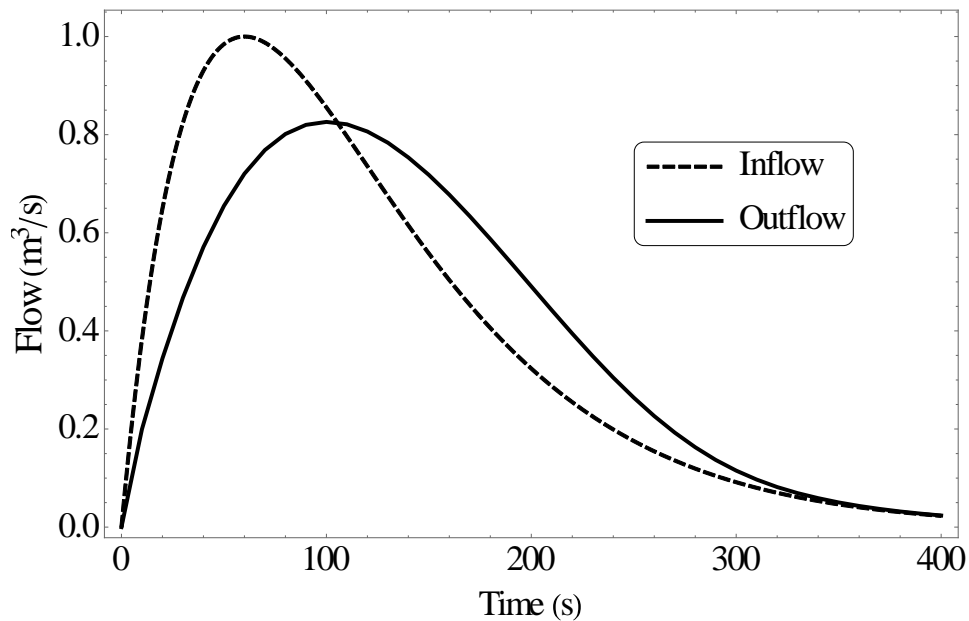


Figure 5 Flood routing in a reservoir with an overflow spillway of example 1.

4.3 Routing through a single channel

4.3.1 Single peak inflow hydrograph

Assume a rectangular channel 5-m wide and 200-m long with Manning's roughness of 0.015, and slope of 0.001. Using Manning's flow resistance equation, we have $a=0.00684819$ and $b=0.4$. The proposed method may then be used to route the inflow through this channel with a time step 10 s. Fig 7 shows the inflow and the routed outflow.

4.3.2 Multiple peak inflow hydrograph

Figure 8 shows the applicability of the proposed model for an inflow hydrograph with multiple peaks, such as periodic waves. The values of $a=0.05$ and $b=0.4$ and time step of 10 s were used for this example.

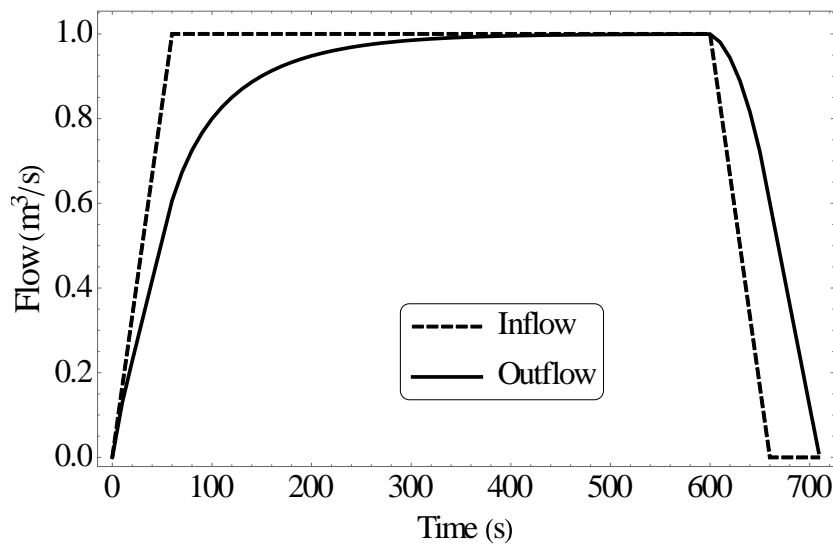


Figure 6 Flood routing in a reservoir with an orifice spillway of example 2.

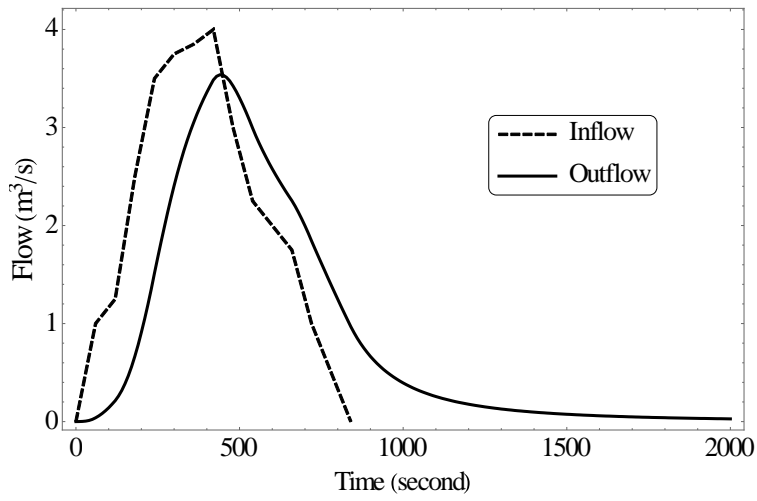


Figure 7 The single peak inflow and routed outflow of hypothetical channel in example 3.

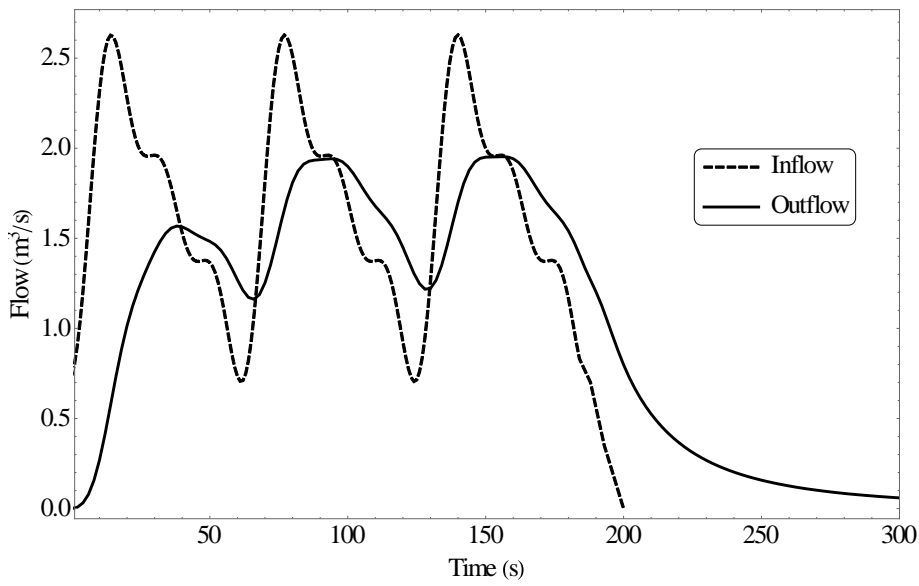


Figure 8 The multiple peak inflow and routed outflow of hypothetical channel in example 3.

4.4 Routing through a network of channels

In this example, arbitrary inflow hydrographs at three locations are routed through a network of five channels. Table 1 summarizes the hydraulic parameters used. Fig 9 shows the channel network. Fig 10 shows the inflow hydrographs used.

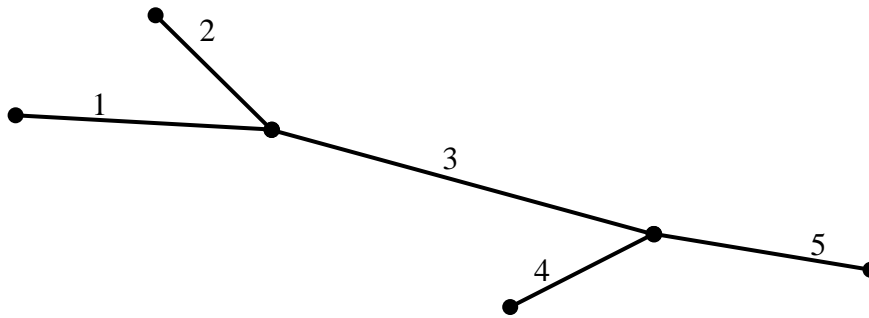


Figure 9 The schematic of the hypothetical network of channels in example 4.

Channel	Length (m)	Slope	Manning's n (m ^{1/2} /s)	Width (m)	a	b
1	3000	0.005	0.010	3	0.001158	0.4
2	2500	0.006	0.013	1	0.001945	0.4
3	5000	0.002	0.010	5	0.00043013	0.4
4	2500	0.005	0.012	2	0.00146446	0.4
5	2750	0.001	0.015	5	0.00049805	0.4

Table 2 The hydraulic properties of the hypothetical network of channels in example 4.

Figs 11-15 show the inflow and outflow in each of the channels. It can be seen that channels 1, 3, and 5 that are longer and have smaller a values, attenuate the flood peak more than channels 2 and 4. Also, channel 2 has a wide inflow hydrograph and shows a larger relative amount of outflow, which makes sense.

due to the mass balance property of the model, its shorter length, and its steeper slope.

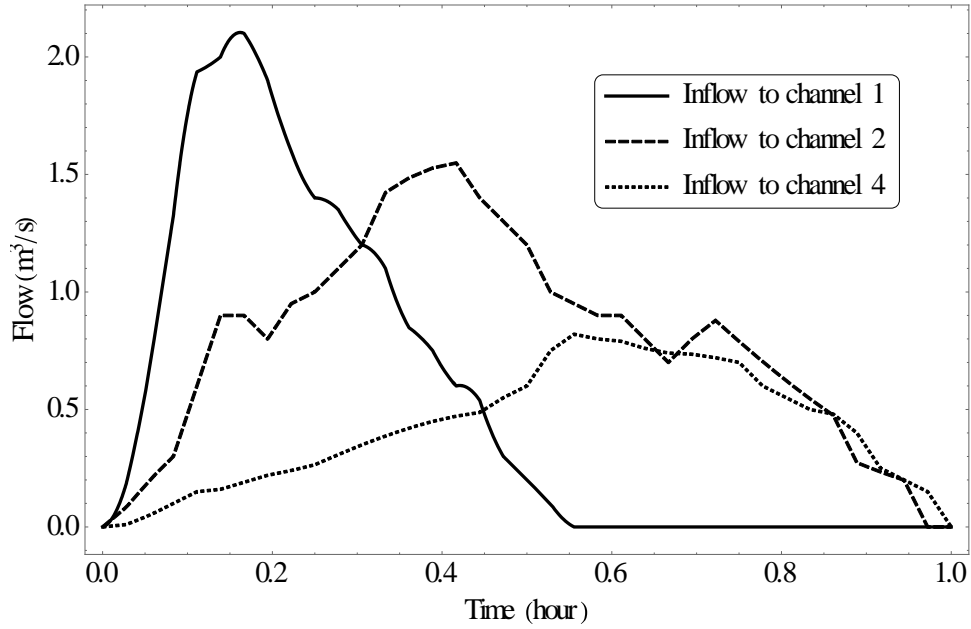


Figure 10 Inflow hydrographs for example 4.

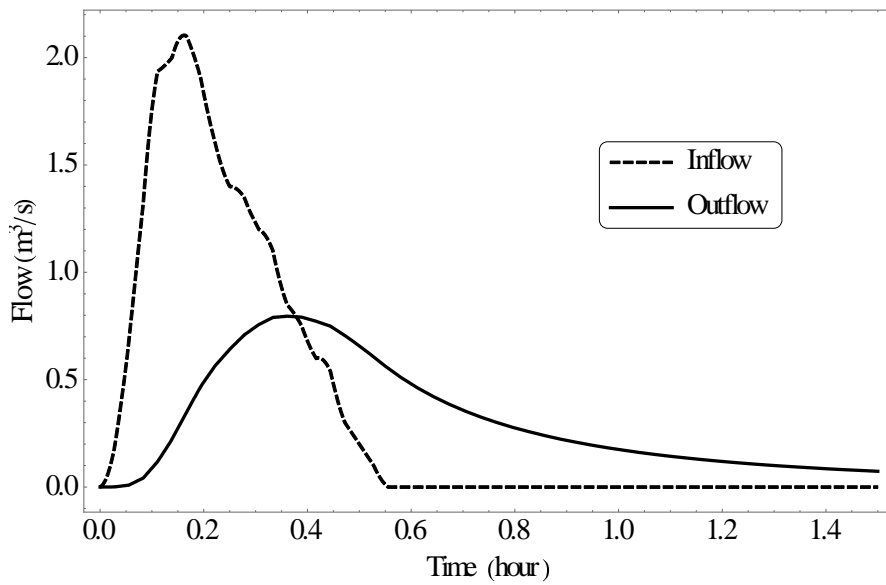


Figure 11 The inflow and routed outflow of channel 1 in example 4.

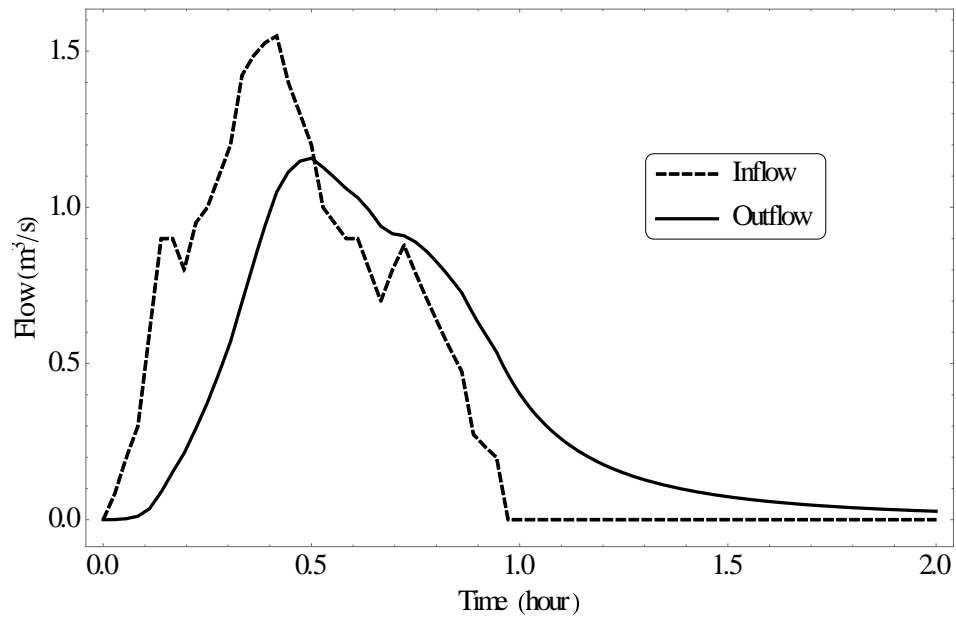


Figure 12 The inflow and routed outflow of channel 2 in example 4.

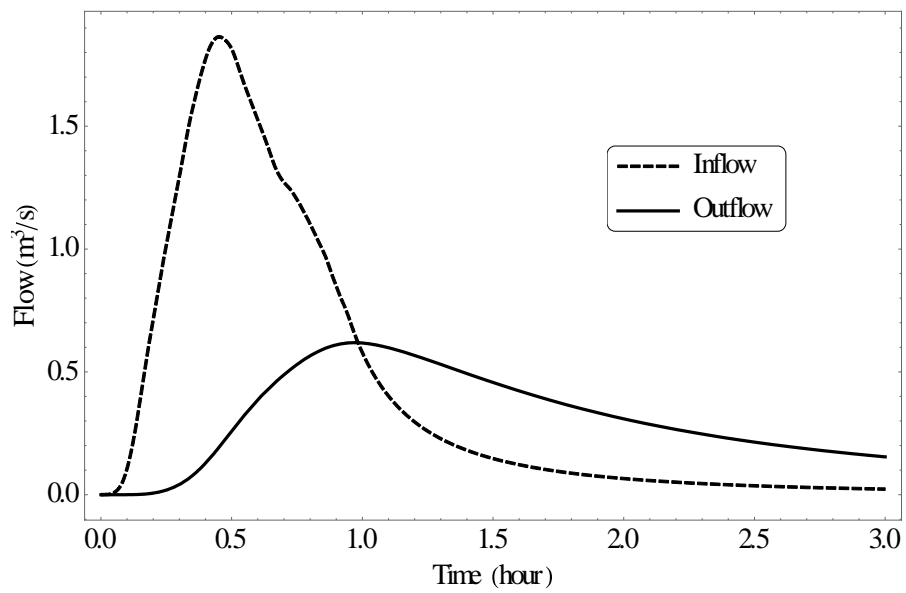


Figure 13 The inflow and routed outflow of channel 3 in example 4.

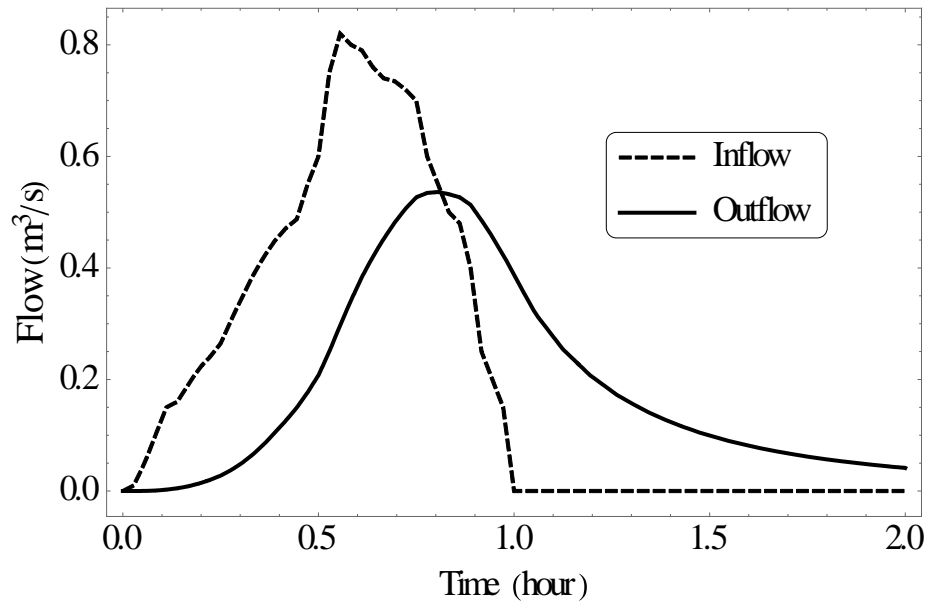


Figure 14 The inflow and routed outflow of channel 4 in example 4.

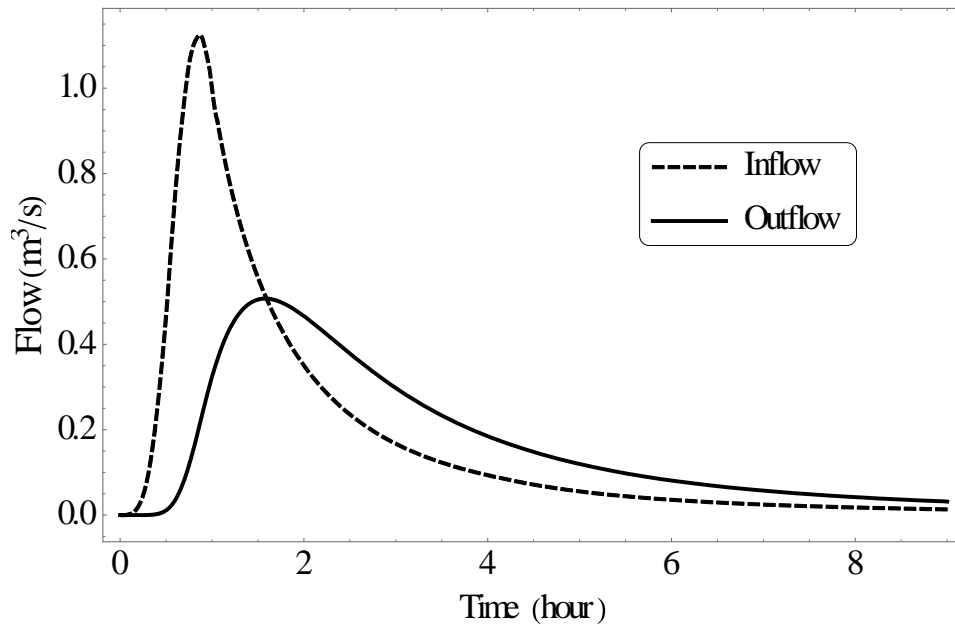


Figure 15 The inflow and routed outflow of channel 5 in example 4.

5 Conclusions and future research recommendations

A new solution to nonlinear routing equation for power-law storage functions with arbitrary exponents was proposed. In addition to flexibility that the proposed formulation offers for using different types of nonlinear reservoirs, general cross sections and flow resistance equations were implemented in the methodology to extend the application of the solution for nonlinear channel routing.

Application of the new exact solution in different routing problems was presented. However, the capability of the proposed method is not limited to these examples. For example, different design and control problems could take advantage of the simplicity of the proposed method. In addition, other components of hydrologic cycle such as ground water aquifers, and various hydraulic structures such as tunnel spillways could potentially be approximated by power-type storage functions and be solved by the presented framework.

One possible limitation of the proposed solution is that some programming environments do not have built-in functions for hypergeometric functions or incomplete beta function. This issue can be remedied by building look-up tables once (using numerical integration methods) and using them many times within the solution framework as an alternative to built-in functions.

Acknowledgements

This material is based upon work supported in part by the National Science Foundation under Grant CyberSEES-1442735 (Dong-Jun Seo, University of Texas at Arlington, PI). This support is gratefully acknowledged.

References

- Ayalew, T. B., Krajewski, W. F., Mantilla, R., & Small, S. J. (2014). Exploring the effects of hillslope-channel link dynamics and excess rainfall properties on the scaling structure of peak-discharge. *Advances in Water Resources*, *64*, 9-20.
- Arora, V., Seglenieks, F., Kouwen, N., & Soulis, E. (2001). Scaling aspects of river flow routing. *Hydrological processes*, *15*(3), 461-477.
- Basha, H. A. (1994). Nonlinear reservoir routing: particular analytical solution. *Journal of Hydraulic Engineering*, *120*(5), 624-632.
- Basha, H. A. (1995). Routing equations for detention reservoirs. *Journal of Hydraulic Engineering*, *121*(12), 885-888.
- Basha, H. A. (2000). Simple nonlinear rainfall-runoff model. *Journal of Hydrologic Engineering*, *5*(1), 25-32.
- Boyd, M. J., Pilgrim, D. H., & Cordery, I. (1979). A storage routing model based on catchment geomorphology. *Journal of Hydrology*, *42*(3-4), 209-230.
- Butler, D., & Davies, J. (2004). *Urban drainage*. CRC Press.

- Camacho, L. A., & Lees, M. J. (1999). Multilinear discrete lag-cascade model for channel routing. *Journal of Hydrology*, 226(1), 30-47.
- Choi, C. C., Constantinescu, G., & Mantilla, R. (2015). Implementation of a hydraulic routing model for dendritic networks with offline coupling to a distributed hydrological model. *Journal of Hydrologic Engineering*, 20(11), 04015023.
- Fiorentini, M., & Orlandini, S. (2013). Robust numerical solution of the reservoir routing equation. *Advances in Water Resources*, 59, 123-132.
- Fread, D. L., & Hsu, K. S. (1993). Applicability of two simplified flood routing methods: level-pool and Muskingum-Cunge. *In ASCE national hydraulic engineering conference. San Francisco, CA: ASCE* (pp. 1564-8).
- Glynn, J. E., & Glynn, P. W. (1996). A diffusion approximation for a network of reservoirs with power law release rule. *Stochastic Hydrology and Hydraulics*, 10(1), 17-37.
- Gradshteyn, I. S., & Ryzhik, I. M. (2014). Table of integrals, series, and products. Academic press.
- Gupta, V. K., & Waymire, E. (1998). Some mathematical aspects of rainfall, landforms, and floods. *Advanced series in statistical sciences and applied probability*, 7, 129-172.

- Gupta, V. K. (2004). Emergence of statistical scaling in floods on channel networks from complex runoff dynamics. *Chaos, Solitons & Fractals*, 19(2), 357-365.
- Hughes, D. A., & Murrell, H. C. (1986). Non-linear runoff routing—A comparison of solution methods. *Journal of Hydrology*, 85(3-4), 339-347.
- Kim, D. H., & Georgakakos, A. P. (2014). Hydrologic routing using nonlinear cascaded reservoirs. *Water Resources Research*, 50(8), 7000-7019.
- Mandapaka, P. V., Krajewski, W. F., Mantilla, R., & Gupta, V. K. (2009). Dissecting the effect of rainfall variability on the statistical structure of peak flows. *Advances in Water Resources*, 32(10), 1508-1525.
- Mantilla, R., & Gupta, V. K. (2005). A GIS numerical framework to study the process basis of scaling statistics in river networks. *IEEE Geoscience and Remote sensing letters*, 2(4), 404-408.
- Mantilla, R., Gupta, V. K., & Mesa, O. J. (2006). Role of coupled flow dynamics and real network structures on Hortonian scaling of peak flows. *Journal of Hydrology*, 322(1), 155-167.
- McCuen, R. H. (1989). Hydrologic analysis and design (pp. 143-147). Englewood Cliffs, NJ: Prentice-Hall.

- Menabde, M., & Sivapalan, M. (2001). Linking space–time variability of river runoff and rainfall fields: a dynamic approach. *Advances in Water Resources*, 24(9), 1001-1014.
- Nash, J. E. (1957). The form of the instantaneous unit hydrograph. *International Association of Scientific Hydrology, Publ*, 3, 114-121.
- Niazkar, M., & Afzali, S. H. (2017). New nonlinear variable-parameter Muskingum models. *KSCE Journal of Civil Engineering*, 1-10.
- Nourani, V., Singh, V. P., & Delafrouz, H. (2009). Three geomorphological rainfall–runoff models based on the linear reservoir concept. *Catena*, 76(3), 206-214.
- Perumal, M. (1992). Multilinear Muskingum flood routing method. *Journal of Hydrology*, 133(3-4), 259-272.
- Reggiani, P., Sivapalan, M., Hassanizadeh, S. M., & Gray, W. G. (2001, January). Coupled equations for mass and momentum balance in a stream network: theoretical derivation and computational experiments. In *Proceedings of the Royal Society of London A: Mathematical, Physical and Engineering Sciences* (Vol. 457, No. 2005, pp. 157-189). The Royal Society.
- Sahoo, B. (2013). Field application of the multilinear Muskingum discharge routing method. *Water resources management*, 27(5), 1193-1205.

- Small, S. J., Jay, L. O., Mantilla, R., Curtu, R., Cunha, L. K., Fonley, M., & Krajewski, W. F. (2013). An asynchronous solver for systems of ODEs linked by a directed tree structure. *Advances in Water Resources*, 53, 23-32.
- Sugiyama, H., Kadoya, M., Nagai, A., & Lansey, K. (1997). Evaluation of the storage function model parameter characteristics. *Journal of hydrology*, 191(1-4), 332-348.
- Tallaksen, L. M. (1995). A review of baseflow recession analysis. *Journal of hydrology*, 165(1-4), 349-370.
- Weisstein, E. W. (2003). Gamma function,
<http://mathworld.wolfram.com/GammaFunction.html>.
- Weisstein, E. W. (2002). Hypergeometric function.
<http://mathworld.wolfram.com/HypergeometricFunction.html>
- Weisstein, E. W. (2003). Incomplete beta function,
<http://mathworld.wolfram.com/IncompleteBetaFunction.html>
- Wolfram Research, Inc., Mathematica, Version 10.3, Champaign, IL (2015).
- Xiong, Y., & Melching, C. S. (2005). Comparison of kinematic-wave and nonlinear reservoir routing of urban watershed runoff. *Journal of Hydrologic Engineering*, 10(1), 39-49.
- Yen, B. C. (2002). Open channel flow resistance. *Journal of hydraulic engineering*, 128(1), 20-39.

Chapter 5

General Conclusions

Accurate and timely forecasting of floods and mapping of inundation extent and severity is one of the largest needs in highly populated urban areas. With urbanization and climate change, this need is fast increasing in many parts of the US and elsewhere. For large areas such as the Dallas-Fort Worth Metroplex (DFW), real-time high-resolution forecasting remains a large challenge due to very large resources required for modeling and computing. The objective of this research is to assess the currently available 1D-2D modeling capability for potential applications for large areas, propose a real world-viable alternative approach and develop key modeling elements that are necessary to realize it.

The first part of this research assessed the applicability of 1D-2D modeling for real-time inundation mapping and the impact of changes in precipitation magnitude and imperviousness on urban inundation using 1D-2D modeling due to climate change and urbanization. The study areas were the Forest Park-Berry Catchment ($\sim 3.3 \text{ km}^2$) and the Edgecliff Branch Catchment of Sycamore Creek ($\sim 12.17 \text{ km}^2$) in the City of Fort Worth in North Central Texas. There are two of the flood-prone areas identify by the City. With respect to the real-time application of 1D-2D model, it was found that:

- 1D-2D hydraulic modeling is currently not viable for real-time forecasting for large areas in which case its accuracy may be significantly compromised,

potentially negating the benefits of such modeling. The limitations of 1D-2D hydraulic modeling for large urban areas are due to modeling complexity and very large requirements for human resources for modeling.

- Detailed hydrologic and hydraulic information (such as slope of pipes, dimensions of inlets and junction boxes, and invert elevation of all the elements) necessary for high-resolution 1D-2D modeling is often not available.
- Due to computational requirements of 1D-2D models,
 - It is impractical to make a very large number of runs required for uncertainty assessment using standard Monte Carlo methods.
 - Simulation in real-time high-resolution inundation mapping is currently practical only for smaller urban catchments.

With respect to the impact assessment, it was found that:

- Large impact of changes in precipitation and impervious cover on local and catchment scale inundation.
- With climate change and continuing urbanization for accurate mapping of inundation in urban areas, high resolution rainfall forcing and physiographic information are essential.

The second and third parts of this research were directed to identifying potential alternatives to 1D-2D modeling with reduced complexity and computational requirements. To that end, a modeling framework was proposed in which coarse-resolution model output is downscaled using high-resolution

physiographic data. Currently, coarse-resolution hydrologic models operate in real time in the DFW area as part of the CASAWX program which may provide the initial and boundary conditions necessary for the downscaling approach. To model the potentially very complex network of channels within each 2D cell, novel physically-based 1D solutions were developed for hydraulic and hydrologic routing. The newly developed approaches avoid solving large systems of linear or nonlinear equations in real-time and hence are computationally efficient as well.

The newly developed hydraulic routing approach offers two continuous-time discrete-space methods for explicit quasi-analytical solution of the 1D diffusion wave equation with a desired number of spatial nodes. In addition, a generic 5-node unit response function to the diffusive wave equation with constant inflow was developed. The proposed quasi-analytical solutions offer a new pathway for simple and efficient modeling of flood waves in real-world applications at a significantly reduced computational cost compared to numerical integration. The main conclusions from this element are:

- CTDS methods offer simple and computationally efficient solutions that can be easily implemented on site on single-board computers such as Raspberry Pi modules for real-time forecasting.
- Using CTDS methods, the complete hydrographs at downstream locations may be obtained via the principle of superposition and proportionality from a fixed-interval pulse representation of the inflow hydrograph. The obtained solutions

are in very good agreement with numerical integration methods and obviate the need for problem-specific model setup.

- The obtained quasi-analytical solutions provide an important reference for both development and validation of new methods.

The second new approach developed in this research offers a new implicit analytical solution for general nonlinear routing with power-law storage functions with arbitrary exponents. Power-law relationships between storage and discharge occur ubiquitously in nature. As such, the new solution has a wide range applications in the real world, including flood routing through large networks of channels, groundwater modeling, and hydraulic structures. Additionally, parametrization of nonlinear channel routing with general flow resistance and cross-sectional area as power-law storage function was presented. With the above parametrization, the proposed analytical solution may be used in nonlinear channel routing for real-time simulation of a very large number of 1D channels over large areas. The main conclusions from this element are:

- Contrary to conclusions drawn from previous studies, it was found that the general nonlinear routing problem with power-law storage functions of any arbitrary exponent has an analytical solution.
- Many components of hydrologic cycle such as ground water aquifers, and various hydraulic structures such as different spillways could potentially be

approximated by power-type storage functions and be solved by the presented solution.

- General cross sections and flow resistance equations were implemented in the methodology to extend the application of the solution for nonlinear channel routing.

Whereas the two new 1D routing models developed in this research will help realize real-time flood forecasting and inundation mapping in large urban areas, they represent only the first steps toward the downscaling approach put forth as an alternative to 1D-2D modeling. The following has been identified as the additional necessary elements:

- Parametrization of power-type storage functions and diffusive wave constants for urban catchments with observational data.
- Downscaling the coarse-resolution model output by prescribing the initial and boundary conditions to the new 1D routing models.
- Delineating large urban catchments into subcatchments and prescribing the upstream simulation results as the boundary condition to downstream subcatchments.
- Integrated real-time simulation over large areas.
- Evaluating the performance and quantifying potential computational savings of quasi-analytical methods for routing a large network of channels or a dense network of small channels in large urban areas.

Finally, the newly developed solutions may also be implemented in the National Water Model (NWM) launched recently into the NWS operations to fill the hydrologic service gaps (Cosgrove et al., 2015). The NWM channel routing currently uses the Muskingum-Cunge (MC) method with variable parameters (Szymkiewicz, 2010) along the channels defined by the NHDPlus Version 2 (Moore and Dewald, 2016). For modeling reservoirs and lakes, the NWM currently uses level-pool routing (Gochis et al. 2013). Whereas the MC method mimics diffusive wave, it requires careful selection of the parameters for stability (Novak et al., 2010). The new routing methods developed in this research may potentially be used in place of or in addition to the existing MC and level-pool routing methods with significant improvement in accuracy, computational efficiency and parsimony (and hence calibration). Such an application may be made at all catchment scales from small urban catchments to large river systems with estuary/ocean BCs incrementally and with spatially varying resolutions based on the need for high-resolution information.

References

Cosgrove, B., Gochis, D., Clark, E. P., Cui, Z., Dugger, A. L., Fall, G. M., ... & Kitzmiller, D. (2015, December). Hydrologic Modeling at the National Water Center: Operational Implementation of the WRF-Hydro Model to support National Weather Service Hydrology. In *AGU Fall Meeting Abstracts*.

- Clark, E., Cosgrove, B., Flowers, T. (2017). *NOAA's National Water Model: Comprehensive Continental-Scale Water Intelligence*. Retrieved from <http://cpo.noaa.gov/sites/cpo/MAPP/Webinars/2017/03-28-17/Clark.pdf>
- Moore, R. B., & Dewald, T. G. (2016). The road to NHDPlus—advancements in digital stream networks and associated catchments. *JAWRA Journal of the American Water Resources Association*.
- Novak, P., Guinot, V., Jeffrey, A., Reeve, D. E. (2010). *Hydraulic modelling—an introduction: principles, methods and applications*. CRC Press.
- Szymkiewicz, R. (2010). *Numerical modeling in open channel hydraulics* (Vol. 83). Springer Science & Business Media.